INFORMATION TO USERS

This manuscript has been reproduced from the microfilm master. UMI films the text directly from the original or copy submitted. Thus, some thesis and dissertation copies are in typewriter face, while others may be from any type of computer printer.

The quality of this reproduction is dependent upon the quality of the copy submitted. Broken or indistinct print, colored or poor quality illustrations and photographs, print bleedthrough, substandard margins, and improper alignment can adversely affect reproduction.

In the unlikely event that the author did not send UMI a complete manuscript and there are missing pages, these will be noted. Also, if unauthorized copyright material had to be removed, a note will indicate the deletion.

Oversize materials (e.g., maps, drawings, charts) are reproduced by sectioning the original, beginning at the upper left-hand corner and continuing from left to right in equal sections with small overlaps.

Photographs included in the original manuscript have been reproduced xerographically in this copy. Higher quality 6" x 9" black and white photographic prints are available for any photographs or illustrations appearing in this copy for an additional charge. Contact UMI directly to order.

ProQuest Information and Learning
300 North Zeeb Road, Ann Arbor, MI 48106-1346 USA
800-521-0600



Downloaded from SHAREOK. Persistent Handle URL: https://hdl.handle.net/11244/400

UNIVERSITY OF OKLAHOMA

GRADUATE COLLEGE

PREDICTION OF CLOUD-TO-GROUND LIGHTNING IN THE WESTERN UNITED STATES

A Dissertation

SUBMITTED TO THE GRADUATE FACULTY

in partial fulfillment of the requirement for the

degree of

Doctor of Philosophy

By

Phillip Dean Bothwell
Norman, Oklahoma
2002

UMI Number: 3034883

Copyright 2002 by
Bothwell, Phillip Dean

All rights reserved.

UMI®

UMI Microform 3034883
Copyright 2002 by ProQuest Information and Learning Company.
All rights reserved. This microform edition is protected against
unauthorized copying under Title 17, United States Code.

ProQuest Information and Learning Company
300 North Zeeb Road
P.O. Box 1346
Ann Arbor, MI 48106-1346

© Copyright by Phillip Dean Bothwell 2002
All Rights Reserved.

PREDICTION OF CLOUD-TO-GROUND LIGHTNING IN THE WESTERN UNITED STATES

A Dissertation APPROVED FOR THE
SCHOOL OF METEOROLOGY

BY

Frederick H. Carr

Charles B. Clark

Kenneth C. Crawford

Donald R. MacGorman

S. Lakshmivarahan

William H. Beasley

ACKNOWLEDGMENTS

I wish to thank all my family for their years of patience as they stood by me while I was taking classes, studying for exams, and working long hours on the research and writing. I am grateful to my wife, Leslie, who encouraged me to "go for it" in the beginning, took care of our large family, and kept me focused through this long journey. I want to thank my sons for understanding why I was often busy with this endeavor. I thank my father, now deceased, and my mother for always supporting my goal of becoming a meteorologist and for expressing their pride in me, each and every step of the way. Without Dr. William Beasley, who kept prodding me to get my doctorate, this would never have been attempted.

My committee has been extremely helpful and has never wavered from "holding me to the standard". I have become very aware of how much time a professor can invest in a graduate student. Dr. Fred Carr has always pushed me to keep my efforts at the highest scientific level and has invested many hours to insure that I produced quality work. Despite my pre-conceived ideas about statistics, Dr. Michael Richman, through our many hours of discussions, has taught me that statistics is an extremely powerful tool and can actually be exciting and interesting. I would also like to thank Dr. William Beasley, Dr. Ken Crawford, Dr. Don MacGorman, and Dr. S. Lakshmivarahan for their invaluable comments and suggestions, for answering many questions, and also for serving on my doctoral committee.

Many thanks to those in the Norman Weather Center who have provided technical and moral support along the way, including Mr. Ron Holle, Mike Baldwin, Dr. Raúl López, Dr. Dave Rust, Dr. Kim Elmore, Dr. Joe Schaefer, and Dr. Russ Schneider. I thank Mr. John Hart for providing additional software that aided in the calculation of some of the parameters.

TABLE OF CONTENTS

Page

ACKNOWLEDGMENTS....iv

TABLE OF CONTENTS....vi

LIST OF TABLES....viii

LIST OF FIGURES....ix

ABSTRACT....xiii

CHAPTER 1 -INTRODUCTION....1
1.1 Statement of the Problem....1
1.1.1 Importance of Accurate Lightning Prediction....2
1.1.2 Thunderstorms in the Western United States....3
1.1.3 Thunderstorm Probabilities and Thunderstorm Flash Rates....5

CHAPTER 2 - RESEARCH OBJECTIVES....6
2.1 Review of Previous Work....7
2.1.1 Perfect Prog vs. Model Output Statistics....7
2.1.2 Previous Research on Thunderstorm Prediction....9
2.2 Differences from Previous Work....16
2.3 The Three Dimensional Model....22

CHAPTER 3 - DATA REQUIREMENTS....27
3.1 Lightning Data....27
3.1.1 Developing Lightning Climatologies....31
3.2 The Rapid Update Cycle 2 (RUC 2) Model....37
3.3 Development of Predictor Predictand Data Sets....42

CHAPTER 4 - DATA ANALYSIS AND STATISTICAL TECHNIQUES....45
4.1 Initial Investigation....45
4.2 Data Set for This Study....46
4.2.1 Original Data Matrix Structure....50
4.3 Correlation of Predictors and Predictands....51
4.4 Stepwise Regression....53
4.5 Principal Component Analysis....56
4.5.1 Procedures....59
4.6 Logistic Regression....64

CHAPTER 5 - RESULTS.....67
5.1 Probability Forecasts.....67
5.2 Conceptual Model for Storms That Produce Lightning.....98
5.2.1 Lightning Versus No Lightning Cases.....98
5.2.2 Low Number of Flashes Versus High Numbers of Flashes.....121

CHAPTER 6 - SUMMARY AND CONCLUSIONS.....127

REFERENCES.....134

APPENDIX A - THE NATIONAL LIGHTNING DETECTION NETWORK.....140
APPENDIX B - DETERMINATION OF LIGHTNING CLIMATOLOGIES.....144
APPENDIX C - CANDIDATE PREDICTORS.....151
APPENDIX D - PREDICTOR CORRELATIONS AND STEPWISE REGRESSION.....157
APPENDIX E - PRINCIPAL COMPONENT ANALYSIS.....162
APPENDIX F - MULTIPLE LOGISTIC REGRESSION.....171
APPENDIX G - MEASURES OF FORECAST SKILL AND ACCURACY.....173

LIST OF TABLES

Page

Table 4.1. Order and descriptor of predictors and correlation with predictands.... 52-53

Table 4.2. Results from stepwise regression and description of predictors.... 55

Table 4.3. Individual Rotated Principal Components.... 62

Table 4.4. Results from stepwise regression on Rotated Principal Components.... 62

Table 5.1 Verification scores for forecast probabilities of one or more flashes.... 96

Table 5.2. Parameter differences between grid boxes without and with lightning.... 113

Table 5.3. Parameter differences between grid boxes with low, moderate and high number of flashes.... 121

Table B.1. Example of lightning data for hypothetical pentad.... 144

Table C.1. Candidate predictors.... 152-156

Table D.1. Correlation values between binary predictand and predictors.... 159

Table D.2. Correlation values between number of flashes and predictors.... 160

Table D.3. Stepwise regression results for two predictands and all predictors.... 161

Table E.1. Principal component loadings.... 170

Table G.1. Summary of terms used to assess forecast skill and accuracy.... 173

LIST OF FIGURES

Page

Figure 2.1. Timeline of operational thunderstorm prediction systems 10

Figure 2.2. Average kinematic and adiabatic vertical velocities between the LCL and 400 mb as computed from the RUC 2 18

Figure 2.3. Schematic showing physical process represented and approximate vertical level 25

Figure 3.1. Locations of the stations in the NLDN 28

Figure 3.2. Detection efficiency after the 1994 upgrade to the NLDN 28

Figure 3.3. Percent of grid boxes reporting 1, 3, 10, 30, or 100 (or more) flashes per 3 hours for both development and independent data sets 30

Figure 3.4. Lightning relative frequency for 2 June pentad 34

Figure 3.5. Lightning relative frequency for 7 July pentad 35

Figure 3.6. Lightning f relative frequency or 1 August pentad 36

Figure 3.7. Horizontal domain of the RUC 2 and smaller domain used in study 38

Figure 4.1. Lightning relative frequencies for July 17 pentad. Times are 18 to 21, 21 to 00, 00 to 03, and 03 to 06 UTC 48

Figure 4.2. Eigenvalues for each of the 208 parameters-development data 61

Figure 4.3. Schematic showing 10 rotated principal component terms and the variance of original data contained in each 63

Figure 5.1. Probability of one or more lightning flashes along with one or more flashes per grid box detected from 00 to 03 UTC for 3 June 1999 68

Figure 5.2. Probability of one or more lightning flashes along with one or more flashes per grid box detected from 00 to 03 UTC for 8 June 1999 69

Figure 5.3. Probability of one or more lightning flashes along with one or more flashes per grid box detected from 00 to 03 UTC for 14 June 1999 70

Figure 5.4. Probability of one or more lightning flashes along with one or more flashes per grid box detected from 00 to 03 UTC for 17 June 1999 71

Figure 5.5. Probability of one or more lightning flashes along with one or more flashes per grid box detected from 00 to 03 UTC for 23 June 1999 72

Figure 5.6. Probability of one or more lightning flashes along with one or more flashes per grid box detected from 00 to 03 UTC for 28 June 1999 73

Figure 5.7 Probability of one or more lightning flashes along with one or more flashes per grid box detected from 00 to 03 UTC for 9 July 1999 74

Figure 5.8. Probability of one or more lightning flashes along with one or more flashes per grid box detected from 00 to 03 UTC for 11 July 1999 75

Figure 5.9. Probability of one or more lightning flashes along with one or more flashes per grid box detected from 00 to 03 UTC for 18 July 1999 76

Figure 5.10. Probability of one or more lightning flashes along with one or more flashes per grid box detected from 00 to 03 UTC for 22 July 1999 77

Figure 5.11 Probability of one or more lightning flashes along with one or more flashes per grid box detected from 00 to 03 UTC for 25 July 1999 78

Figure 5.12. Probability of one or more lightning flashes along with one or more flashes per grid box detected from 00 to 03 UTC for 29 July 1999 79

Figure 5.13. Probability of one or more lightning flashes along with one or more flashes per grid box detected from 00 to 03 UTC for 13 August 1999... 80

Figure 5.14. Probability of one or more lightning flashes along with one or more flashes per grid box detected from 00 to 03 UTC for 14 August 1999 81

Figure 5.15. Probability of one or more lightning flashes along with one or more flashes per grid box detected from 00 to 03 UTC for 22 August 1999 82

Figure 5.16. Probability of one or more lightning flashes along with one or more flashes per grid box detected from 00 to 03 UTC for 24 August 1999 83

Figure 5.17. Box plots showing number of observed flashes per 3 hours per grid box versus the forecast probability of one or more flashes 88

Figure 5.18. Box plots showing number of observed flashes per 3 hours per grid box versus the forecast probability of 10 or more flashes 89

Figure 5.19. Box plots showing number of observed flashes per 3 hours per grid box versus the forecast probability of 100 or more flashes 90

Figure 5.20. Probability of 10 or more lightning flashes along with one or more flashes per grid box detected from 00 to 03 UTC for 17 June 1999 92

Figure 5.21. Probability of 100 or more lightning flashes along with one or more flashes per grid box detected from 00 to 03 UTC for 17 June 1999 93

Figure 5.22. Reliability diagram for all independent forecasts 95

Figure 5.23. POD, FAR, CSI and Bias for 16 independent days 97

Figure 5.24. Box plots showing climatological thunderstorm probability when each flash category (none, 1-9, 10-99, 100-999) is observed 99

Figure 5.25. Box plots showing average length of time lightning occurs (in minutes) from lightning climatology when each category (none, 1-9, 10-99, 100-999) is observed 101

Figure 5.26. Box plots showing average number of flashes per grid box per 3 hours from lightning climatology when each flash category (none, 1-9, 10-99, 100-999) is observed 102

Figure 5.27. Convective Inhibition (CIN) for cases when most unstable CAPE (MUCAPE) is greater than 0 103

Figure 5.28. Layer CAPE (-15 to -20 °C) when MUCAPE greater than 0 105

Figure 5.29. Most unstable parcel Layer CAPE and percent of grid boxes with one or more flashes when there is positive CAPE in the respective layer 107

Figure 5.30. Layer CAPE (LFC to -20 °C) for MUCAPE greater than 0 108

Figure 5.31. Cloud depth when MUCAPE is greater than 0 for grid boxes reporting no flashes, 1-9, 10-99, and 100-999 flashes 110

Figure 5.32. Cloud base temperature when MUCAPE is greater than 0 for grid boxes reporting no flashes, 1-9, 10-99, and 100-999 flashes 112

Figure 5.33. Normalized CAPE from LCL to -20 degrees C for grid boxes reporting no flashes, 1-9, 10-99, and 100-999 flashes 115

Figure 5.34. Normalized (total) CAPE for grid boxes reporting no flashes, 1-9, 10-99, and 100-999 flashes 116

Figure 5.35. Potential/convective instability between 400 and 700 mb, for cases of no flashes, 1-9, 10-99, and 100 to 999 flashes 118

Figure 5.36. Temperature at EL for MUCAPE greater than 0 for grid boxes reporting no flashes, 1-9, 10-99, and 100 to 999 flashes 119

Figure 5.37. Precipitable water (inches) for grid boxes reporting no flashes, 1-9, 10-99 flashes, and 100 to 999 flashes 120

Figure 5.38. Total number of flashes per grid box per 3 hours and potential vorticity for the full 54 day development data set 124

Figure 5.39. Total number of flashes per grid box per 3 hours and tropopause pressure (mb) for the full 54 day development data set 125

Figure B.1. Weights applied data in development of 7 June pentad 147

Figure B.2. Lightning relative frequency for each three hour time period of the day for grid box located at point A (shown in Fig. B.4)..... 148

Figure B.3. Pentad lightning relative frequency for 00 to 03 UTC for grid box located at point A (shown in Fig. B.4)..... 149

Figure B.4. Map of western United States and grid point "A"..... 150

Figure E.1. Pair-wise plot for 10 rotated PCs using all loadings 168

Figure E.2. Pair-wise plot for 10 rotated PCs (absolute values) using 0.4 cutoff... 169

Figure F.1. Example of response of predictand from logistic regression..... 172

Figure G.1. Contingency table..... 173

Figure G.2. Contingency tables for grids sized 80 and 40 km per side..... 175

Figure G.3. Contingency tables for two time periods and sample grid..... 176

Figure G.4. Pie chart of number of lightning flashes..... 178

ABSTRACT

During the past 30 years, many schemes have been developed to predict lightning (i.e., thunderstorms). These schemes, either extrapolative in nature for the short term or dependent on model output for the longer term, have met with limited success. Yet, more accurate prediction of thunderstorms could help mitigate billions of dollars in annual property damage as well as reduce death, injury, and disruption of human activities. To predict lightning and storms with high flash rates, it is necessary to understand what factors determine when and where thunderstorms develop, as well as determine what factors cause storms to produce high flash rates.

This dissertation focuses specifically on identifying the thermodynamic environment and forcing mechanisms across the western United States that create precipitation systems with lightning. The majority of these convective systems are non-severe. With some thunderstorms, very little precipitation may reach the ground; yet, these "dry" storms spark deadly wildfires in the West every summer.

The goals of this dissertation are: to develop a statistical prediction system that will improve the forecasts of thunderstorms, particularly thunderstorms with high numbers of flashes; to produce forecasts that bridge the gap which exists between extrapolative systems and model-based systems by using both analysis and model forecasts; and to improve the understanding of environmental characteristics which support general thunderstorms and storms with high flash rates.

Predictors are derived from the high-resolution model output (temporal and spatial) of the numerical model known as the Rapid Update Cycle 2 (RUC 2). Additional predictors are from a lightning climatology developed for this study. The RUC 2 model is used in a "Perfect Prog" approach with the predictive equations evaluated using independent data. Using principal component analysis, over 200 candidate predictors from the RUC 2 and the lightning climatology are reduced to a set of 10 new predictors, each representing similar thermodynamic or dynamic processes. Logistic regression is used to produce reliable forecasts of one or more flashes out to three hours.

Comparisons with previous methods show that these forecasts represent a significant improvement in thunderstorm forecasting. Since they have been designed to cover any time period, these forecasts are the first forecasts that fill the gap between current extrapolative techniques and model forecasts covering the critical zero to six-hour time frame. They can be produced quickly from any model analyses or forecasts and are not tied to a specific model. These procedures are also used to successfully predict the probability of convection with higher flash rates and can be easily adapted to predict other lightning related quantities such as positive cloud to ground flashes. Lightning is shown to be especially favored when conditions support a vigorous updraft from the cloud base to at least the –20°C level in the environment. Large numbers of lightning flashes are supported by storms that have vigorous updrafts with higher, colder cloud tops.

CHAPTER 1

Introduction

1.1 Statement of the Problem

Each year, across the United States, lightning is responsible for deaths and injuries, forest fires, personal and business property losses, and airline delays. In addition, lightning can be associated with other forms of hazardous weather such as heavy rain and flooding, wind, hail, and tornadoes. Lightning can even be associated with dangerous winter storms that produce heavy accumulations of snow, sleet, and/or freezing rain.

As part of its mission, the Storm Prediction Center (SPC) works in partnership with National Weather Service (NWS) forecast offices to provide forecasts of thunderstorms, wind, hail, and tornadoes to the public and various federal and emergency management concerns. New techniques that produce better predictions of thunderstorms and lightning offer the chance to minimize human and property losses, as well as airline delays and societal disruptions. Through better forecasts, the finite resources (man and machine) available to fight wildfires sparked by lightning can be used more effectively. The purpose of this dissertation is to develop a system that can produce probabilistic forecasts for general thunderstorms and for thunderstorms with high rates of cloud-to-ground lightning.

1.1.1 Importance of Accurate Lightning Prediction

Lightning from thunderstorms is acknowledged as one of the most deadly forms of weather in every corner of the United States. The 30-year average (1966-1995) number of storm-related deaths per year reveals that lightning is second among all weather-related fatalities; on average, 87 deaths occur (flooding and flash flooding rank first with 139 fatalities; Holle et al. 1999). Nearly 500 people are injured each year by lightning. Most lightning deaths occur during the warm season when people are engaged in outside activities. In some cases, those fighting forest fires have been struck and killed by lightning.

The National Lightning Safety Institute (NLSI) estimated that lightning related losses approach $5 billion per year (Kithil 1999). This amount included losses due to forest fires, residential fires and damage to electrical components in the home, lightning strikes to petroleum storage tanks, mishaps/damage to aircraft and airline passenger delays, electric power outages, damage to sensitive electronic components, and activations of safety features at nuclear power plants.

On average, more than 13,000 lightning-caused forest fires occur each year; the majority are sparked by dry thunderstorms and burn an estimated 80 percent of the total acres burned in the United States (National Interagency Fire Center (NIFC) 2000). A "dry thunderstorm" (also referred to as "dry lightning") can be viewed as any thunderstorm that produces minimal rain at the surface, usually less than 2.54 mm. Canada has similar problems. Lightning starts approximately 34% of the nearly 10,000 fires recorded annually, but fires started by lightning account for 87% of the total area burned nationwide (Ramsey and Higgins 1986).

While lightning strikes cannot be prevented, accurate and continually updated thunderstorm forecasts could potentially have a large economic impact. Probabilistic thunderstorm forecasts would allow decisions to be based on pre-determined probability thresholds. Proactive measures could be taken to pre-position repair and fire fighting crews, give people time to seek appropriate shelter, reroute electric power through the nation's power grids, safeguard sensitive equipment, and move or reroute aircraft. While it is impossible to put an exact dollar value on the potential savings from improved lightning forecasts, the airline industry alone could recoup a substantial part of the estimated $2 billion dollar losses in annual operating costs and passenger delays. Better positioning of repair crews and equipment would help minimize losses from power outages caused by lightning. As part of the nearly $1 billion effort to fight wildfires each year, fire fighters in the West could have time to access the lightning fires in remote areas before they could grow and become costly and damaging. The goal would be to better position fire fighters and equipment. Curran et al. (1997) determined the annual vulnerability to lightning was a constant and widespread threat to human life. One way to reduce these nearly constant numbers is to move people from harm's way. The key is longer lead times (via better forecasts) of lightning strikes.

1.1.2 Thunderstorms in the Western United States

Thunderstorm forecasts issued by the SPC now address the prediction of dry thunderstorms in the western United States (Bothwell 2000). Many thunderstorms in the western United States, including dry thunderstorms, are less intense compared to

those that typically occur in the central and eastern United States. Non-severe thunderstorms, particularly in the West, have been studied less extensively than have their strong and violent counterparts in the central United States. The western thunderstorms are more difficult to forecast because of limited moisture, highly complex and variable terrain, and the shift of the primary upper-level storm track northward into Canada during the summer. Even the day-to-day variability in the Southwest Monsoon over Arizona and New Mexico is difficult to forecast. This dissertation aims to improve our knowledge and prediction of thunderstorms in the western United States, including dry thunderstorms.

Historically, the SPC thunderstorm outlooks are issued to highlight areas where a ten percent or greater chance of thunderstorms exists, and/or where a likelihood exists that severe storms may occur. Forecasters are accustomed to evaluating the threat of severe weather by monitoring areas of moist, unstable air that are co-located with strong upper-level systems which "trigger" convection. In the West however, especially in the case of dry thunderstorms, storms form where instability and upper-level forcing are weak. As noted previously, dry thunderstorms seldom produce severe weather, aside from brief strong winds. Many western storms do not produce large numbers of cloud-to-ground flashes. Even so, the flashes that do occur can spark forest fires when surface fuels are dry. Throughout this dissertation, the terms "lightning" and "thunderstorms", while not the same thing, will be used interchangeably because they refer to the same class of threat.

Dry thunderstorms are typically high-based storms (i.e., a high Lifted Condensation Level (LCL)) and are common over the western United States where the low

level moisture is limited. Dry thunderstorms also are more difficult to predict because the storms usually develop in association with elevated plumes of moisture advecting around the periphery of an upper-level high pressure system over the West. These plumes interact with complex heating and wind patterns associated with the mountains, and in certain locations, destabilize the environment to cause high-based thunderstorms.

1.1.3 Thunderstorm Probabilities and Thunderstorm Flash Rates

The probability that thunderstorms might occur is not the only critical item. The maximum (cloud-to-ground) flash rates, or total number of flashes in any given area, are also vital. The ability to distinguish between storms that may produce only a few flashes, versus those that produce hundreds of flashes, is important. Statistics from Global Atmospheric Inc. (GAI), the company that maintains lightning detection networks across the U.S. and Canada, indicate that total flashes across North America can exceed 500,000 flashes per day. In addition to increased safety risks posed to persons, areas with high lightning flash rates (or large numbers of flashes) have increased electrical system interruptions or failures and experience airline delays or cancellations at major hubs. Predicting when and where a high probability exists for a large number of flashes can provide valuable advance information to those at risk so to minimize human or economic losses. Meisner et al. (1994) determined the number of fire starts in southwestern Idaho was highly correlated with the total number of cloud-to-ground flashes and suggested "...there is some potential for predicting fire starts".

CHAPTER 2

Research Objectives

The primary objective of this dissertation is to develop a prediction system that will produce three-hour grid point probability forecasts of cloud-to-ground lightning for the western United States. Another objective is to produce a set of lightning climatological predictors that contain sufficient detail to represent diurnal lightning trends as well as intraseasonal trends such as the development of the Southwest Monsoon. The prediction system should be able to use either an analysis or forecast from any model. Since it is not normally known in advance which vertical levels contribute the most information, predictors from many vertical levels are included in the development of the prediction system, rather than just the surface and standard pressure levels (850, 700, 500 mb, etc.). Through statistical analysis, this study seeks to determine which predictors are important and if distinct physical processes can be ascertained from groups of these predictors.

Additionally, this research seeks to expand the value of these lightning probability forecasts by predicting areas where significant numbers of lightning flashes are expected. Probability forecasts for one or more flashes, 10 or more flashes, and 100 or more flashes are derived. The methodology developed in this dissertation is designed to be expanded to cover the entire United States. It is also capable of producing probabilities for specific types of lightning, such as the flashes that deliver positive charge to ground.

This lightning prediction system is designed to bridge the gap that currently exists between extrapolative techniques (for lightning that is already occurring) and

model forecasts which are usually presented in increments of six hours after the model analysis time. Finally, this work seeks to improve the understanding of what environmental characteristics support thunderstorms and storms with high flash rates and to show that the Rapid Update Cycle 2 (RUC 2) contains sufficient information to support a reliable operational thunderstorm prediction system.

2.1 Review of Previous Work

While sophisticated computer models predict many surface parameters such as surface wind (10 meter), surface temperature, and dew point (2 meter), other important quantities are not forecast directly. Fields such as amount of cloud cover, ceiling, visibility, probability and type of precipitation, thunderstorm probability, and severe thunderstorm probability are not explicitly predicted by most models. Two basic methods have been used to compute fields not specifically forecast by a model: the Model Output Statistics (MOS) and the Perfect Prog (prognosis) methods.

2.1.1 Perfect Prog vs. Model Output Statistics

The perfect prog method was first presented by Klein et al. (1959). A statistical relationship is developed between the variable to be estimated and selected variables which can be forecast by a model. The predictors and predictand are observed quantities in the developmental sample. This relationship is applied using the output fields from the forecast models as predictors to estimate the predictand, treating the model forecast as a perfect prognosis. As improvements to the model are made, fore-

casts of the predictors should improve with corresponding improvement of the perfect prog forecasts.

The other approach, called Model Output Statistics (MOS; Glahn and Lowry 1972), involves determining a statistical relationship between the predictand and the predictors from a numerical model at a predetermined projection time. MOS equations in the past have been able to out-perform a perfect prog approach because they take into account model biases and the decline in the model accuracy with increasing forecast projection. The most serious drawback to MOS is that it requires a stable numerical model. Given the rate with which changes and improvements are made to today's models, it is doubtful that any model will remain static long enough to develop new MOS equations. Alternatively, the use of the MOS approach requires the newer version of any model to be "rerun" on a minimum of one year (and usually two to three years) of model output data (Glahn et al. 1991).

Because today's complex computer forecast models change more frequently than those of the past, recent research in thunderstorm forecasting has not been transferred to the MOS statistical forecast system. Other MOS-based statistical forecasts have ended when the particular model they were based on was discontinued (e.g., the Limited area Fine Mesh (LFM) model). MOS equations derived from the older models such as the Nested Grid Model (NGM) have not been updated since the NGM code was "frozen" in 1991.

The perfect prog approach is used in this research because it can be applied to different computer models at any forecast (or analysis) time and can be applied even as the models change.

2.1.2 Previous Research on Thunderstorm Prediction

This section will discuss U.S. efforts to develop thunderstorm forecasting techniques. A summary of this work is also presented in Fig. 2.1. Reap (1974) developed an early MOS predictive scheme called PEATMOS (Primitive Equation And Trajectory Model Output Statistics) to produce gridded 24- hour thunderstorm forecast fields. It used predictors from the 24-hour forecast of the six-layer primitive equation model (Shuman and Hovermale 1968) and the three-dimensional trajectory model (Reap 1972). The predictand was tabulated from radar summary maps by noting radar tops of 7621 meters or higher (7621 meters or 25,000 feet was used to denote thunderstorms at that time). Each grid box was approximately 190 km on a side. Thus, the predictive scheme produced probability forecasts for an area of roughly 36,000 square kilometers.

Reap and Foster (1979) changed the forecast equations to use a three-year predictand sample of manually-digitized radar (MDR) data. The MDR grid blocks were approximately 80 km on a side. They showed that most thunderstorms were identified by the presence of a MDR code value of 4 or greater which indicated a convective rainfall rate of 1 to 2 inches per hour. An interactive predictor (KF) was formed by multiplying the large-scale K index by the daily thunderstorm relative frequencies obtained from the MDR data. Reap and Foster stated that this combination, stability and relative frequency, forced the climatology, as represented by the thunderstorm frequencies, to be more responsive to the presence (or absence) of instability. Without this term, they found unreasonably high probability values on occasions when the synoptic situation was not favorable for thunderstorm formation. They found the ten lead-

Operational Thunderstorm Prediction Systems

YEAR

72 73 74 75 76 77 78 79 80 81 82 83 84 85 86 87 88 89 90 91 92 93 94 95 96 97 98 99 2000 2001

A B C D E F G H I J K

[Cntrl & Ern U.S. A-F]	POD	FAR	CSI	BIAS	SS	Forecast Length	Grid Size
A Reap	Not available					24 hour	190 km
B Charba				1.17	21.9%	2-6 hour	80 km
C Reap	Not available					24 hour	80 km
D Reap and Foster	0.75	0.47	0.45			24 hour	80 km
E Reap							80 km
F Charba			0.31	1 to 1.5		2-6 hour	80 km
						Values are for dependent data	
G Reap	0.72	0.44	0.46	1.3		6 hour	48 km
H Bower					20%	6 hour	135 km
I Reap	0.72	0.55	0.40		9%	24 hour	48 km
						Values are for dependent data	
J -K Hughes					25%	24 hour	48 km

Fig. 2.1. Timeline showing time evolution and comparison (when data available) of different thunderstorm forecasting systems in the U.S. over the past 30 years. See Appendix G for complete definition of POD, FAR, CSI, BIAS, and SS and discussion of CSI and SS as a function of grid size and forecast length.

ing thunderstorm predictors (based on linear correlation) to be the interactive predictor (KF), the K index, the 24-hour relative frequency of thunderstorms, the Showalter index, the surface dew point, the Total Totals index, the convective instability, the 1000-400 mb mean relative humidity, boundary-layer moisture divergence, and boundary layer potential temperature. To allow the forecaster to prepare a categorical yes/no forecast of thunderstorms, the methods of Donaldson et al. (1975) to compute the Probability Of Detection (POD), False Alarm Ratio (FAR), and Critical Success Index (CSI) were used.

Charba (1977) reported on an operational system for predicting thunderstorms two to six hours in advance for areas east of the Rocky Mountains. These forecasts were issued three times daily for the spring and summer and covered the period 1700-0300 UTC, the period of diurnal maximum in thunderstorm frequency. His technique represented the first attempt at an operational short-term forecast system for the probability of thunderstorms. The probabilities were produced by multiple linear regression equations. The predictors were derived from objectively analyzed surface observations, MDR data, climatic frequencies of thunderstorms and numerical model output (only at mandatory levels, 850, 700, and 500 mb) from the LFM. The predictand was the occurrence or nonoccurrence of a thunderstorm (1 or 0 value, respectively) which was represented by a MDR code value of 4 or greater within an MDR box during the four-hour period (i.e., the 2-6 hour forecast period).

The system used development data from mid-March to mid-June from 1974 and 1975 and was tested on data from 1976. A phase correction was added to allow for predictor offsetting by one or more grid points. The optimal position for the offset

was defined as the grid point for which the predictor variable had the highest linear correlation with the predictand. This modification allowed the system to be more representative of the typical structure of severe weather systems (e.g., warm, moist air to the south and cool, dry air to the west of thunderstorms). In the example used by Charba, by offsetting the grid points, the grid point used to represent warm, moist air was placed one grid point to the south, and the grid point representative of cool, dry air was one grid point to the west of the actual predictand grid point.

Many of the individual predictors exhibited a markedly nonlinear relationship to the predictand. The stability indices in particular had a strong non-linear relationship to the predictand which meant the linear regression model did not adequately represent the true relationship. This obstacle was overcome by converting some of the predictors to binary variables or by transforming other variables such that the transformed variables were linearly related to the predictand. This transformation allowed the screening procedure to select new variables as predictors. Predictors selected by this method of multiple linear regression included stability terms such as the modified K index, modified Total Totals index, and modified Showalter index (where "modified" indicates that surface observations were combined with LFM upper-air forecasts in the computations). Selected predictors were the thunderstorm relative frequency, surface moisture divergence, terms involving mixing ratio at the surface or at 850 and 500 mb, surface or 850 mb Theta-E, 500 mb wind, and MDR data (one half-hour prior to the surface observations).

Charba (1984) added a set of cool season regression equations to his previous probability equations for the 2 to 6-hour prediction of thunderstorms during the spring

and summer. As a result, year-round coverage became possible for most of the United States east of the Rockies. Separate equations were used for the Great Plains, the Northeast, and the Gulf Coast. The input data consisted of (1) hourly objectively analyzed surface variables, (2) forecasts of the basic variables above the surface using the Limited area Fine Mesh (LFM-II) model (Newell and Deaven 1981), (3) MDR data, and (4) the climatic frequency of the predictand. He also added additional potential predictor variables, derived from pairs of variables (e.g., the modified Total Totals Index and 700 mb vertical velocity). As before, each predictor was developed on a grid with spacing of approximately 80 km.

The western United States presented a unique challenge in the derivation of thunderstorm probabilities. Until the addition of the WSR-88D Doppler radars across the West, radar coverage was poor. Thus the MOS approach using MDR values was of little use. Prior to 1986, the operational thunderstorm forecast equations were all derived by applying screening regression techniques to relate MDR data to large-scale predictors from the numerical forecast models.

Reap (1986b) used lightning data from the Bureau of Land Management (BLM), to develop experimental 6 hour forecast equations for thunderstorms and for several categories of lightning density (i.e., 2, 20, ... 100 flashes per grid block). His results for the 1985 season revealed that the predictability of high lightning densities is very low, although this may have been due, in part, to the model data not resolving small scale features. The results were successful in identifying general areas of lightning activity, but not successful in identifying localized regions of high-density strikes. He hypothesized that storms with high strike rates apparently respond to small-scale

features in the temperature, moisture, and wind fields that were not resolved by existing numerical models. Reap also found a high correlation between the terrain elevation and the time of maximum lightning frequency (three to five hours after local noon in the western mountains). He found a pronounced increase in the average number of lightning strikes with increasing terrain elevation. As a result, a strong influence on the timing and frequency of lightning activity appears in the western United States due to topographic features.

Lightning data was used in Alaska to determine lightning relative frequencies during the time period from 1987 to 1989 (1 May through 30 September) as reported by Reap (1991). Linear screening regression analysis and the MOS approach were used to statistically relate lightning data to Nested Grid Model (NGM) forecast fields. These equations were used as guidance by forecasters in estimating the potential hazard of wildfire initiation in Alaska. Not surprisingly, the large-scale static instability and local convergence in the wind and moisture fields were key parameters in lightning occurrences over Alaska. His study also showed that the mean number of flashes generally increased with increasing elevation.

Reap had theorized that local moisture convergence could have been responsible for the production of high flash accumulations. He showed that in Alaska, nearly 80% of the flashes occurred on only 20% of the sample days. When he applied screening regression to just the days with high flash accumulations (400 or more flashes), he found that low-level moisture convergence was important in the production of high lightning flash accumulations. The first two terms selected were the static stability term (500-850mb temperature lapse rate) and the 850 mb moisture convergence.

Bower (1993) developed NGM MOS thunderstorm forecasts for selected surface stations but was not able to include lightning data in the development. Reap (1994b) used 2 or more lightning flashes in deriving NGM based 24 hour grid point probability forecasts at 48 km resolution for the U.S.

The Interactive Computer Worded Forecast (ICWF) available to NWS forecasters has a thunderstorm probability derived from linear regression equation that uses only the Lifted Index from the Eta model. No other fields were considered in the development of the equation (Brill 1999).

Except for the recent work on AVN/MRF model-based MOS equations (Hughes 2001), which uses surface-based CAPE, no one has developed a model-based predictive system that relates thunderstorm occurrence to the most unstable CAPE and or any measure of the capping inversion (e.g., Cap strength (°C) or Convective INhibition (CIN; J kg^{-1})).

One recent effort at lightning prediction for the zero to three-hour time period is the System for Convection Analysis and Nowcasting (SCAN; Smith et al. 1998). This technique is an extrapolative-statistical method based on three years of lightning, radar and satellite developmental data. The algorithms use extrapolated forecasts of radar reflectivity, satellite-estimated cloud-top temperatures, and current lightning strike rates. These routines do not extend very far into the future because they rely so heavily on the extrapolation of current conditions. They also are not able to predict when and where new storms will develop. With the exception of the SCAN extrapolative forecasts, no short-term (0 to 6 hour) lightning forecasts are in operational use.

2.2 Differences from Previous Work

The work herein differs from previous attempts at thunderstorm/lightning prediction in a number of ways. Rather than using data that is tied just to the surface or an arbitrary level (e.g., 850 mb, or 700 mb, etc.), as in past studies, a large number of predictors will be computed from a multitude of model levels (every 25 mb in the vertical). For example, the level of the most unstable parcel below 500 mb will be included. Although the AVN/MRF MOS equations (Hughes 2001) have recently used the Surface Based Convective Available Potential Energy (SBCAPE), no other model-based predictive system has used the Most Unstable parcel Convective Available Potential Energy (MUCAPE) and Most Unstable parcel Convective INhibition (MUCIN) together as a fundamental component of its system for thunderstorm prediction. For example, the current thunderstorm probability forecasts available to NWS forecasters from the Eta model are based only on the Lifted Index from the Eta and do not take into account the capping inversion or any other parameters. When CAPE and CIN are used together, areas of positive CAPE can be eliminated simply because the capping inversion (as measured by the CIN) is too strong for convection to develop.

Another unique aspect of this work is that, rather than analyzing only the total MUCAPE, the total MUCAPE between 0 and -40 °C is sub-divided into layers that are 5 °C thick based on the environmental temperature (e.g., 0 to -5 °C, etc.). In addition, when there is positive CAPE, the lowest and highest layers are computed from the Level of Free Convection (LFC) to 0 °C and from -40 °C to the Equilibrium Level (EL), respectively. The CAPE in these layers is defined as Layer CAPE (LCAPE). These layers will be used to determine if there is any relationship between them and

the presence of lightning and the number of flashes. Also, the relationship of Normalized CAPE (NCAPE) (i.e., CAPE divided by the depth of the CAPE - with units of acceleration (m s^{-2})) to lightning and storms with high numbers of flashes will be examined. Finally, the Best CAPE (BCAPE) and CIN are computed from the parcel with the "Best" (larger) CAPE from either of (1) the mean mixing ratio and potential temperature in the lowest 50 mb or (2) a parcel above the lowest 50 mb and below 500 mb. The Best CAPE and CIN can give a better representation of the CAPE and CIN when there are unrealistically large surface moisture or super-adiabatic layers near the surface and can also capture the contribution of warm, moist air above a frontal surface or nocturnal inversion.

The presence of a strong capping inversion can suppress thunderstorm development, even when large amounts of CAPE are present. Yet, the capping inversion has largely been ignored in previous regression techniques. The strength of the capping inversion will be investigated by three diagnostic measures. These are the Convective INhibition (CIN - measured in J kg^{-1} or m^2 s^{-2}), the Normalized CIN (m s^{-2}) (CIN divided by the depth of the CIN), and the strength of the capping inversion measured in degrees C.

The predictive equations can be applied at the model analysis time, as well as forecast times. With the RUC 2, there is essentially no "spin-up" of the model, as the vertical velocities are "diagnosed" using the adiabatic method. In addition, to anticipate that vertical velocities might be unavailable in other model analyses, the kinematic vertical velocities were also computed. As shown in Fig. 2.2, both methods, adiabatic and kinematic, returned similar values of vertical motion. The methods in

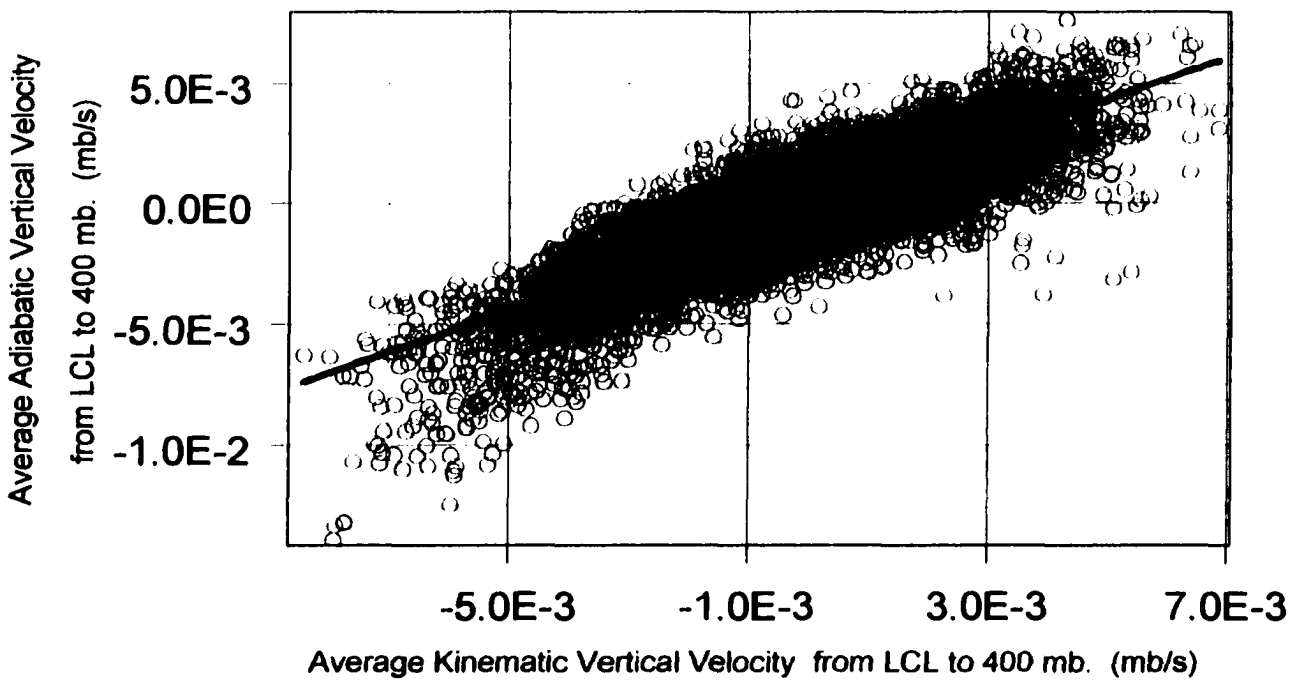

Fig. 2.2. Average kinematic vertical velocity computed from RUC 2 data compared to average vertical velocity computed adiabatically from RUC-2 (Averages are from LCL to 400 mb). Red solid line is least squares line fitting all points. Black dashed line represents a line where kinematic and adiabatic vertical velocities would be exactly equal within the range -0.005 to -0.005 mb/s.

this work can be applied to an hourly 3-dimensional RUC 2 analysis or any other similar objective analysis.

The present research is the first to use the hourly three-dimensional data sets generated by the RUC 2 analyses as the basis for generating thunderstorm probability forecasts. The RUC 2 has the advantage of rapidly incorporating all hourly surface data and any other off-time (i.e., non-radiosonde time) observations. Previous attempts to generate thunderstorm probabilities have had to rely on developmental data sets initialized only from the normal analysis times (00 and 12 UTC) and then the thunderstorm forecast became valid 6 to 12 hours after the analysis. Since the RUC 2 is able to capture important changes (especially at the surface) on an hourly basis, this can translate into hourly updated model forecast parameters which are important to the accurate prediction of thunderstorms.

When the RUC 2 model became operational in April 1998, it marked the first time that a three-dimensional analysis was available hourly. The RUC 2 also contained the parameters necessary to evaluate the conditions needed for convection (pressure, temperature, moisture and wind). In this dissertation, the physical processes that (1) initiate, (2) organize (3) sustain and/or terminate convection will be examined by computing a large number of relevant diagnostic fields from the RUC 2 data.

With the RUC 2 model output and high speed computers to process and store the data, it is now possible to calculate a wide spectrum of diagnostic quantities in addition to traditional model output at any desired level(s) in the atmosphere that might be physically related to thunderstorm genesis and maintenance. These diagnostic fields are then evaluated to gain a better understanding of the processes that are

related to thunderstorm growth and development. This study includes a larger number of diagnostic quantities and more vertical levels than previous attempts at thunderstorm prediction. Much like the learning experience used in Biology, the atmosphere will be "dissected" and studied "element by element", from the surface to the upper-levels, in order to gain a better understanding of the individual components related to thunderstorm initiation, organization and maintenance in the western United States.

One advantage in deriving probabilities for every three-hour period is that different processes may dominate during different time periods. By deriving separate equations for each three-hour time period, each of the equations are more likely to capture this difference (e.g., daytime versus nocturnal storms, or early afternoon development versus early evening decay of storms). While some predictors may be active through all eight of the three-hour periods, it is not reasonable to expect all terms to be acting in the same way throughout the course of any 24-hour period.

This research is also unique in that it will attempt to account for the influences of terrain features in the western United States, as well as the Southwest Monsoon by incorporating a set of time-dependent lightning climatological predictors developed especially for this study.

Despite the general increase in model resolution, important small-scale features in terrain, temperature, moisture and wind fields still occur below current model resolution. Reap (1986b) and Hughes (2001) increased the skill of MOS forecasts through the incorporation of lightning climatologies. However, these lightning climatologies have been monthly averages of 6, 12, and/or 24 hour time periods

Lightning climatological predictors used in this study are determined for the eight contiguous three-hour periods in a day and are updated every five days by using an average derived for each five day period (pentads; see Chapter 3). These predictors include the average (1) number of flashes, (2) relative frequency (or probability) of 1 or more flashes, (3) percentage of flashes over all grid boxes that occurred in each box, and (4) the percentage of the three-hour interval that lightning is observed (i.e., the number of 15 minute intervals with lightning divided by 12).

Daytime heating over the elevated terrain and local mountain/valley circulations may figure prominently in the initiation of these storms. Reap (1986a) found that storms initially formed over higher terrain elevation in the early to mid afternoon and that the topography exhibited a strong control on the timing, location, and number of flashes. In his MOS development of thunderstorm forecast equations for the West, Reap (1986b) used lightning frequencies to account partially for small-scale topographic effects and improve the temporal and spatial resolution of the MOS forecasts. Fosdick and Watson (1995) observed that summer convection over New Mexico usually forms first over higher elevations before moving off the mountain peaks late in the afternoon. Since the resolution of current model data is insufficient to incorporate small scale features and circulations, the lightning climatological predictors, developed for each three-hour time period of the day (00 to 03,...,21 to 00 UTC) at a resolution of 40 km, attempt to account for the diurnal variability of the sub-grid scale heating and forcing processes that cannot be resolved in the models. No current thunderstorm predictive system has a lightning climatology comprised of three-hour climatologies per five day (pentad) period.

The methods and procedures developed herein for the prediction of thunderstorms in the western United States can be applied to the prediction of all thunderstorms across the United States (including large, violent thunderstorms). Forecasters familiar with forecasting severe weather can many times be confident that "IF" storms develop, the storms may become severe. However, the most difficult part of the forecast often is to predict the probability of thunderstorms developing. That is where the efforts of this research are directed.

Although current technologies are beginning to map lightning sources in three-dimensions and examine relationships between in-cloud (IC) and cloud-to-ground (CG) flashes, this work will concentrate only on cloud-to-ground flashes since these are what are reported in real time across the West. Cloud-to-ground flashes are also of particular importance because they produce nearly all of the damage, deaths and injuries caused by lightning. However, it is anticipated that in the future, the techniques developed in this work could easily be applied to the prediction of total lightning (in-cloud and cloud-to-ground).

2.3 The Three Dimensional Model

Observational evidence from plots of lightning data indicate that lightning is often organized within certain areas and/or lines. In this investigation, grid boxes that had only an isolated single flash per three hours comprised less than 20 percent of the grid boxes that reported lightning for June, July and August in 1999. Thus, 80 percent of the boxes had more than one flash. Generally, the lightning plots show that even the

single flash events are in close proximity to other grid boxes that have two or more flashes. It is rare to have isolated single strike events scattered randomly. Thus, it seems likely that some degree of organization must result from multiple processes in the atmosphere acting simultaneously to trigger thunderstorms. The goal is to develop a physically-based conceptual model that can account for the most significant processes in thunderstorm development. The model should account for as many physical processes as possible. A conceptual model is proposed that is able to incorporate different mechanisms associated with the development of thunderstorms.

The model begins with what are generally accepted as the ingredients necessary to produce thunderstorms: (1) moisture, (2) instability, (3) a source of lift (Doswell 1987). While McNulty (1983) also includes divergence aloft, that is not to say that strong divergence aloft is needed beforehand; rather, it would be more physically correct to say that the absence of strong convergence aloft, leading to strong downward motion that would retard convection, is desired. Often, only weak divergence is noted prior to convection, and the convection itself may strengthen the divergence. Since it is likely that the "lift" needed for convection arises through different processes (heating, upslope flow, convergence, etc.) and at different levels, this conceptual model must be able to take into account different modes of convective initiation. The model should also be able to account for unstable air parcels originating at different levels.

It is assumed that there is a source of unstable air, or CAPE, that is capable of supporting an updraft with mixed-phase precipitation, (graupel, ice, and super-cooled water). Given that there is a source of unstable air, whether at the surface or aloft,

some process or processes must act on air parcels originating in the potentially unstable air, in a way that causes the parcels to reach the Level of Free Convection (LFC). This requires either intensive surface heating or some form of lifting. As air parcels rise and mix with the environment, there must be sufficient moisture such that they do not ingest dry air and become negatively buoyant. Also, the atmosphere must not be experiencing strong, large scale downward motion that would restrict upward moving parcels.

A wide variety of computed fields, including (but not limited to) the wind convergence, moisture flux convergence, and vertical motion, are calculated from the most unstable parcel level (MUPL) to the Lifted Condensation Level (LCL) and from the MUPL to the Level of Free Convection (LFC) when present (or at the LCL level if NO LFC is present). Throughout the troposphere, the temperature lapse rates are evaluated, as is the vertical motion. Wind shear and storm relative flow are evaluated at different levels to determine which, if any, of the wind values can contribute to charge generation. Finally, in the upper-levels, fields are evaluated to see which would aid in strong thunderstorm development. Simply put, a thunderstorm would be most likely to form where there is (1) unstable air that is not strongly capped, (2) a lifting mechanism sufficient to allow the air parcel to reach its Level of Free Convection, and (3) sufficient moisture present in the environment to minimize the effect of mixing.

Since there are more than 200 candidate predictors, the predictors have been grouped for convenience according to physical process and the vertical level they best represent (see Fig. 2.3).

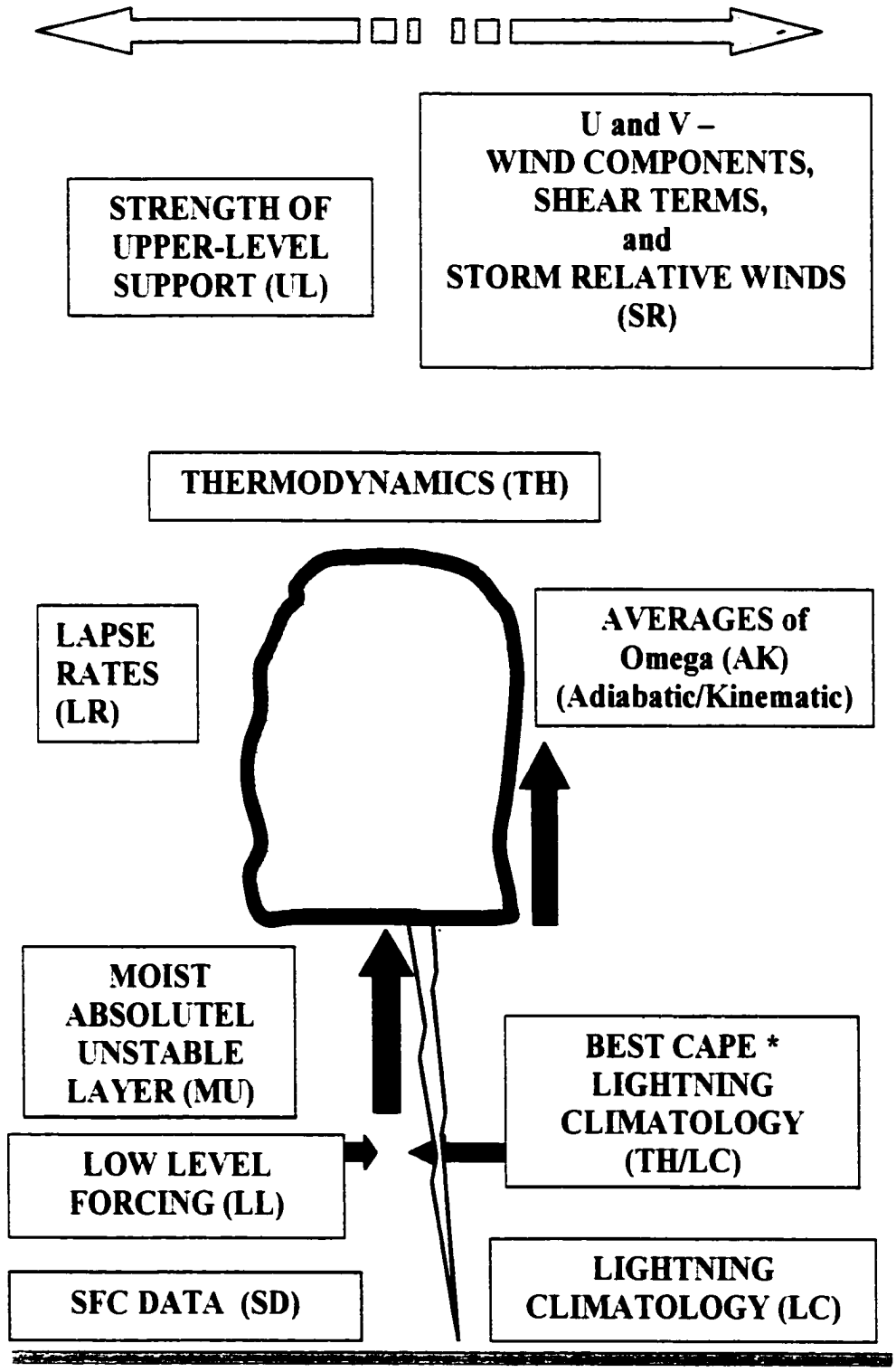

Fig. 2.3. Schematic showing approximate vertical levels for groups of similar variables.

These groupings are:

1) Upper-level support
2) U and V wind components, shear terms and storm relative winds
3) Thermodynamics
4) Averages of vertical motion (adiabatic/kinematic)
5) Best CAPE * Lightning climatological predictors
6) Lightning climatology
7) Surface data
8) Lower-level forcing
9) Moist Absolutely Unstable Layer (MAUL), Byran and Fritch (2000)
10) Lapse rates

The following hypothesis will be tested as part of the conceptual three-dimensional thunderstorm model:

If, as is generally accepted, thunderstorms form where there are sources of (1) moisture, (2) instability, and (3) lifting mechanisms, the RUC 2 model data contains sufficient information to evaluate these conditions and predict thunderstorm formation over the next three hours. Additionally, if the model analyses show skill for any thunderstorm (one or more flashes) in the short term (forecasts from zero to three hours using the perfect prog equations) they will also exhibit skill for the prediction of thunderstorms with high flash rates.

CHAPTER 3

Data Requirements

3.1 Lightning Data

Since the prediction of lightning is a goal of this work, it is important to understand how detection of cloud-to-ground flashes by the National Lightning Detection Network (NLDN) occurs and how the network has changed and improved since it began in 1989. Global Atmospherics Inc. (GAI) has operated the NLDN (Fig. 3.1) the past 12 years. During the years from 1989-1993, the NLDN operated throughout the United States with gated, wideband magnetic direction finders (MDFs) (Wacker and Orville, 1999). Time-of-arrival (TOA) instruments were added in 1992. Beginning in 1994, the NLDN underwent a system-wide network upgrade using both MDFs and TOA sensors plus enhanced signal processing algorithms to improve location accuracy and detection efficiency (see Appendix A for the details of lightning detection by NLDN).

The primary objective of the nationwide upgrade was to (1) improve location accuracy (2) improve data processing infrastructure in order to deliver stroke and flash data in real time and (3) improve detection efficiency of weak flashes (as low as 5 kiloAmps (kA)). The upgrade resulted in the improvement of flash location accuracy from 2.5 miles to 0.3 miles (0.5 km) (Cummins et al., 1998). After the upgrade, the detection efficiency, which had been as low as 40% in a few locations, improved to 80-90% (Fig. 3.2). Huffines and Orville (1999), have shown that since the upgrade, the nation-wide detection efficiency is high enough (greater than 80% in most areas) to reliably detect single flashes.

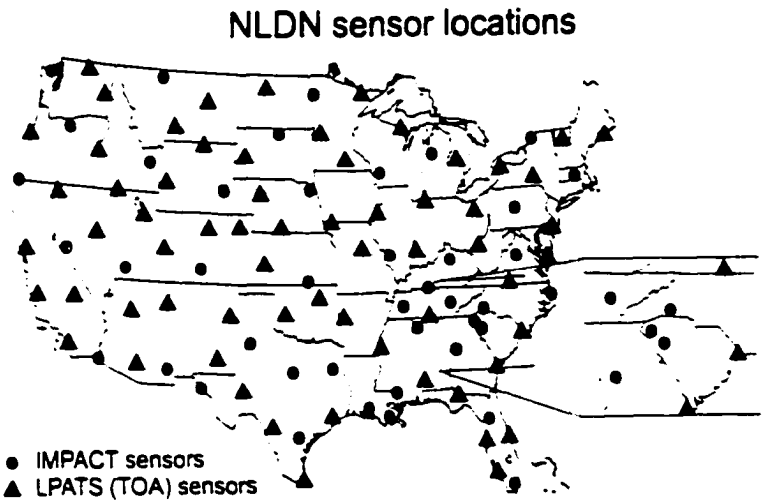

Fig. 3.1. Location of stations in the National Lightning Detection Network (NLDN). From Orville and Huffines (1999).

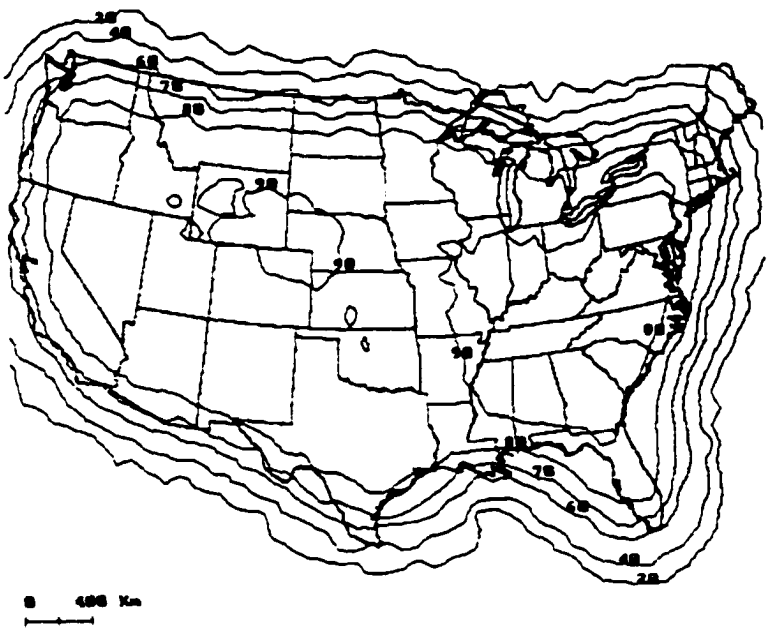

Fig. 3.2. Detection efficiency after the 1994 upgrade to the NLDN. From Cummins et al. (1998).

Since the upgrade of the NLDN was completed by the end of 1994, only data from 1995 through 1998 are used to derive the lightning climatologies. Data from 1999 are not used since the lightning predictand data are from 1999.

The predictand lightning data from 1999 for each three-hour period are developed for the entire U.S. on the same 40 by 40 km grid as the predictors from the lightning climatologies using the years 1995 to 1998. This is the same grid on which the RUC 2 predictors were calculated. In 1999, for the 00 to 03 UTC time period in this study, the lightning flash densities (1, 3, 10, 30 and 100 or more flashes per three hours) in the western states are shown in Fig. 3.3 to vary according to a logarithmic distribution. In Fig. 3.3 the percent of grid boxes with lightning (development and testing data sets) are plotted against the log of the flash densities (number of flashes per three hours per grid box). While approximately ten percent of the grid boxes had one flash or more observed, less than one percent had 100 or more flashes. Figure 3.3 illustrates how rare the events with one hundred or more flashes are in the western United States for the time period 00 to 03 UTC.

A similar type of logarithmic distribution was reported by López and Holle (1986). They observed a distinct "skewness" in the flash density distribution for both Colorado and Florida (the two areas of their study). Although the time periods for their flash densities were different than in this investigation (five-minute peak flash densities versus three-hour flash densities in this study), the size of the grids were similar (1000 km^2 versus 1600 km^2 in this study). Their results indicated the flash density could be represented as a logarithmic distribution.

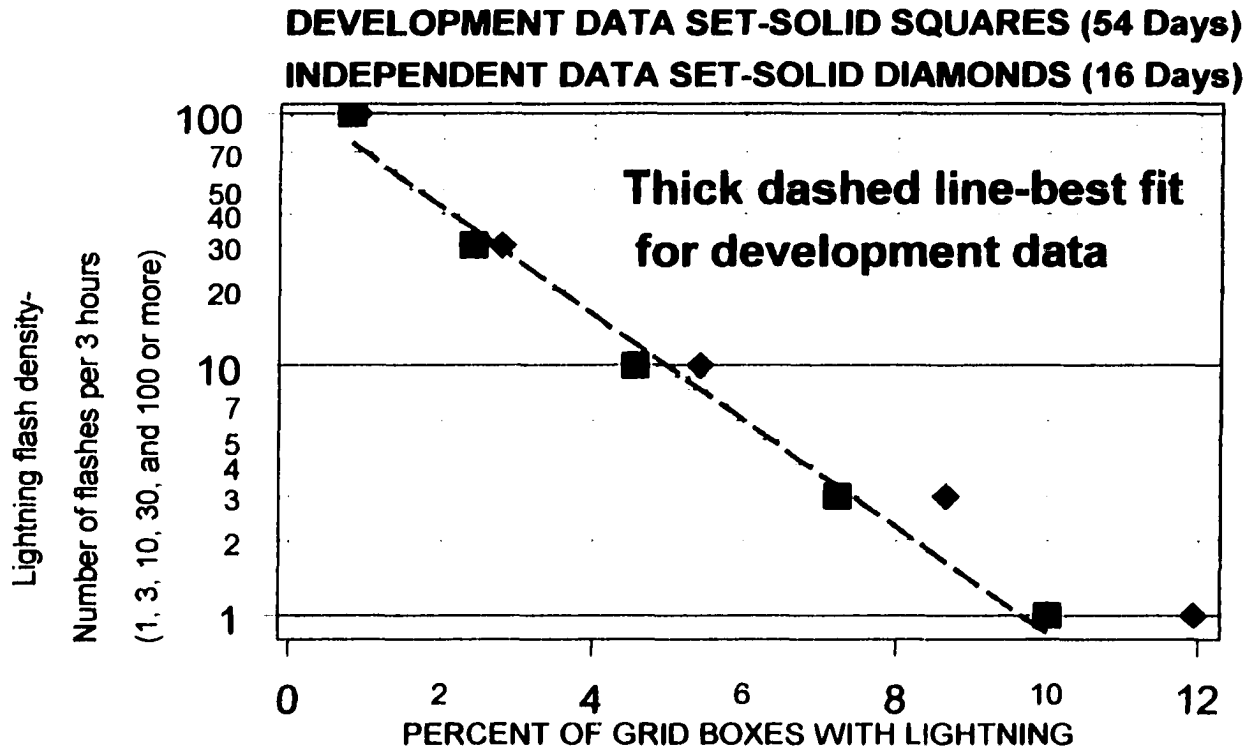

Fig. 3.3. The percent of grid boxes reporting 1 (or more), 3, 10, 30, or 100 (or more) flashes per 3 hours for both development and independent data sets.

3.1.1 Developing Lightning Climatologies

The problem with deriving lightning climatologies, given a short 4 year record of lighting data, was how to provide a stable measure on a day-by-day basis of such a variable phenomena.

Reap (1986a) was the first to use archived lightning data from a lightning network to develop lightning climatologies that could be used as candidate predictors in thunderstorm regression equations. Initially, seasonal climatologies were developed and covered hourly intervals. Climatologies were later developed for 6-hour intervals (Reap, 1986b). Monthly climatologies have also been developed that cover 6, 12 and 24 hour forecast valid times (Hughes, 2001).

In this study, lightning climatologies are developed on the same 40 by 40 km grid as the RUC 2 model data for every three-hour time period of the day for each of the 73 contiguous five-day periods (pentads) of the year (e.g., Jan. 1-5, 6-10, 11-15, etc.). Pentad climatologies were chosen rather than monthly climatologies (Hughes, 2001) to better describe subseasonal climatic variations as recommended by Wang and Xu (1997) and better represent the lightning flash population which is unknown. The methodology for deriving the lightning climatologies is shown in Appendix B. For each grid box, the lightning climatologies that are developed include the average (1) number of flashes, (2) relative frequency (or probability) of 1 or more flashes, (3) percentage of flashes over all grid boxes that occurred in each box, and (4) the percentage of the three-hour interval that lightning is observed (i.e., the number of 15 minute intervals with lightning divided by 12).

Initially, using the four years of archived lightning data, 365 pentad climatologies were developed for each day of the year. February 29th (leap year) was included in the same pentad as February 28th. These original daily pentads had 4 years of data, resulting in 20 total 3-hour periods. However, these initial 365 daily pentads exhibited significant day-to-day variability.

The following procedure (described more completely in Appendix B) is used to produce 73 contiguous lightning climatologies with less variability. For each contiguous pentad of the year, as shown in Appendix B, nine daily pentad climatologies that include at least one day of the contiguous pentad were averaged together. Since the months of June through August are used in this study, one example is the pentad centered on 7 June (defined to be time t=0). All nine of the original daily pentads involved in the June 5-9 pentads are averaged together. This average is then assigned to each of the days in the 7 June pentad (i.e., June 5-9). For each of the lightning climatological predictors listed earlier in this section, the 73 pentad averages for the year are calculated according to the formula derived in Appendix B as follows:

$$L_t = (0.2 * Lavg_{t-6} + 0.4 * Lavg_{t-5} + 0.6 * Lavg_{t-4} + 0.8 * Lavgrf_{t-3} + 1.0 * Lavgrf_{t-2} + 1.0 * Lavgrf_{t-1} + 1.0 * Lavg_t + 1.0 * Lavg_{t+1} + 1.0 * Lavg_{t+2} + 0.8 * Lavg_{t+3} + 0.6 * Lavg_{t+4} + 0.4 * Lavg_{t+5} + 0.2 * Lavg_{t+6}) / 9$$

where each of the terms on the right hand side are defined in Appendix B.

Thus, 13 days (days t-6 to t+6) contribute to the contiguous pentad average. In a similar development of severe weather climatologies (wind, hail and tornado) with data spanning 50 years (more than ten times longer than the development sample for the lightning climatologies), Brooks (1999) has found that stable results were achieved

when using a Gaussian weight over a 15 day period, since severe reports, even over 50 years, exhibit wide temporal and spatial variability.

The climatologies are developed for the 19 contiguous pentads of June, July, and August, and the resulting values are then assumed to apply equally to each of the days within the pentad. This approach captures the growth and expansion of the southwest monsoonal thunderstorms and produces general agreement with earlier studies across the northern Rockies (Fuquay, 1962). Figures 3.4, 3.5 and 3.6 are examples of the relative frequency (or probability) of 1 or more flashes from 00 to 03 UTC for the pentads centered on 2 June, 2 July, and 1 August. The data have been spatially smoothed for display purposes.

As can be seen in Fig. 3.5, one of the highest areas for the lightning relative frequency appears in northwestern Mexico where there are no lightning sensors. In this area, the NLDN theoretical detection efficiency drops to 20 percent or below. The NLDN data is normally terminated at approximately 600 km from the U.S. coasts and borders. The operators of the NLDN, GAI, are aware of this apparent high number of flashes in an area where the detection efficiency if low. According to Holle (personal communication, 2001), the area is likely experiencing an extraordinary large number of flashes, although no scientific study has yet been attempted to verify the number of lightning strikes in northwestern Mexico

Preceding the NLDN upgrade, Douglas et al. (1993), studied this area by examining rainfall reports, satellite imagery and rawinsonde data. They found that this area received 60 to 70 percent of the yearly rainfall over the three-month period from July to September, during the "Mexican monsoon". Using monthly mean fre-

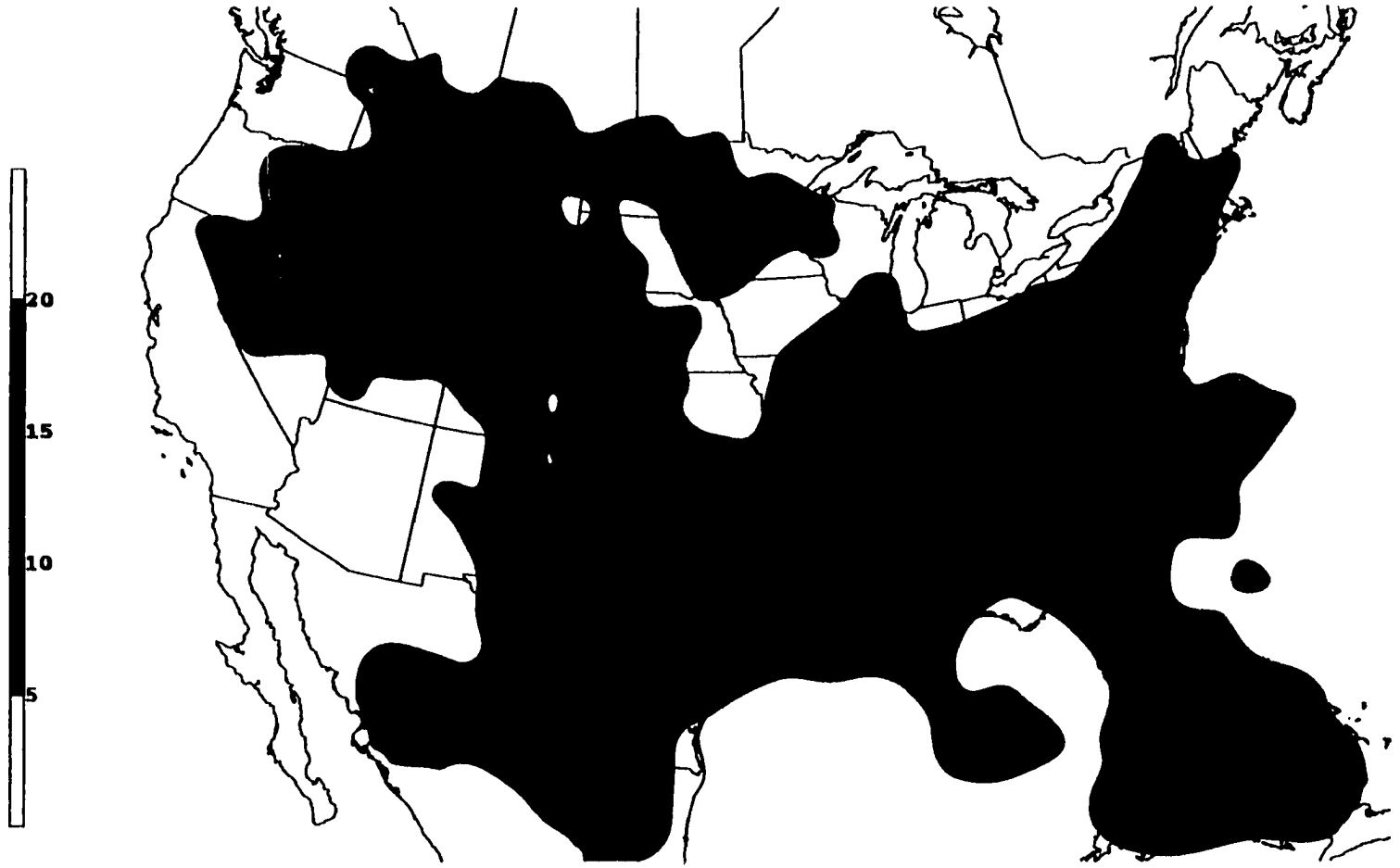

Fig. 3.4. Lightning relative frequency (00 to 03 UTC) for the pentad centered on 2 June.



Fig. 3.5. Lightning relative frequency (00 to 03 UTC) for the pentad centered on 2 July.



Fig. 3.6. Lightning relative frequency (00 to 03 UTC) for the pentad centered on 1 August.

quencies of the Geostationary Operational Environmental Satellite (GOES) infrared temperatures colder than -38 °C as a surrogate indicator for deep convection, they also found good agreement between the cold cloud tops and the precipitation maximum during July, the first full month of the monsoon. Thus, it is likely that the area does experience a large number of flashes.

3.2 The Rapid Update Cycle 2 (RUC 2) Model

The current version of the Mesoscale Analysis and Prediction System (MAPS) model, developed at the Forecast Systems Laboratory (FSL), runs operationally every hour as the Rapid Update Cycle 2 (RUC 2) at the National Centers for Environmental Prediction (NCEP) (Benjamin et al., 1998). It replaced the previous version of the RUC in 1998. This model offers many advantages for a center such as the SPC, not only in severe weather forecasting, but forecasting of all hazardous weather. Accurate short-term forecasts that are updated hourly are clearly indispensable for the NWS mission of protection of life and property. The RUC 2 runs at the highest frequency of any forecast model at NCEP, assimilating recent observations aloft and at the surface to provide high frequency updates of current conditions and short-range forecasts. The RUC 2 forecasts begin about 20 minutes after the hour except for 55 minutes after 00 and 12 UTC. The RUC 2 model produces hourly forecasts out to 3 hours every hour, plus forecasts out to 12 hours every 3 hours (00, 03, 06, 09, 12, 15, 18 and 21 UTC).

The horizontal grid resolution of the RUC 2 is approximately 40 km (Fig. 3.7), with 40 levels in the vertical. The increased vertical resolution, combined with the

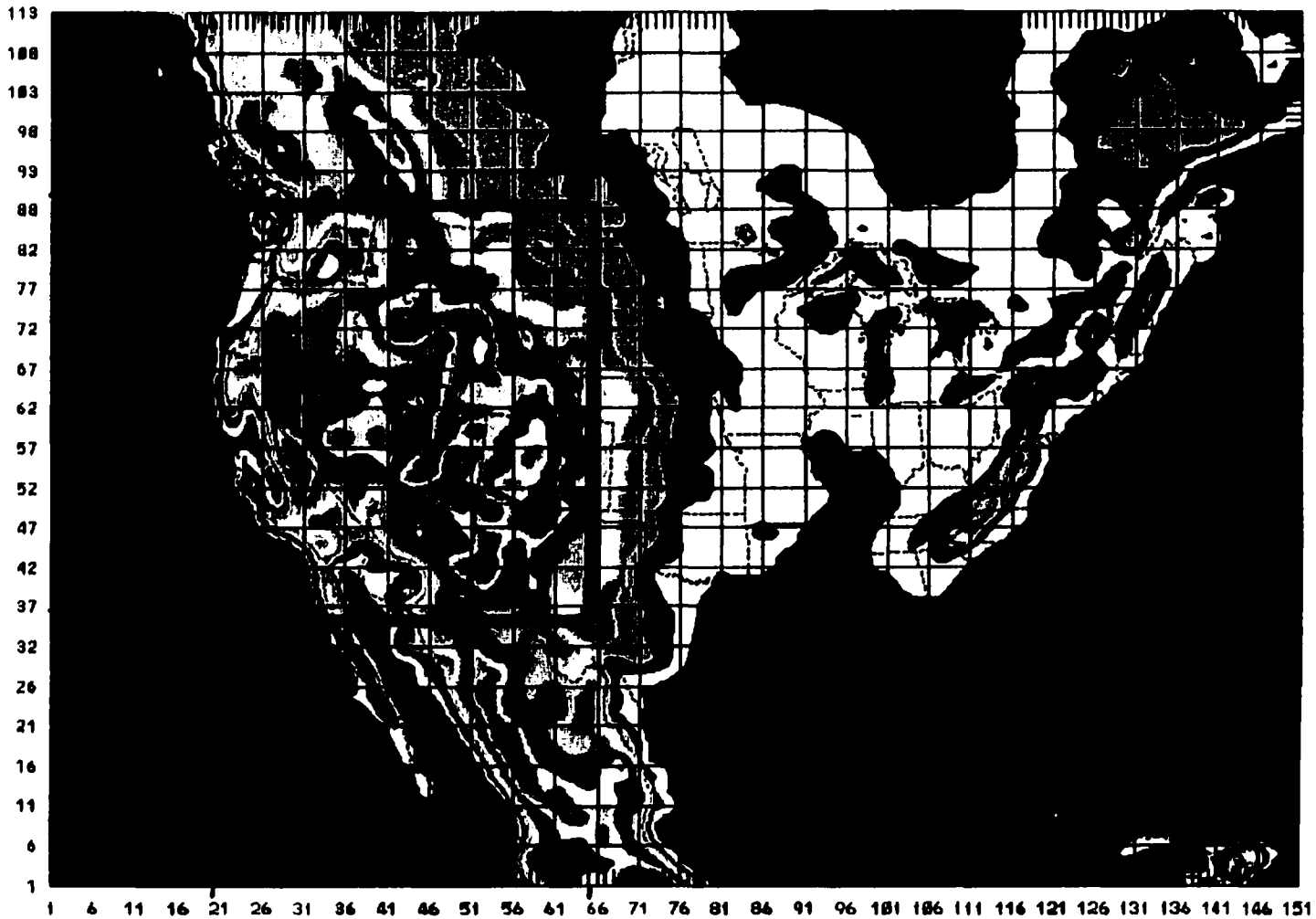

Fig. 3.7. Horizontal domain of the RUC 2. Each large square is comprised of 25 smaller squares (each 40 km on a side). Domain used in this dissertation (2530 grid points) is enclosed by thick black line.

hybrid isentropic-sigma coordinate system which maintains an isentropic coordinate representation down to within 2-3 km above the ground, provides for sharper resolution near fronts and the tropopause. Since the model levels follow the terrain in the lowest levels, the RUC 2 has excellent resolution of the boundary layer with approximately 7 levels in the lowest 400 meters even over higher terrain. Since each vertical level has a virtual potential temperature associated with it, the actual number of sigma levels above the ground varies depending on the topography and how warm or cold the lower levels are.

The surface elevation of the RUC 2 is defined by a "slope envelope" topography instead of the full envelope topography. According to Benjamin et al. (1998) the envelope topography is defined by adding the sub-grid-scale terrain standard deviation (calculated from a 10-km terrain field) to the mean value over the box. For the slope envelope topography, the terrain standard deviation is calculated with respect to a plane fit to the high-resolution-topography within each grid box and added to the mean value of the box. This gives more accurate terrain values at locations such as Denver and Salt Lake City (e.g., locations which are situated close to large mountain ranges).

In the optimal interpolation multivariate analysis for the RUC 2 (Benjamin et al., 1998), an isotropic weighting scheme is used on the hybrid isentropic-sigma surfaces except for the wind analysis which is anisotropic and oriented along the direction of the flow. Critical to the evolving moisture patterns, the RUC 2 better captures moisture transport because most moisture advection takes place on isentropic surfaces rather than on the quasi-horizontal surfaces used in other models. Since the adiabatic

component of the total vertical motion in the model is represented by the flow along the sloping isentropic surfaces, the adiabatic vertical motion fields can be diagnosed from the horizontal winds.

The RUC 2 is able to incorporate nearly all available observations including traditional radiosondes and aircraft dropwindsondes, wind profilers, and commercial aircraft temperature and wind data. The latter data are provided by the Aircraft Communications Addressing and Reporting System (ACARS) from en route aircraft as a function of pressure; numerous high resolution ascent and descent reports at major airport hubs are also available. Satellite derived fields of integrated precipitable water and cloud drift winds, and Doppler Velocity Azimuth Display (VAD) winds are also used by the RUC 2. The RUC 2 modified optimal interpolation multivariate analysis also provides for a closer fit to observations and better use of aircraft ascent/descent winds and temperatures.

In the RUC 2, the hourly surface analyses are produced directly out of the hourly three-dimensional cycle rather than a stand-alone system as in the previous version of the RUC (Benjamin, 1999). Since surface stations report every hour, and radiosonde times are only at 00 and 12 UTC, the lowest levels of the model just above the surface are adjusted to be dynamically consistent with the surface analysis. Over 95% of the surface temperature and dew point observations in the West are used in the 3-dimensional analysis. Station pressure (altimeter) and surface wind observations are used, regardless of the difference between the station and model elevation. The new RUC 2 surface analysis is designed to draw more closely to the data and have better consistency and reliability than the analysis from the previous version of the RUC. In

addition, the use of a 1-hour forecast background allows for improved quality control of the hourly surface, profiler, and VAD observations. As a result, many of the frequent bullseyes in the previous, 60 km version of the RUC surface analysis have been eliminated. Aircraft data is now closer to the analysis time since the time window for aircraft data is now –1h to 0h, instead of the –2 to +1h used with the RUC 1.

The six prognostic variables analyzed by the RUC 2 on the model coordinate surfaces are pressure, height, virtual potential temperature, water vapor mixing ratio, and the horizontal grid relative wind components (u and v). Although the output moisture variable predicted by the RUC 2 is water vapor mixing ratio, the RUC-2 integration is carried out using the condensation pressure, since this variable varies with fewer orders of magnitude (e.g., 100 to 1000 mb) over the depth of the troposphere than water vapor mixing ratio (e.g., 0.1 g kg^{-1} to 20 g kg^{-1}). Five hydrometeor species: cloud water, rain water, snow, ice, and graupel are predicted in the model, using the explicit microphysics scheme from the NCAR/Penn State mesoscale model MM5. Cloud variables are "cycled", meaning there are initial cloud fields available for each run. The RUC 2 has a 6-layer soil/vegetation/snow model, in order to better model the surface conditions. The model accumulates liquid and solid precipitation at the ground, allowing snow accumulation, melting, liquid infiltration into the soil, or surface runoff. The model also allows for evapotranspiration in the soil/vegetation scheme. The convective parameterization scheme is a version of the Grell (1993) convective parameterization. According to Benjamin et al. (1998), modifications to the downdraft detrainment resulted in smaller-scale details in RUC-2 warm season precip-

itation patterns than are evident from the 80 km Eta model (which uses Betts-Miller-Janjic convective parameterization).

These significant improvements make the RUC 2 potentially superior for short term forecasting. Normally, since the data cut-off time is about 20 minutes after analysis time, the model forecast is available between 35 and 40 minutes past the hour (aside from the 12 and 00 UTC runs, which are delayed until 55 minutes past the hour to allow for complete receipt of radiosonde data). Thus, forecasts are rapidly transmitted to the forecasters, with most forecasts available to NWS meteorologists by the beginning of the subsequent hour. This frequency of forecast data is unparalleled in National Weather Service (NWS) operations.

Comparisons of radiosonde and RUC 2 soundings (Benjamin et al., 1999; Thompson and Edwards, 2000) have shown that the RUC 2 can capture important details of the sounding. In addition, a subjective comparison of radiosonde observations overlayed with RUC 2 soundings from the analysis at the raob locations (through bi-linear interpolation of isobaric grids at 25 mb intervals), the RUC 2 analyses appear to accurately reproduce the temperature and moisture profiles, as well as the wind profiles. Thus, it is believed that fields such as CAPE and CIN are accurately represented where observations are available.

3.3 Development of Predictor/Predictand Data Sets

The initial step was to derive a set of predictors from the 1999 RUC 2 analyses. The time period for which RUC 2 data and lightning data were both available covered approximately 70 days from 1 June to 31 August, 1999. The initial three-hour forecast

time interval selected was 00 to 03 UTC since the RUC 2 predictors would be derived from the analyses at 00 UTC which included all upper-air data. Also, the 00 to 03 UTC time period normally falls just slightly after the convective maximum in the West (22 to 00 UTC; Reap 1986a).

During the time period in which initial data were collected, it was discovered that the archived RUC 2 data were the "early" RUC 2 analyses for 00 and 12 UTC. The early analysis, which used only about 25% of the upper-air data because of an early data cut-off, had been archived rather than the final RUC 2 analysis at 00 and 12 UTC. Since the one hour forecasts from the "final" 00 UTC analyses were already incorporated as part of the 01 UTC analyses and most one hour differences in RUC 2 analyses are small, the 01 UTC analyses were used in place of 00 UTC. Predictive equations were derived for the 00 to 03 UTC time period, although the technique developed herein can be applied to each of the remaining three-hour RUC 2 runs (03, 06, 09, 12, 15, 18 and 21 UTC). This technique can also be applied to forecasts valid at 00 UTC.

The candidate predictors (see Appendix C for a complete listing) were designed and selected to represent the majority of the major components of a physically based and dynamically consistent conceptual model (section 2.3 of Chapter 2). Many of the previous attempts at developing predictive equations for thunderstorms have used data from a limited set of model levels (e.g., surface, 850, 700 mb, etc.). This study uses data from the surface and every 25 mb above the surface up to 100 mb to compute the candidate predictors. For example, all levels are evaluated to find the most unstable parcel and the level it occurs at, rather that assuming (*a priori*) that lev-

els such as the surface or one of the standard pressure levels such as 850 or 700 mb, represent the most unstable air.

The RUC 2 gridded data is transformed into the format of a vertical sounding, with temperature, dew point, and wind from the surface through 100 mb at every grid point. Additionally, this study is unique in that it first calculates fields such as convergence, vorticity, frontogenesis, etc. at the surface and on each of the isobaric surfaces and then merges that with the other vertical sounding data at each grid point. Thus there are vertical profiles of these fields at each grid point, in addition to temperature, wind and humidity (see Appendix C for full details). When it was not possible to calculate certain fields, such as CIN where there was no CAPE, default values were assigned to the fields.

Since the RUC 2 model runs every hour, it is able to capture rapidly changing mesoscale situations, such as outflow boundaries, frontal movements, rapid destabilization, etc. Even if the model does not capture a significant feature the first hour, it is more likely to catch it the next hour. In this manner, the RUC 2 can respond to rapidly changing weather, "correcting" itself in the newer runs, and thus provide better predictors.

CHAPTER 4

Data Analysis and Statistical Techniques

4.1 Initial Investigation

Beginning in 1998, data displays covering the contiguous United States were developed to plot hourly lightning data in relation to two 500 mb Lifted Indices (LIs). These indices were derived by subtracting the hourly objectively analyzed surface parcel temperature lifted to 500 mb from the hourly forecast 500 mb model temperature for both the Eta model and RUC 2. These showed good results when the convection was surface-based. Not surprisingly, the surface based LIs did not pick up convective areas when the instability was not surface-based (elevated convection).

Next, lightning data were plotted with the Convective Available Potential Energy (CAPE), using the analysis from both the Eta and RUC 2. CAPE is more robust in that it can capture small amounts of instability anywhere in the sounding, even if the 500 mb LI is zero or slightly positive. The Eta calculations search the lowest 180 mb for the parcel with the highest instability. The LI for this parcel is called the "best LI" and the CAPE is the "best CAPE". Lightning often occurred within the area where the best CAPE was positive. The best CAPE (BCAPE) in the RUC 2 is the larger CAPE from either (1) the value computed from the average of potential temperature and mixing ratio in the lowest 7 sigma layers (within about 40 mb of the surface) or (2) a single layer above the first 7 sigma layers (within 300 mb of the surface).

The third step in the research was to add an analysis of the capping inversion, the Convective INhibition (CIN), to the best CAPE and lightning plots. Lightning plots were then compared to Eta and RUC 2 CAPE/CIN analyses. It was found that

across the central United States, where the CIN often appeared to be the strongest (most negative), areas with high CAPE did not experience convection if the capping inversion was strong (large negative CIN values were usually more negative than -100 J kg^{-1}). The CIN could be used to eliminate the probability of storms from any area that has a strong capping inversion. It has not been used as a candidate predictor in previous predictive equations for lightning or in any screening regression applied to thunderstorm predictions. A subjective evaluation of the RUC 2 CIN over the West indicated that the CIN was often not as strong as it was in the central and eastern U.S.

The final investigation using the RUC 2 and Eta for 1998 involved testing a simple linear equation developed by the Techniques Development Laboratory (Brill 1999) for thunderstorm prediction. This equation is currently used in the NWS Interactive Computer Worded Forecast (ICWF) and relates the Lifted Index (LI) to a thunderstorm probability. Aside from the obvious problem of using only one term, another serious deficiency is that the equation does not take into account the capping inversion. When the plots with CIN were graphically overlaid with the computed thunderstorm probabilities and lightning, it was clear that, by using either the RUC 2 or the Eta, areas with high thunderstorm probabilities could be eliminated, if they had large negative CIN values.

4.2 Data Set for This Study

The RUC 2 and lightning data available for the development and testing of the predictive equations were from June, July, and August of 1999. As mentioned in the previous chapter, a lightning climatology was developed separately, using the years

1995 to 1998. See Appendix C for a complete list of the predictor data set. The remaining sections of this chapter will describe the methods used to obtain the predictive equations using these quantities for the time period 00 to 03 UTC.

Although lightning in the West can be very active into early September, the lightning climatologies developed herein confirm that the months of June, July and August normally represent the most active months for thunderstorms. Also, as shown in Fig. 4.1, the climatologies confirm that the time period from 00 to 03 UTC is just after the convective maximum Reap (1986a) reported in the West (22 to 00 UTC). Finally, in interpreting the forecast probabilities, it is realized that lightning over a three-hour period in a grid box that is 40 by 40 km is likely to represent multiple thunderstorms. The forecast probabilities do not attempt to represent individual thunderstorms; rather, they may represent a group of storms within each grid box.

During the three months of June, July and August 1999, a total of 70 days had both RUC 2 and lightning data. Out of the 70 days, 54 days were used to develop the regression equations. Sixteen days were picked at random from contiguous pentads and withheld as independent data in order to test the equations. Since data from only one summer were available, the equations developed should be redeveloped when more data become available to improve the stability of the equations. Even with data from just one summer, Chapter 5 will show that results are encouraging.

Except when only one day was available in a pentad, one day per pentad was selected at random for the independent data set used to test the predictive equations.

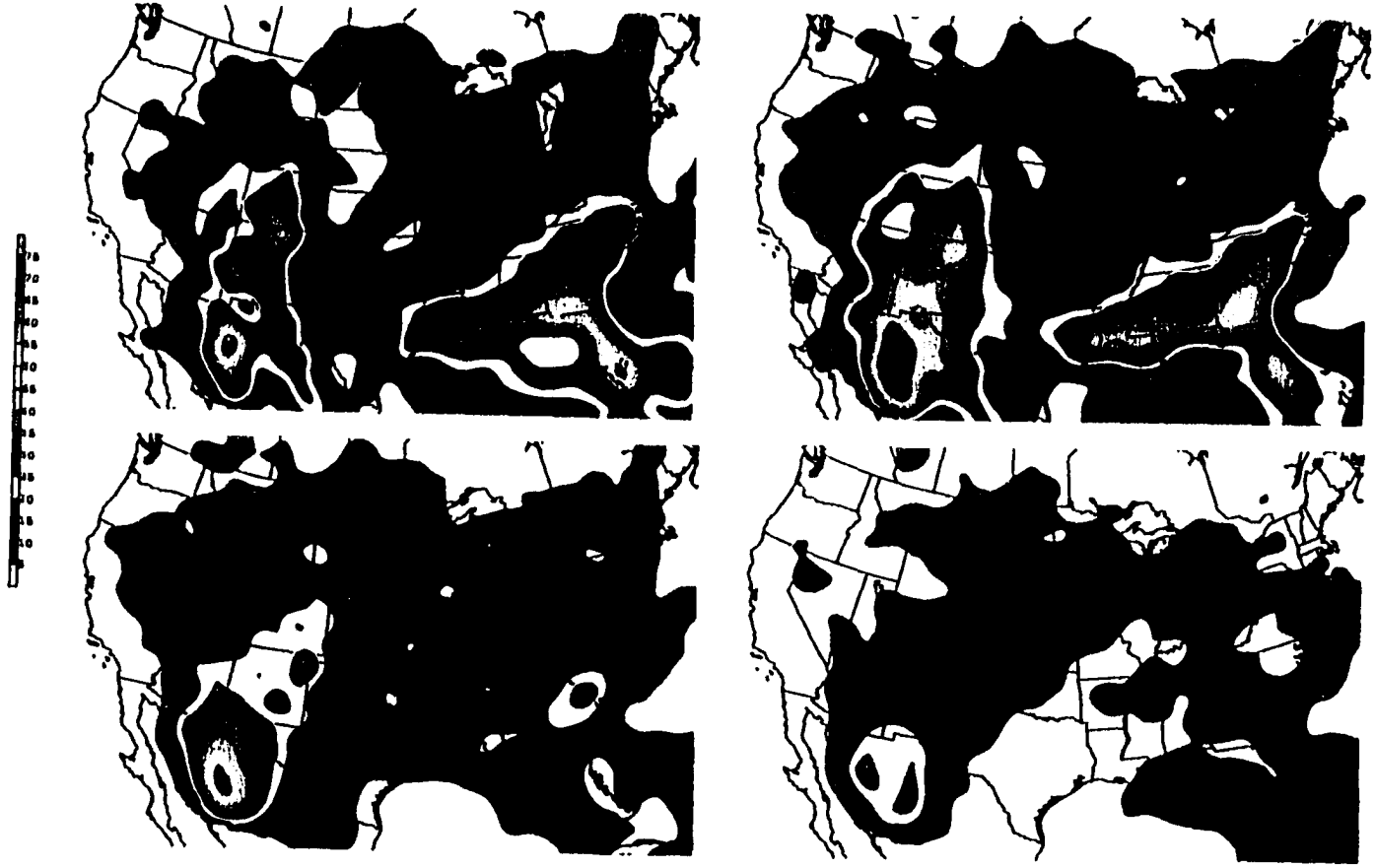

Fig. 4.1. Lightning relative frequency for the pentad centered on 17 July. Upper left is for 18 to 21 UTC, Upper right is for 21 to 00 UTC, lower left is for 00 to 03 UTC, and lower right is for 03 to 06 UTC.

Of the original 19 pentads, the 16 days withheld for testing were:

Pentad 1 (5/31-6/4): 3 June 1999
Pentad 2 (6/5-6/9): 8 June 1999
Pentad 3: (6/10-6/14) 14 June 1999
Pentad 4:(6/15-6/19) 17 June 1999
Pentad 5:(6/20-6/24) 23 June 1999
Pentad 6:(6/25-6/29) 28 June 1999
Pentad 7:(6/30-7/4) missing data (only one day available)
Pentad 8:(7/5-7/9) 9 July 1999
Pentad 9: (7/10-7/14) 11 July 1999
Pentad 10: (7/15-7/19) 18 July 1999
Pentad 11:(7/20-7/24) 22 July 1999
Pentad 12:(7/25-7/29) 25 July 1999
Pentad 13:(7/30-8/3) 29 July 1999
Pentad 14:(8/4-8/8) missing data (only one day available)
Pentad 15:(8/9-8/13) 13 August 1999
Pentad 16:(8/14-8/18) 14 August 1999
Pentad 17:(8/19-8/23) 22 August 1999
Pentad 18: (8/24-8/28) 24 August 1999
Pentad 19: (8/29-9/2) missing data (only one day available)

A total of 208 candidate quantities (see Appendix C) were developed to be used as potential regression predictors. These fields were designed to encompass terms that diagnosed instability, moisture, and lift, as they relate to thunderstorm initiation and development at different levels in the atmosphere.

This body of work seeks to determine: (1) which variables are most correlated with lightning and total number of flashes, (2) which variables explain the most variance along with the amount of variance they explain, and (3) if there are any distinctive groupings of variables that may predict lightning better. It was realized that many of the candidate predictors were at least partially correlated. For example, approximately 10% of the candidate predictors in Appendix C are related to various forms of CAPE (e.g., most unstable CAPE, normalized CAPE, layer CAPEs, best CAPE, Lifted Indices, etc.). The multivariate data analysis techniques covered in this chapter

include (1) correlation of predictors to predictand, to find the strongest correlation to the predictands among the variables, (2) stepwise regression, to determine, among all 208 candidate predictors, which group of single predictors explains most of the variance, (3) Principal Component Analysis (PCA), to determine a much smaller, distinctive physical set of predictors (to serve as new predictors for regression), and (4) logistic regression to derive the predictive equations for lightning.

4.2.1 Original Data Matrix Structure

The original data matrix was 136,620 rows by 208 columns. It was composed of 208 candidate predictors in the columns, and grid point data for all 54 days in the rows (i.e., 2530 grid points for 54 days). Initially, the first statistical analyses were attempted using all 136,620 grid points, even those without CAPE. However, since the purpose was to search for physical relationships between groups of predictors and lightning, only the grid points where the Most Unstable parcel CAPE (MUCAPE) was present (greater than 0) and extended from the LFC to at least the -15 to -20°C range (discussed in Chapter 5) were included in the final developmental matrix, **[X]** (89,115 rows by 205 columns). Many of the predictors (Appendix C) are only defined in the presence of CAPE, otherwise, default values had to be applied (e.g., LFC, EL, etc.)

The CAPE computed from the Most Unstable Parcel (MUP) was used to represent an "upper-bound" for the CAPE calculations. In reality, the actual CAPE values of a rising parcel could be far less than the MUCAPE, since the air at the Most Unstable Parcel Level (MUPL) may not be representative of the air going into the updraft.

The layer CAPE from -15 to -20 °C was found to be a good discriminator between cases with CAPE and lightning and cases with CAPE and no lightning (see Chapter 5). In other words, when any amount of CAPE was present, in over 98 percent of the cases when lightning occurred, the CAPE extended to at least the layer from -15 to -20 °C. Therefore, in order to concentrate on the cases where lightning was more likely (layer CAPE greater than zero from -15 to -20 degrees C), the rows of data with no CAPE in this layer were removed from the matrix, leaving 89115 rows of data. This resulted in only 150 out of 13,523 grid boxes (1 percent) with 1 or more flashes being discarded. However, 47,505 grid boxes (39 percent) without lightning were excluded from the analysis as a result of this condition.

All 208 candidate predictors were used in the correlation study and stepwise regression. However, out of the original 208 candidate predictors, 205 candidate predictors were used in the PCA because the I, J, and K grid point locations were excluded, as these are fixed points with zero variance. The fundamental PCA method is called a "R mode analysis" since a R mode (Cattel 1952; and Richman 1986) is defined where the columns of the matrix are the predictors and station data (grid points in this case) are the rows. The PCA is termed a "Hybrid R mode" because a normal R mode analysis is for one time period and in this case 54 days are included in the rows.

4.3 Correlation of Predictors and Predictands

Correlation analyses were performed between each of the predictors and the binary predictand (1 for one or more flashes, 0 otherwise) and again for when the pre-

dictand was the total number of flashes. Table 4.1a shows that no single atmospheric variable/predictor exhibited a high correlation with either predictand, as the highest correlation was 0.33 and 0.32 for lightning/no lightning and total number of flashes, respectively. Also, the predictor correlations to the binary predictand were higher than the correlations to the total number of flashes. It is also interesting to note that out of 208 predictors, the first 17 predictors with the highest correlation were the same for both predictands, although in different order. From Table 4.1b it can be seen that the predictor with the highest correlation for one or more flashes is the climatological relative frequency. The highest correlation with the total number of flashes is the product of the best CAPE and the average number of flashes.

1=LTG/0=NO LTG		Total number of flashes	
IONE	0.33	BOTF	0.32
ITSM	0.31	BTFR	0.30
ML47	0.30	IOTF	0.27
BONE	0.29	BTSM	0.26
BTSM	0.28	ITFR	0.25
ML48	0.26	BONE	0.24
CDPM	0.26	BECP	0.21
SMXR	0.26	ITSM	0.21
WBZH	0.25	SMXR	0.17
BECP	0.25	INPW	0.17
IOTF	0.25	IONE	0.17
INPW	0.24	ML47	0.16
ITFR	0.24	MXMX	0.15
MLCT	0.23	CDPM	0.15
BTFR	0.23	MLCT	0.15
MXMX	0.23	ML48	0.14
BOTF	0.23	WBZH	0.13

Table 4.1a. Order of predictors and correlation (absolute value) for binary predictand (left column) and for total number of flashes (right column).

ONE OR MORE FLASHES and (TOTAL NUMBER of FLASHES)

1	(11)	IONE	Lightning relative frequency for one or more flashes
2	(8)	ITSM	Percentage of time lightning reported
3	(12)	ML47	Change in Theta-E from 400 to 700 mb
4	(6)	BONE	Best CAPE * relative frequency of one or more flashes
5	(4)	BTSM	Best CAPE * Percentage of time lightning reported
6	(16)	ML48	Change in Theta-E from 400 to 700 mb
7	(14)	CDPM	Depth of cloud from LCL to EL
8	(9)	SMXR	Surface Mixing Ratio
9	(17)	WBZH	Height of wet-bulb zero
10	(7)	BECP	Best CAPE
11	(3)	IOTF	Average number of flashes per three-hour period
12	(10)	INPW	Inches of precipitable water
13	(5)	ITFR	Average percent of total flashes
14	(15)	MLCT	Cloud base temperature
15	(2)	BTFR	Best CAPE * Percentage of flashes in each box
16	(13)	MXMX	Mixing ratio at level of most unstable parcel
17	(1)	BOTF	Best CAPE * Average number of flashes per three- hour period

Table 4.1b Descriptor of predictors (from Table 4.1a and order of predictors for binary predictand (first column) and for total number of flashes (second column).

4.4 Stepwise Regression

Forward stepwise regression was performed using all 208 predictors to examine how the predictors selected from this data set would be ordered in terms of their contributions to the reduction of variance in the prediction equation. Complete results for all predictors are listed in Appendix D. Stepwise regression was run with (1) 208 predictors and the binary response of 0 for no flashes and 1 for one or more flashes, FONE, and (2) 208 predictors and the total number of flashes per grid box as the predictand, TOTF. Tables 4.2a and 4.2b show the top 12 terms retained from the stepwise regression for each predictand. Twelve terms were chosen because the amount of additional variance explained by including the 12th term dropped to less than 0.005 for

FONE. This is consistent with Glahn's (1985) recommendation of stopping when the added reduction of variance of the next predictor is less than 0.005. An inspection of both sets of predictors revealed that several variables were common to both groups. However, there were substantial differences between the remaining predictors in the two groups.

No attempt was made to linearize the predictors or predictand since the primary emphasis was to compare the order of the terms by the reduction of variance. Tests were performed using a linear regression equation derived from the top terms selected by stepwise regression to predict one or more flashes, and the results showed significant areas between the 10 and 30 percent probability contours that did not have any lightning. Also, when predicting one or more flashes and the total number of flashes, very little skill was shown as evidenced by the Multiple R-Squared statistic (cumulative variance explained) for 12 terms of 21 and 14 percent, respectively (Table 4.2a). Tests were performed using linear regression to predict the total number of flashes and results were that the predictive equations failed to predict the cases where more than a few tens of flashes occurred.

The stepwise regression approach in this study was not optimized as the main objective of this work was to explore the principal component analysis technique to determine if there were groupings of predictors that would produce a better result and if the groupings could identify distinct physical processes.

FONE	Cumulative Variance	TOTF	Cumulative Variance
IONE	0.1061	BOTF	0.1021
INPW	0.1440	VKAV	0.1107
VKCL	0.1621	BTSM	0.1185
LP78 (1)	0.1767	IOTF	0.1248
ML47 (2)	0.1909	BECP	0.1297
BONE (3)	0.1943	LC67 (5)	0.1325
MFCN (4)	0.1971	LP78 (1)	0.1358
AUDV	0.1996	ML47 (2)	0.1378
LC67 (5)	0.2001	MFCN (4)	0.1394
MLCH	0.2048	MCAP	0.1404
TL75	0.2097	PTND	0.1413
SMXR	0.2122	BONE (3)	0.1422

Table 4.2a Stepwise regression results for top 12 terms.

ONE OF MORE FLASHES (FONE)

IONE	Climatological relative frequency of one or more flashes
INPW	Inches of precipitable water
VKCL	Kinematic vertical velocity at cloud base
LP78 (1)	Change in Theta-850 to 700 mb
ML47 (2)	Change in Theta-E from 400 to 700 mb
BONE (3)	Best Cape * relative frequency of one or more flashes
MFCN (4)	Surface moisture flux convergence
AUDV	Average divergence from 400 to 250 mb
LC67 (5)	Change in Theta-700 to 600 mb * avg convergence in layer
MLCH	Most unstable parcel cloud base height (msl)
TL75	Temperature difference from 700 to 500 mb
SMXR	Surface mixing ratio

TOTAL NUMBER OF FLASHES (TOTF)

BOTF	Best CAPE * Average number of flashes from climatology
VKAV	Kinematically computed average mid level vertical motion
BTSM	Best CAPE * percentage of time lightning reported
IOTF	Average number of flashes from climatology
BECP	Best CAPE
LC67 (5)	Lapse Rate-700 to 600 mb * avg convergence in layer
LP78 (1)	Lapse Rate from 850 to 700 mb
ML47 (2)	Change in Theta-E from 400 to 700 mb
MFCN (4)	Surface moisture flux convergence
MCAP	Most unstable parcel cap strength
PTND	3-hour surface pressure tendency
BONE (3)	Best Cape * relative frequency of one or more flashes

Table 4.2b Description of parameters in Table 4.2a. Terms that are the same in bothgroupings are identified in parenthesis.

4.5 Principal Component Analysis

The multivariate statistical method, Principal Components Analysis (PCA) (see Appendix E), was first applied to atmospheric data by Lorenz (1956). He called the technique Empirical Orthogonal Function (EOF) analysis. Related to this is the PCA method, where the difference is that the unit length eigenvectors from the EOF analysis are multiplied by the square root of each corresponding eigenvalues. PCA (or EOF) has been used extensively in the atmospheric sciences to reduce data sets containing large numbers of variables to a single set containing many fewer variables, but still representing a large fraction of the variability contained in the original data set (Wilks 1995). This can be achieved via PCA if there are substantial correlations (or covariances) among the original variables. Each of the new variables derived from the PCA is called a principal component (PC). Another desirable aspect of the use of PCA output for regression input is that the variables in the new data set are uncorrelated.

In addition to data compression, PCA can also help us gain a better physical interpretation of atmospheric processes and can yield substantial insights into both the spatial and temporal variations of the fields being analyzed. However, although the first PC may represent an important physical process, there is the possibility that it may also include aspects of other physical processes (i.e., several distinct physical processes being jumbled together in a single PC). To avoid this pitfall, a procedure to minimize the problem of PCs with mixed processes is to apply a linear transformation (called "rotation") to a subset of the data. Even though the original variables may be

correlated, the new variables which are the rotated principal components (RPCs) retain all of the variability in the truncated series of unrotated PCs, yet are uncorrelated if an orthogonal rotation is used because of the coordinate transformation. It was for these reasons that PCA was used to reduce the 205 candidate predictors to a more manageable data set. Appendix E shows how the 205 predictors were reduced to 10 new predictors.

While the PCA is extremely powerful for data compression and can yield substantial insights into both the spatial and temporal variation of the fields being analyzed, the linear transformation ("rotation") should be applied to assure the PCs do not contain mixed processes. This is because of the basic properties of the PCA. One of the properties of the PCA is that the eigenvectors of symmetric matrices are perpendicular (orthogonal) to each other. In the PCA, the eigenvectors calculated from a symmetric data matrix, serve to define an alternative coordinate system to view the data. It is the orthogonality constraint on the eigenvectors that can cause problems with the interpretation. This new coordinate system is oriented such that each new axis is aligned along the direction of the maximum joint variability of the data, consistent with that axis being orthogonal to the preceding ones (Wilks 1995). The first eigenvector is the vector associated with the largest eigenvalue and is aligned parallel to the direction in which the data jointly exhibit maximum variation. While the first principal component may represent an important atmospheric process, the maximal variance property of the PCA makes it likely that other distinct atmospheric processes

are also combined and mixed in with the first principal component (as well as the other PCs).

Since one purpose of a PCA is to gain a better physical interpretation of the atmospheric processes leading to thunderstorms in the West, it is desirable to apply the linear transform (rotation) to a subset of the original PCs, in order to form a new set of rotated PCs (RPCs). The advantage is the RPCs are physically consistent with subsets of the original 205 variables which coincide with specific atmospheric processes (i.e., the RPCs support the observed correlation between the variables). Hence, the RPCs allow us to gain better insight into the physical basis of the problem being studied which was one of the primary goals of the analysis.

To illustrate how this works, in his review article on the rotation of principal components (RPCs), Richman (1986) includes an example from an experiment by Thurstone (1947), and the analysis by Harman (1976), in which 20 non-linear measurements (i.e., combinations of X, Y, and Z) were taken of a set of boxes. It would be logical to assume that X, Y, and Z are the important physical measurements that uniquely identify the boxes. However, as in most investigational cases, the underlying "order" may not be known at all, or at least not known completely. The 20 non-linear measurements were formed into a correlation matrix and analyzed, with the final rotated solution correctly identifying the three RPCs as length, width, and height of the boxes (X, Y, and Z). Thurstone (1947) defined a set of requirements for the transformed solution, which he called "simple structure". The goal of simple structure was to aid in "the scientific problem of discovering an underlying order in the domain". That is the purpose herein.

Suppose, for example, we were to assume (perhaps erroneously) that we had devised "the perfect set of predictors", where each predictor represented a distinct physical process in the atmosphere and each of the predictors was uncorrelated. The principal component analysis could independently confirm or disprove our original predictor assumptions. Even if we did not know or understand (in advance) the underlying physical processes (such as how thunderstorms form), the PCA would be able to take a large set of predictors and assign them to a much smaller set of rotated vectors that could best describe the atmospheric building blocks for thunderstorms.

4.5.1 Procedures

The complete procedure for the principal component analysis (PCA) is shown in Appendix E. First, a correlation matrix (205 by 205) was computed from the data matrix, **[X]**, (89,115 rows by 205 columns). The diagonal elements of the correlation matrix are the correlations of each of the variables with themselves and are always equal to 1. Since the correlations, r_{ij}, between the i and j variables are the same as the correlations, r_{ji}, the matrix is symmetric. The correlation matrix is used rather than the covariance matrix, because the correlation matrix uses the variance-normalized variables and these help to assure that variables with large differences in magnitude, such as potential vorticity (10^{-6} m^2 s^{-1} K kg^{-1}) and the 500 mb height field (10^3 meters), receive equal weight in the analysis.

The eigvenvalues (scaler quantities) and eigenvectors (a set of nonzero vectors) of the correlation matrix were obtained. Next, the individual elements, also called coefficients or PC loadings, of each of the eigenvectors were computed. Mathemati-

cally, there are as many eigenvectors as there are variables. However, if all the eigenvalues are plotted versus the corresponding principal component number, on what is called a scree graph, Cattel (1952) (see Fig. 4.2), only the eigenvalues with the largest values that retain the largest amount of variance from the original data need to be retained. As can be seen from Fig. 4.2, the first 10 principal components contain the most information. The first 10 loadings were deemed significant after also evaluating the rate of change of slope on Fig. 4.2. These first 10 loadings were then "rotated". Several tests (see Appendix E) were run by rotating 10, 12, 14, and 16 PCs, and these did not produce significant improvement. These results are discussed in Appendix E.

The rotation of the original principal components gives rise to a new set of vectors. Each of these vectors, or rotated PCs (RPCs), contains all of the original quantities, and each vector can be defined by the largest (absolute value) coefficients (Appendix E). In this case, the coefficients with a value below 0.40 were not used because they contribute little information to the analysis (Richman and Gong, 1997). The new variables (RPCs) and percent of original variance explained are shown in Table 4.3, 4.4 and Fig. 4.3.

Plots of the geographic distribution of the mean values of each of these individual RPCs can provide information indicating in which areas of the West they are most important (e.g., where instability (Term 1) or low level forcing and vertical velocity (Term 4) would normally be the strongest). The variance of each of these RPCs can show where they exhibit the most variability during the course of the summer.

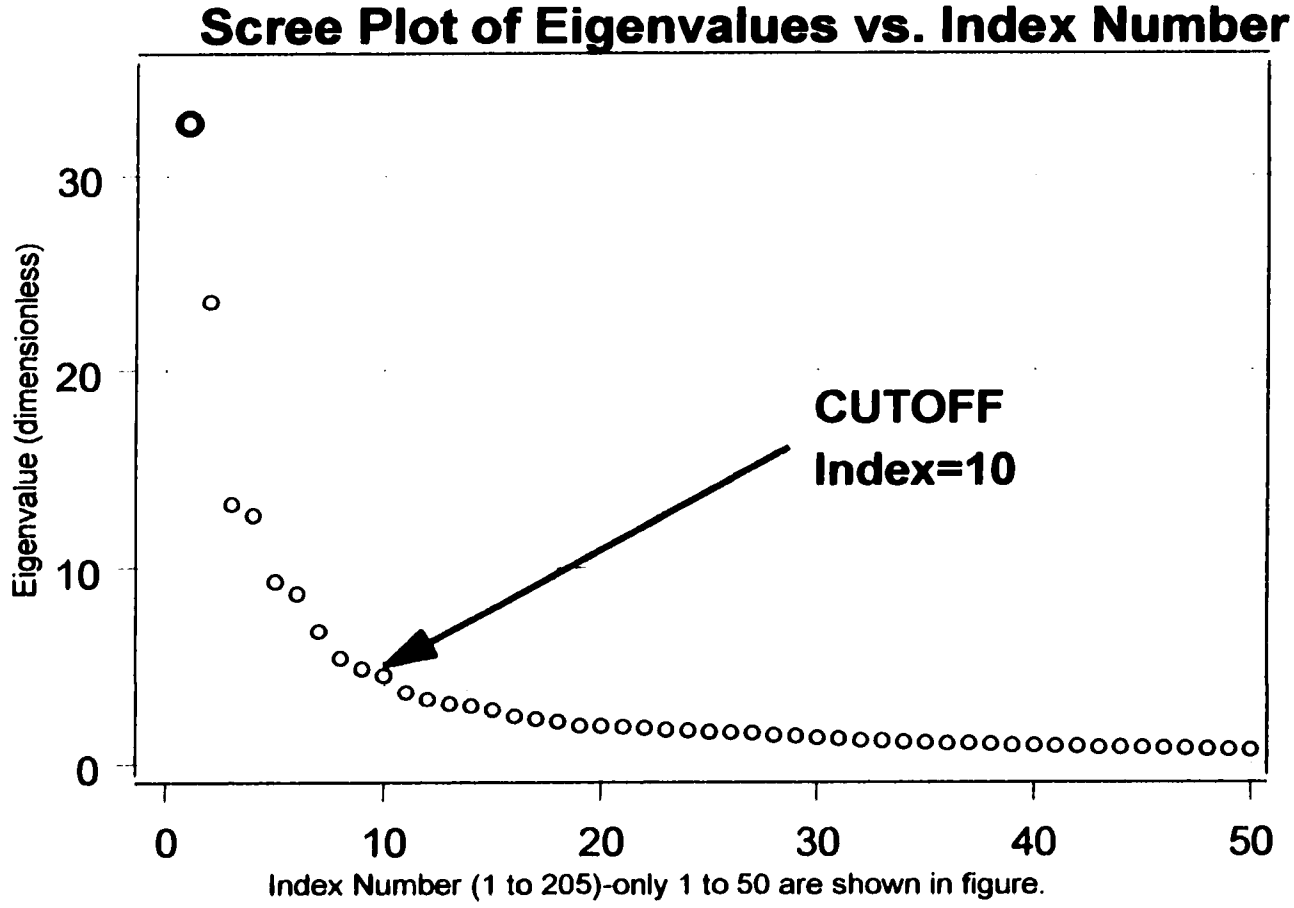

Fig. 4.2. Scree plot with first 50 of 205 Eigenvalues from development data.

1) **(T)**	(13%)	CAPE
2) **(T)**	(10%)	Lapse rates/relative humidity
3) **(D)**	(6%)	Upper-level potential vorticity, saturated and moist geostrophic potential vorticity (above 400 mb), tropopause pressure, temperature,500 mb height, height of 0, -10, and -20 °C, WBZ
4) **(D)**	(5%)	Low level forcing and vertical velocity through LFC
5) **(D)**	(5%)	U wind components, shear and storm relative terms
6) **(D)**	(5%)	V wind components, shear and storm relative terms
7) **(D)**	(3%)	Mid-level saturated geostrophic potential vorticity (below 400 mb), mid and low level cyclonic circulation.
8) **(T)**	(4%)	Convective Inhibition/Capping inversion
9) **(T)**	(5%)	Best CAPE*LTG Climo, LTG Climo, potential instability
10)**(D)**	(3%)	Forcing from LCL to LFC, mid-level vertical velocity, upper- leveldivergence, pressure at most unstable parcel level
	(59%)	Total variance from all predictors contained in the 10 RPCs

Table 4.3 Individual Rotated Principal Components (RPCs) from Varimax rotation. RPC Terms: (T=related to Thermodynamics; D=related to Dynamics). Percentage is amount of variance contained from original data.

The 10 RPCs were submitted to a stepwise regression to test for the significance of each of the ten fields. Based on the variance explained by each term, the stepwise regression ordered the 10 RPCs in the following order:

1) (9.5%)	Best CAPE*LTG Climo, LTG Climo, potential instability
2) (12%)	Low level forcing and vertical velocity through LFC
3) (14%)	Forcing from LCL to LFC, mid-level vertical velocity, upper- leveldivergence, pressure at most unstable parcel level
4) (15.4%)	CAPE
5) (16.5%)	Lapse rates/relative humidity
6) (17.30%)	V wind components, shear and storm relative terms
7) (18.2%)	Upper-level potential vorticity, saturated and moist geostrophic potential vorticity (above 400 mb), tropopause pressure, temperature,500 mb height, height of 0, -10, and -20 °C, WBZ
8) (18.6%)	U wind components, shear and storm relative terms
9) (18.6%)	Convective Inhibition/Capping inversion
10) (18.6%)*	Mid-level saturated geostrophic potential vorticity (below 400 mb), mid and low level cyclonic circulation.

Table 4.4 Rotated Principal Components (RPCs) in the order from stepwise regression and cumulative variance explained by each term in stepwise regression. Term 10 was rejected by the regression, but is included here for completeness.

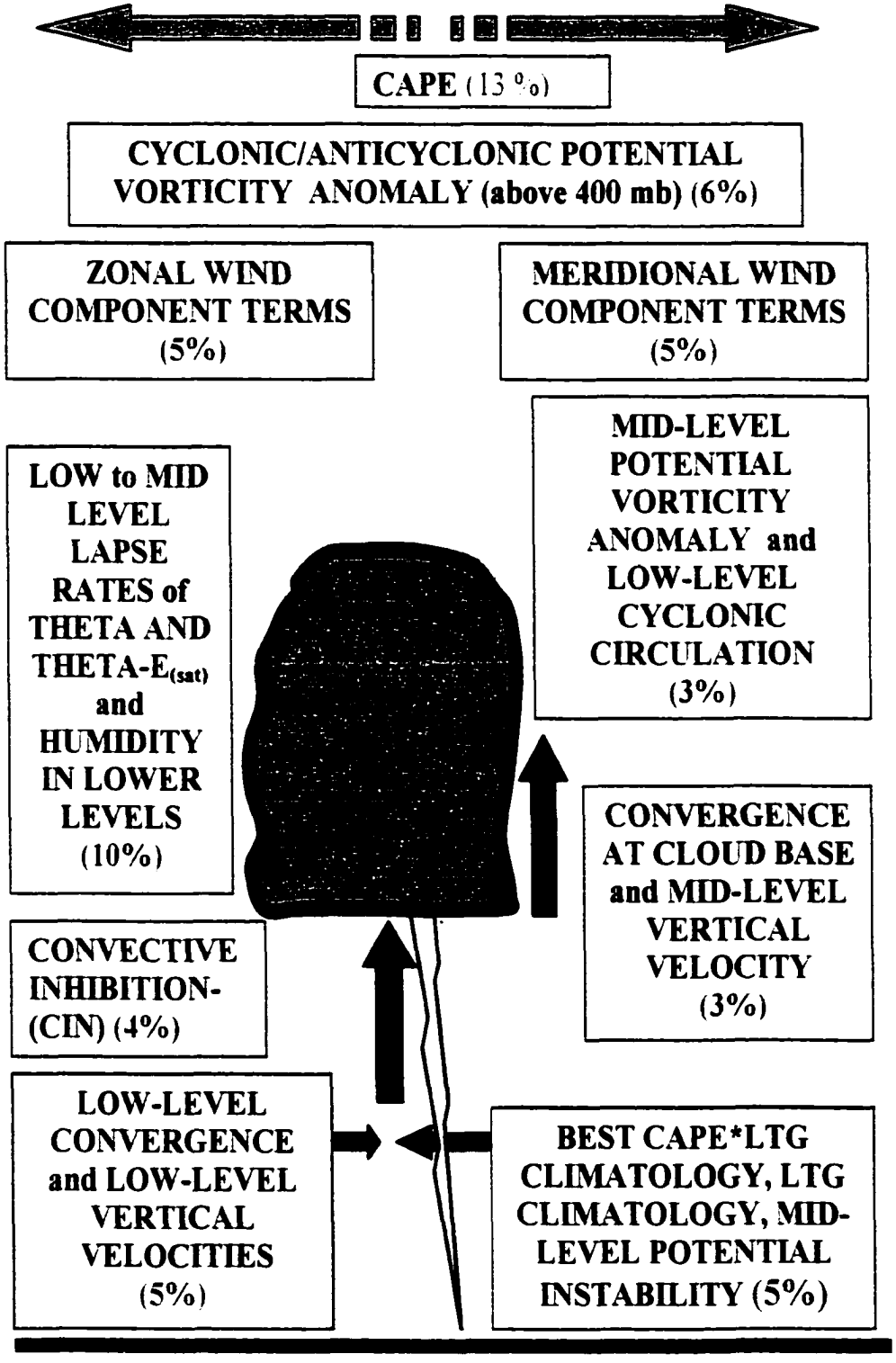

Fig. 4.3. Schematic showing 10 RPC terms and the percentage of the variance explained by each term. Total variance from all predictors contained in the 10 RPCs is 59%.

The result from the stepwise regression of the 10 RPCs accounts for 18.6% of the variance explained. This is lower than the 21.2% of the variance explained by the first 12 terms from the original predictor data set (see Tables 4.4 and 4.2, respectively). However, the 12 original predictor terms have some correlation with each other and the variance explained is measuring that also. Thus, some of the variance is measured twice. Because the varimax orthogonal rotation used to derive the 10 RPCs, there is no correlation between any of the 10 terms. Secondly, the variance explained by the 10 RPCs appears lower because the terms that accounted for 40% of the variability in the training data set were indistinguishable from noise and have been eliminated by rotating only 10 PCs. Thus, a significant part of the noise in the original data set has been greatly reduced. For these two reasons, the 18.6% should be a better representation of the true (signal) variance that is explained by the stepwise regression. Even though variable number 10 (Table 4.4), mid-level saturated geostrophic potential vorticity and low to mid-level cyclonic circulation was not selected in the stepwise regression, it is included because it accounted for three percent of the original data variability.

4.6 Logistic regression

One of the goals of this dissertation was to derive probabilistic forecasts for a binary event, (i.e., lightning either does or does not occur). Two primary regression approaches can be used when the predictand is binary. The simplest approach, called Regression Estimation of Event Probabilities (REEP), involves using multiple linear regression to derive a forecast equation for a binary predictand. However, it is possible with this method to forecast probabilities that are either negative or greater than 1.

Even though someone using the probabilities could "adjust" negative values to 0 and those greater than 1 back to 1, this is not very satisfying from a theoretical viewpoint. Another regression method, called logistic regression, fits the regression parameters to a non-linear equation with an exponential in the denominator that produces an S-curve configuration with properly bounded results for the probabilities, (ranging from 0 to 1; described in more detail in Appendix F). In addition to always producing a prediction between 0 and 1, the S-shape of the logistic function, f(z), is appealing because it combines the contributions of the predictors and produces results that are slowly changing for low values of z until a threshold is reached, then rises rapidly for intermediate values of z and finally levels off for high values. Historically, the parameters had to be estimated from an iterative technique that was computationally intensive and limited its use in statistical weather forecasting. However, many statistical computer software packages now include logistic regression.

Prior to beginning the logistic regression, two possible methods to develop the testing predictor set were evaluated. In the first test, the independent data matrix was scaled and then the new independent PC elements (or scores) were calculated using the independent scaled matrix and the loadings correlation matrix, as derived from the independent data set. A test was also performed calculating the independent PC scores using the independent scaled matrix and the loadings correlation matrix as computed from the development data set. As expected, the results (not shown) using predictors derived from the loadings correlation matrix from the development data set were found to produce better forecasts compared to those using the loadings correlations matrix from the independent data set. A test of the independent PC scores still

showed that the new predictors, as calculated with the development loadings correlation matrix, remained essentially uncorrelated (highest inter-correlation between any of the predictors using this method as 10^{-13}).

Linear regression was also attempted to determine if the PC scores could predict the total number of flashes per grid box per three-hour period. This method exhibited little skill for flash rates above 50 flashes per three-hour period and was not used further. This poor performance may have been partially due to the small sample size used and the rarity of events with 100 or more flashes. It was observed that the data sets were dominated by the large number of grid boxes with no flashes (>87% in both dependent and independent sets) and there were a relatively few number of grid boxes with flash rates greater than 100 per three-hour period (<3%).

Since the linear regression methods tested herein failed to predict large flash rates, rather than using regression to derive the forecast number of flashes, the higher flash events were also transformed into binary outcomes. Logistic regression was used in three different regressions for each of the following cases:

1) 0 for no flashes and 1 for one or more flashes
2) 0 for less than 10 flashes and 1 for 10 or more flashes
3) 0 for less than 100 flashes and 1 for 100 or more flashes.

With this method, it is possible to compute the probability of any number of flashes desired. The PC scores were calculated for the development data (54 days worth of data) and each of the 16 independent days. The computed PC scores (Appendix E) served as the predictors for the logistic regression.

CHAPTER 5

Results

5.1 Probability Forecasts

The forecast equations developed through the PCA and logistic regression in Chapter 4 were derived from the 54 day developmental data set for the following categories of lightning flash densities (number of flashes from 00 to 03 UTC in each 40 by 40 km grid box):

1) one or more flashes
2) ten or more flashes
3) one hundred or more flashes.

The equations were evaluated on independent data comprised of 16 days selected at random within each contiguous pentad from the summer of 1999 (except for pentads with only one day available). For each of the three categories, this resulted in 40,480 forecast probabilities generated for all of the 2,530 grid boxes for 00 to 03 UTC, for each of the 16 days. To eliminate cases where the most unstable CAPE was shallow, the probabilities were made conditional on CAPE extending from the LFC through the -20 °C level in the environment. This was supported by the fact that over 98 percent of all grid boxes with most unstable CAPE greater than zero and reporting lightning, had layer CAPE (LCAPE) from -15 to -20°C.

Results showing the observed lightning, along with the forecast probabilities of one or more flashes, for the independent days are shown in Figs. 5.1 through 5.16. In general, the figures show that the 10 percent line encompassed nearly all lightning

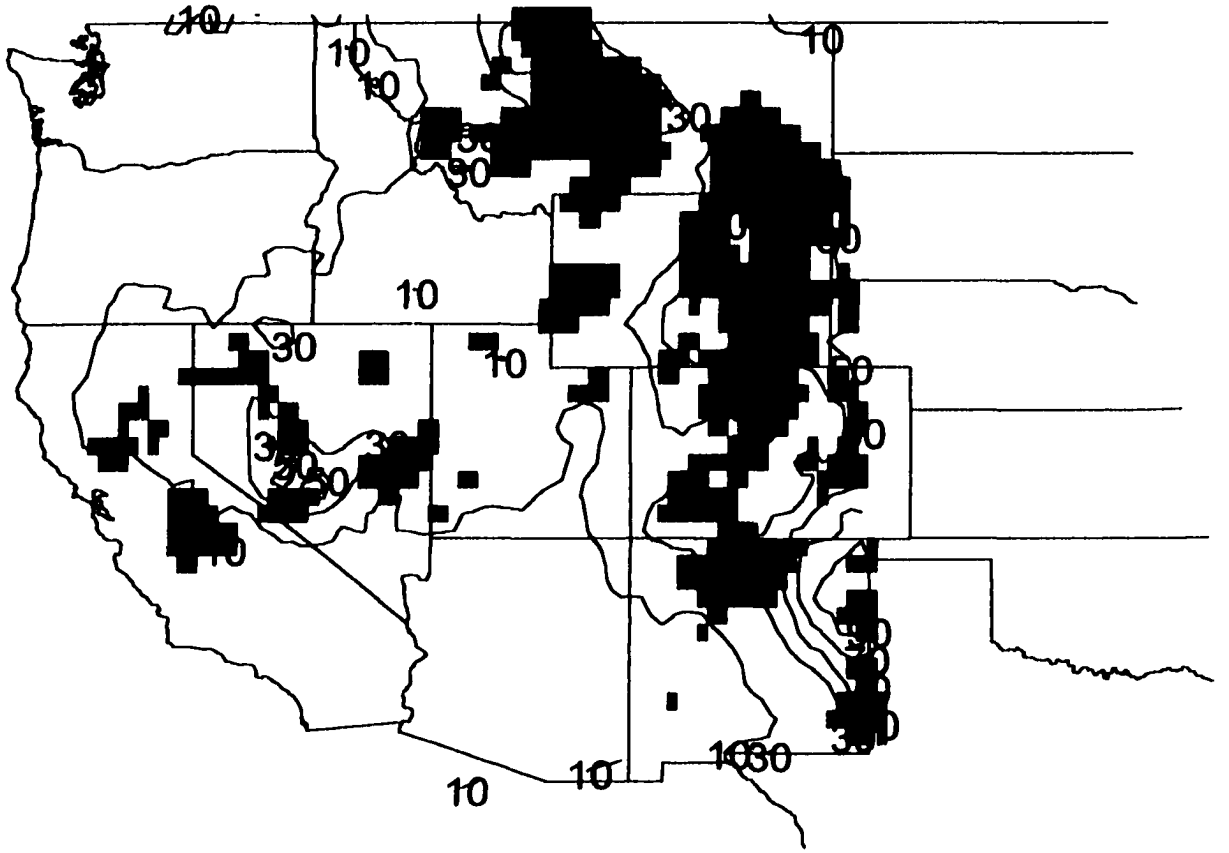

Fig. 5.1. Probability of one or more lightning flashes -solid contours (10, 30, 50, 70, and 90%) for 3 June 1999 and one or more lightning flashes per grid box detected from 00 to 03 UTC-solid color fills.

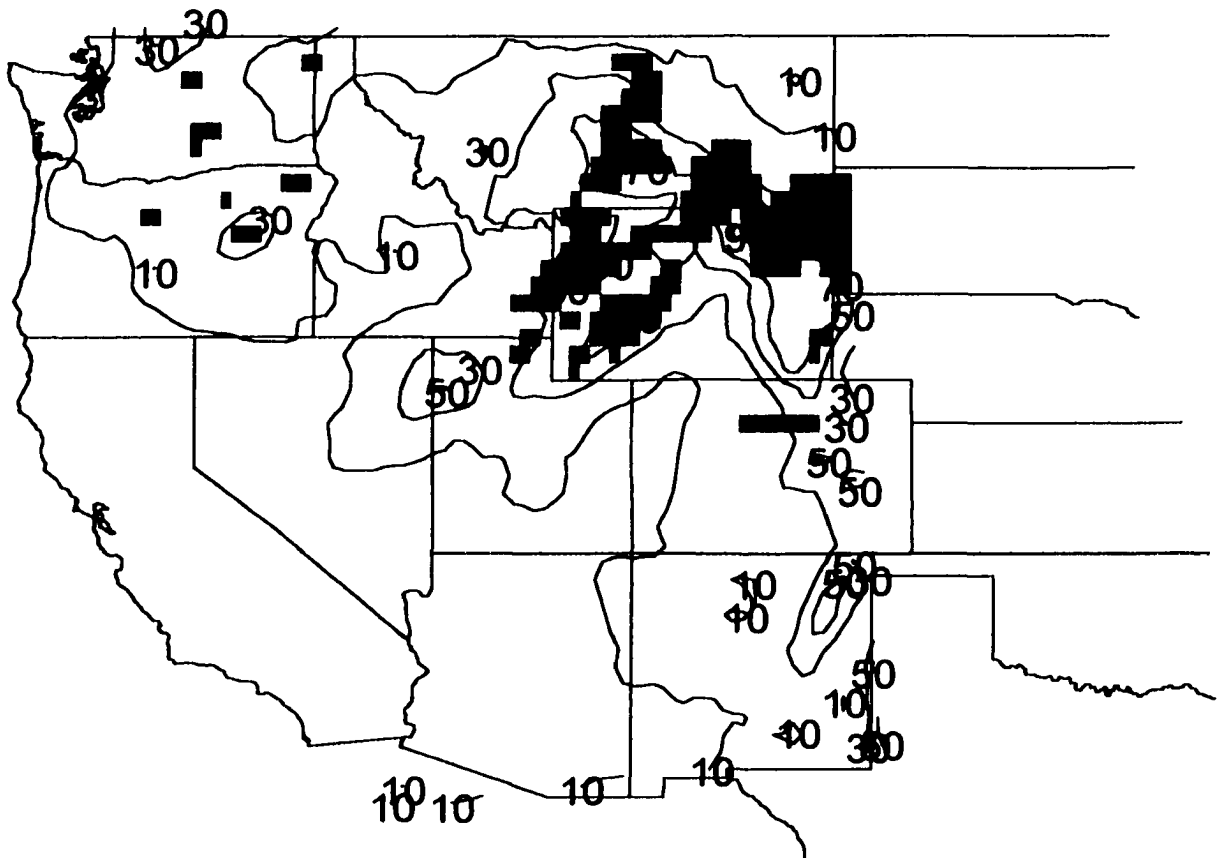

Fig. 5.2. Probability of one or more lightning flashes -solid contours (10, 30, 50, 70, and 90%) for 8 June 1999 and one or more lightning flashes per grid box detected from 00 to 03 UTC-solid color fills.

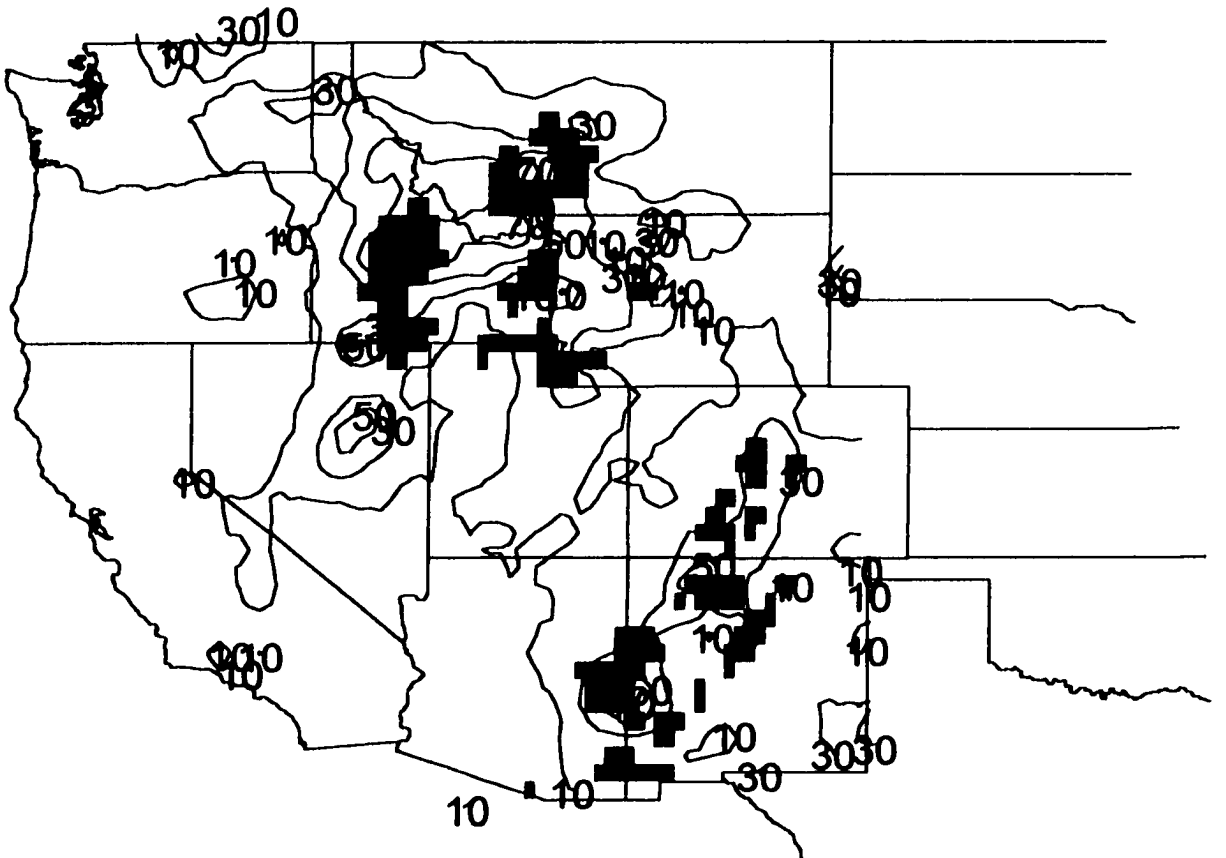

Fig. 5.3. Probability of one or more lightning flashes -solid contours (10, 30, 50, 70, and 90%) for 14 June 1999 and one or more lightning flashes per grid box detected from 00 to 03 UTC-solid color fills.

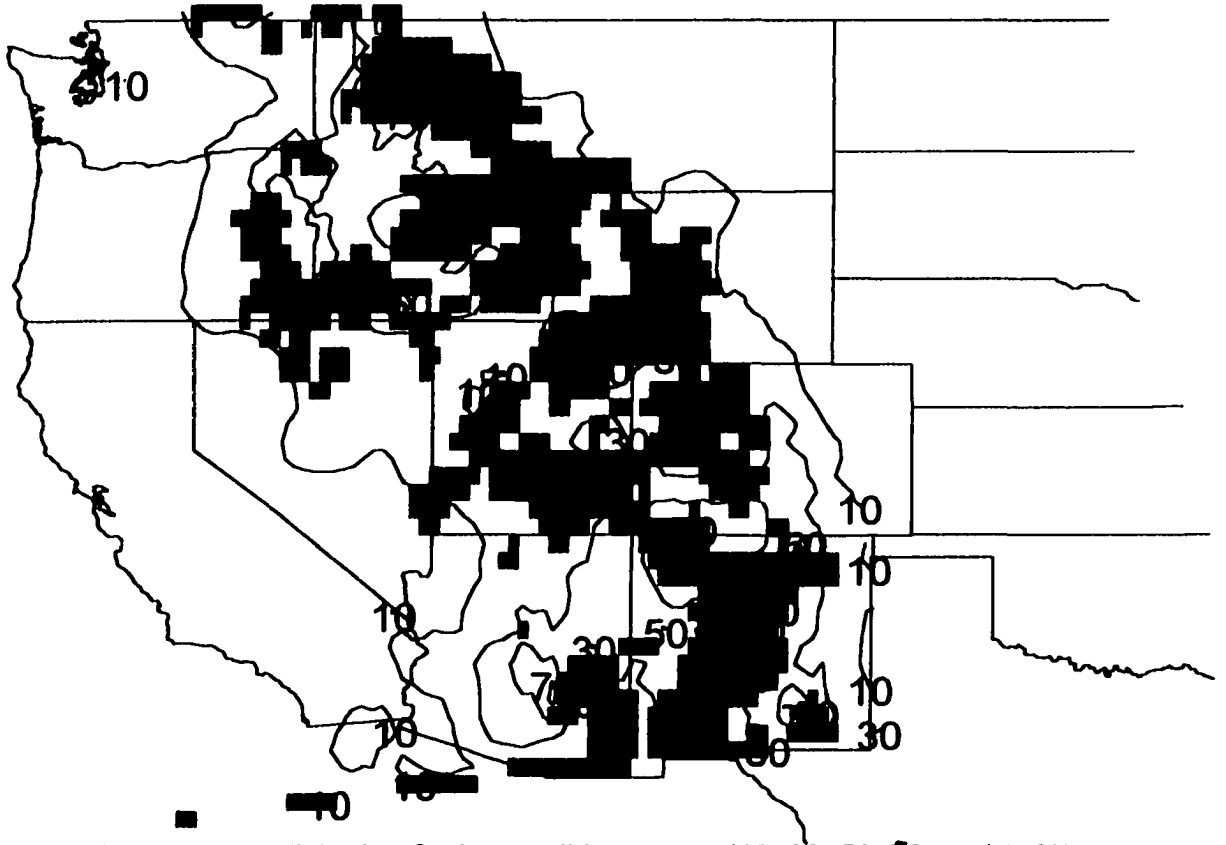

Fig. 5.4. Probability of one or more lightning flashes -solid contours (10, 30, 50, 70, and 90%) for 17 June 1999 and one or more lightning flashes per grid box detected from 00 to 03 UTC-solid color fills.

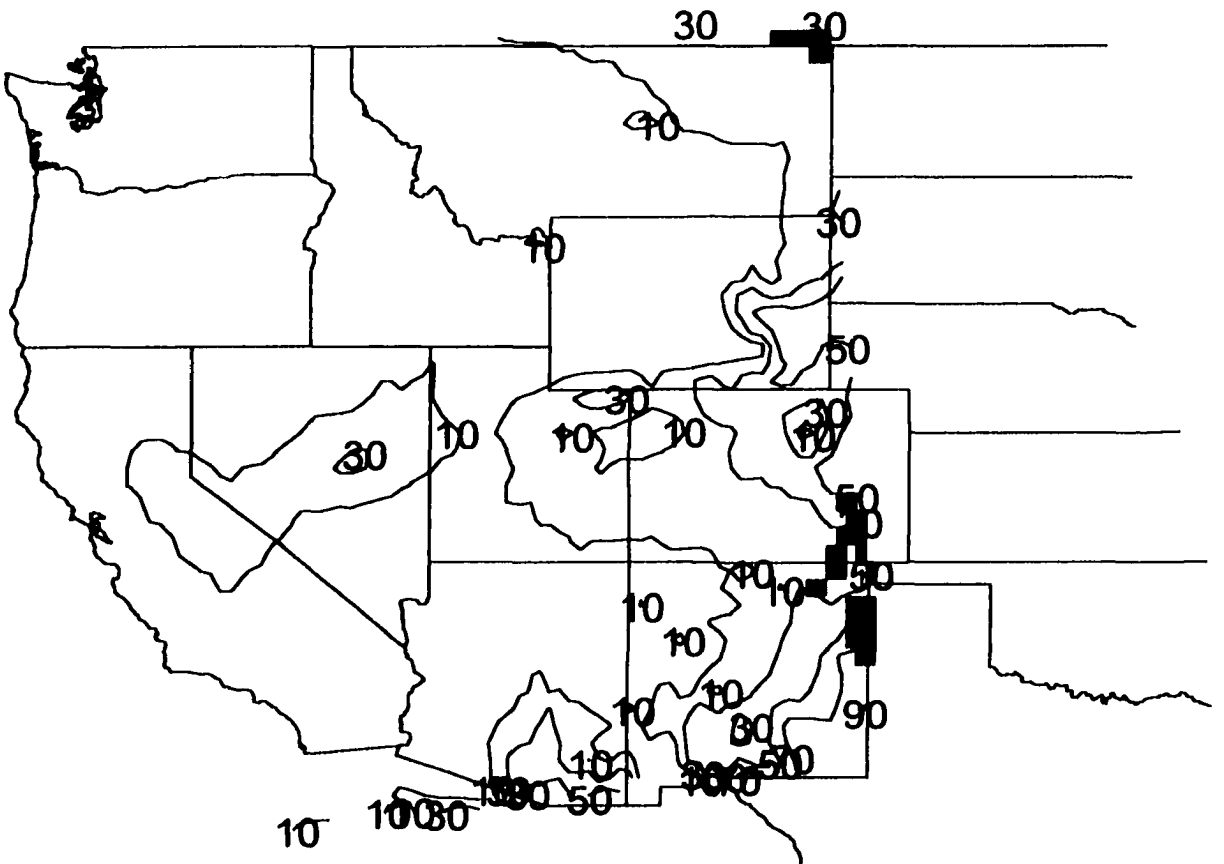

Fig. 5.5. Probability of one or more lightning flashes -solid contours (10, 30, 50, 70, and 90%) for 23 June 1999 and one or more lightning flashes per grid box detected from 00 to 03 UTC-solid color fills.

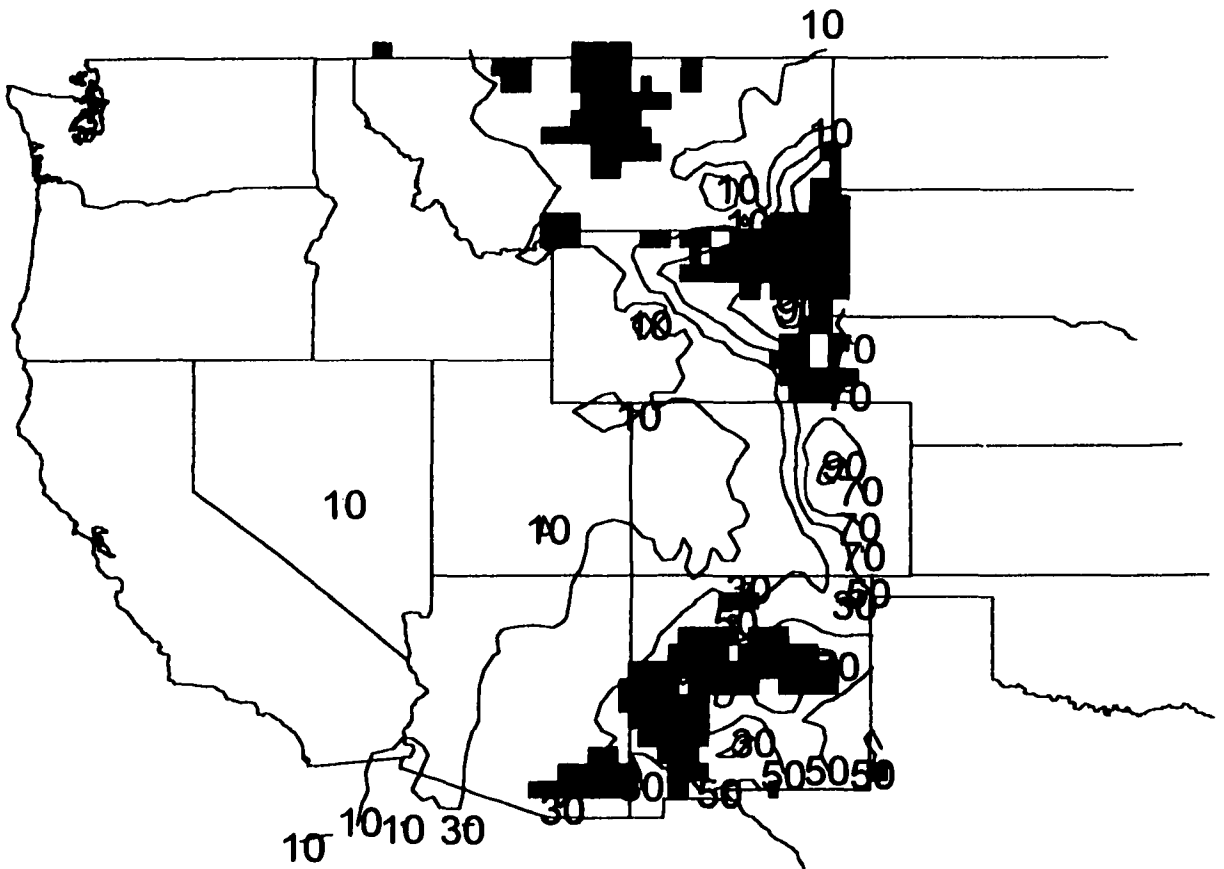
10
10
10

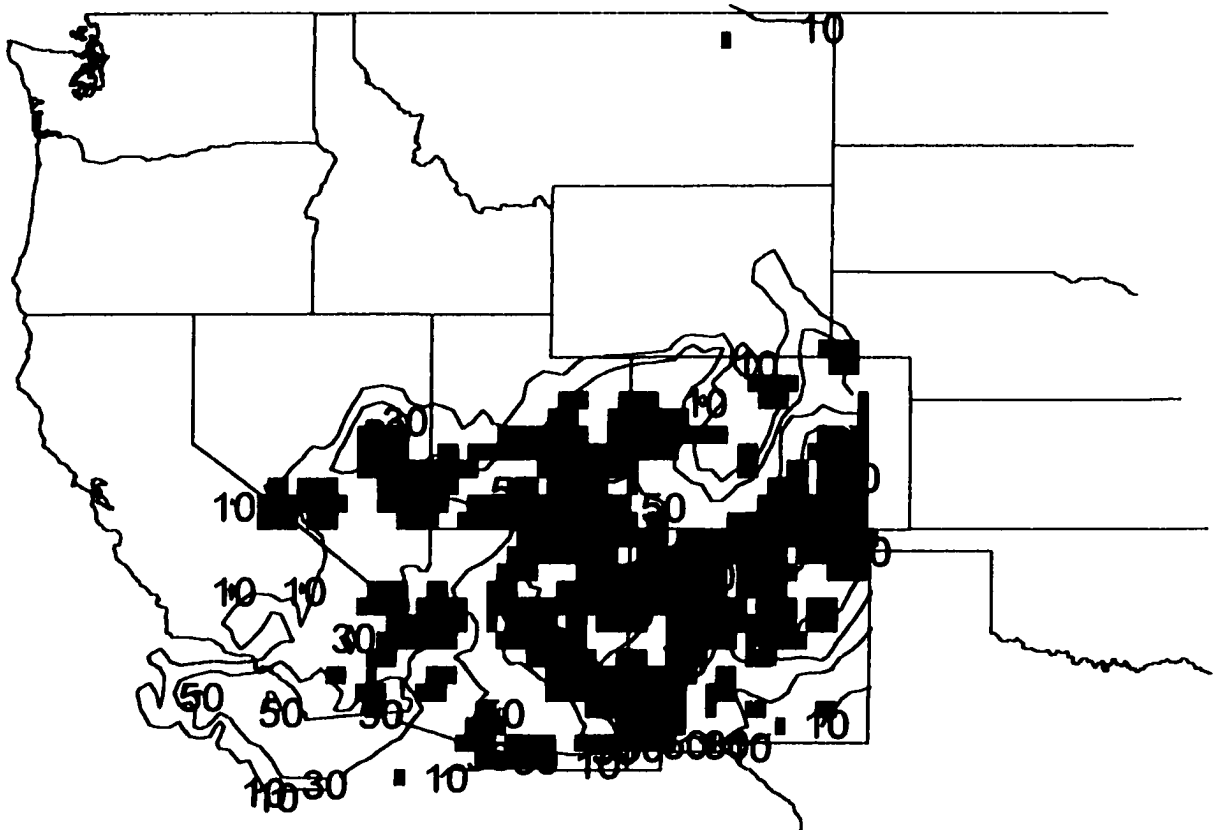

Fig. 5.7. Probability of one or more lightning flashes -solid contours (10, 30, 50, 70, and 90%) for 9 July 1999 and one or more lightning flashes per grid box detected from 00 to 03 UTC-solid color fills.

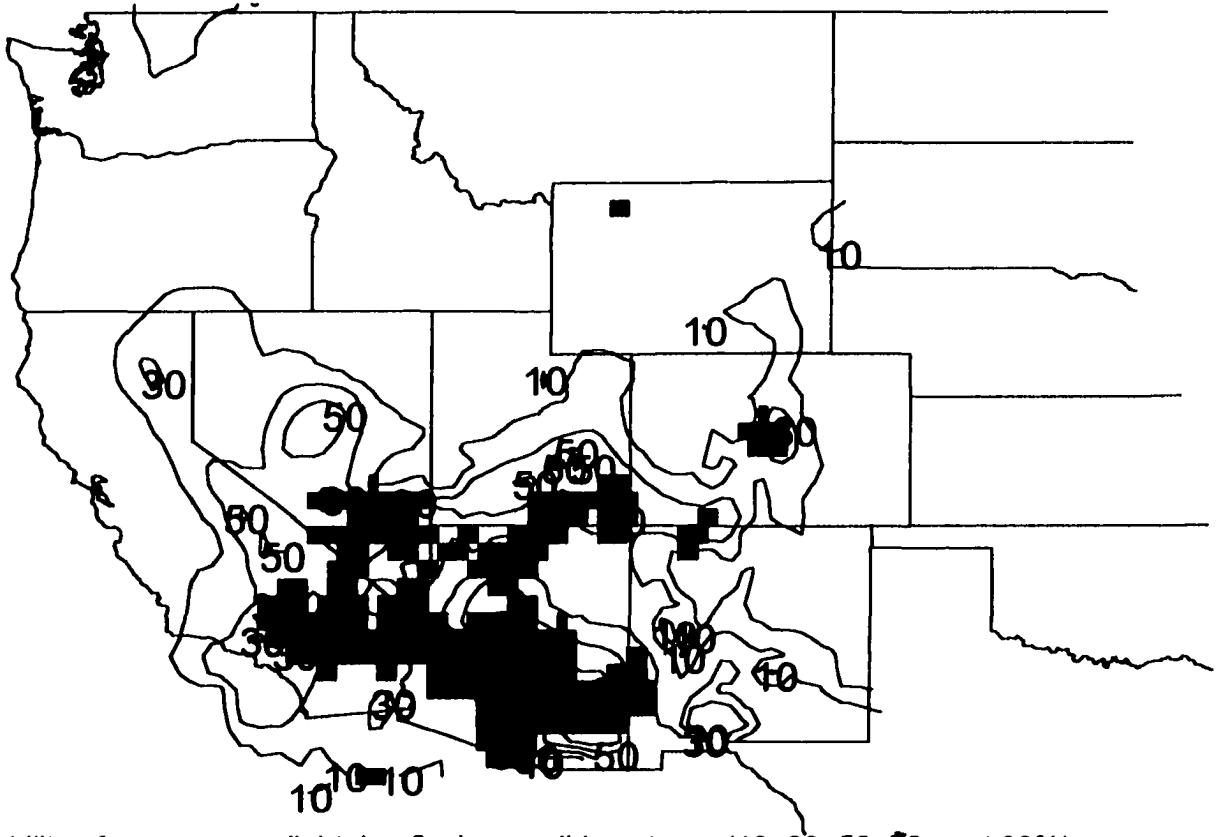

Fig. 5.8. Probability of one or more lightning flashes -solid contours (10, 30, 50, 70, and 90%) for 11 July 1999 and one or more lightning flashes per grid box detected from 00 to 03 UTC-solid color fills.

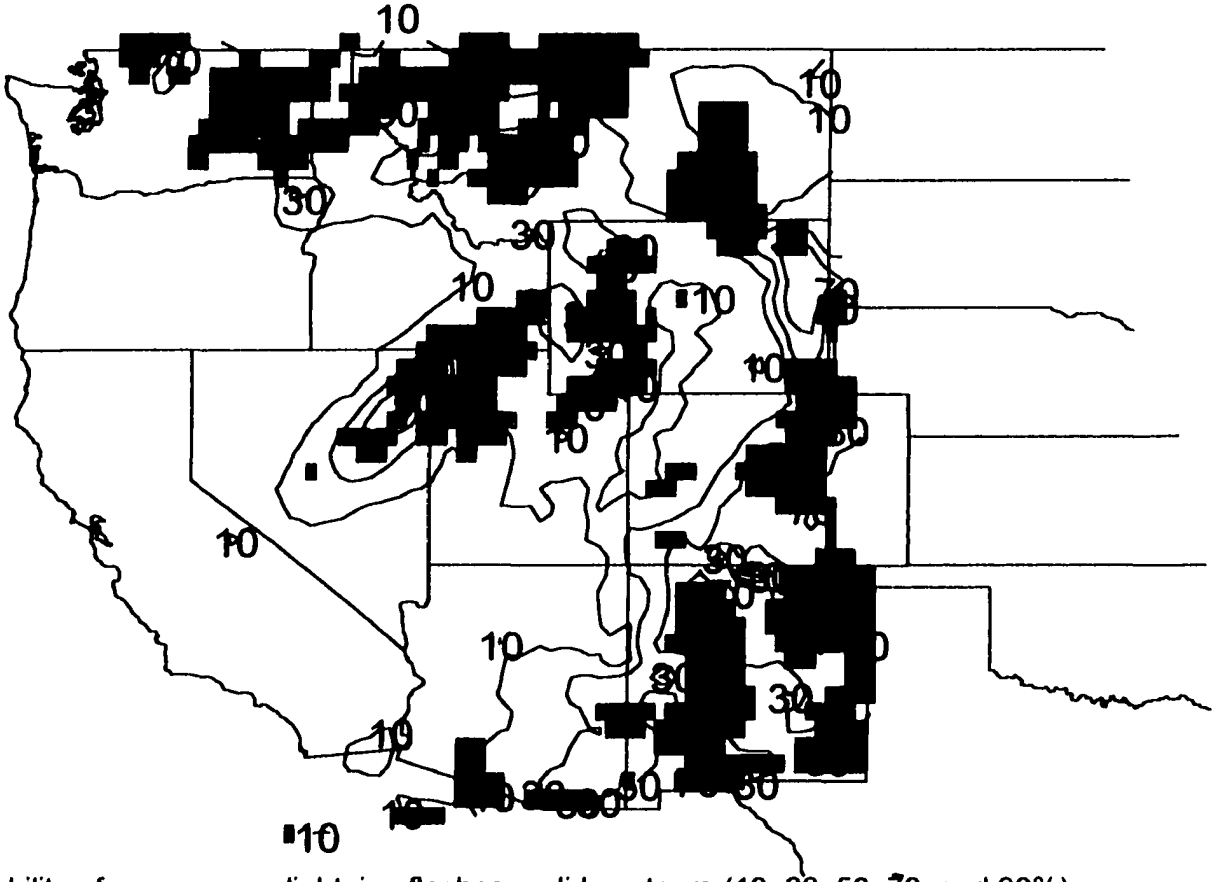

Fig. 5.9. Probability of one or more lightning flashes -solid contours (10, 30, 50, 70, and 90%) for 18 July 1999 and one or more lightning flashes per grid box detected from 00 to 03 UTC-solid color fills.

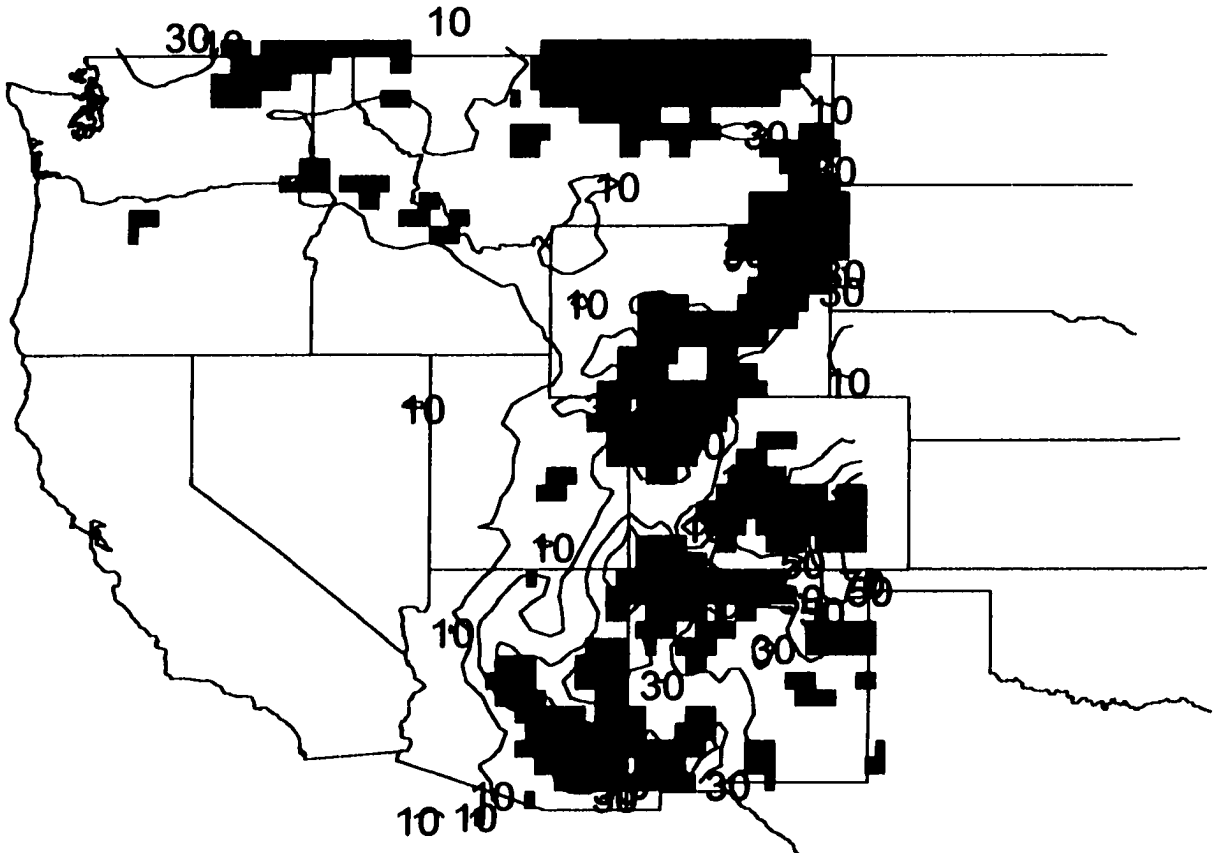

Fig. 5.10. Probability of one or more lightning flashes -solid contours (10, 30, 50, 70, and 90%) for 22 July 1999 and one or more lightning flashes per grid box detected from 00 to 03 UTC-solid color fills.

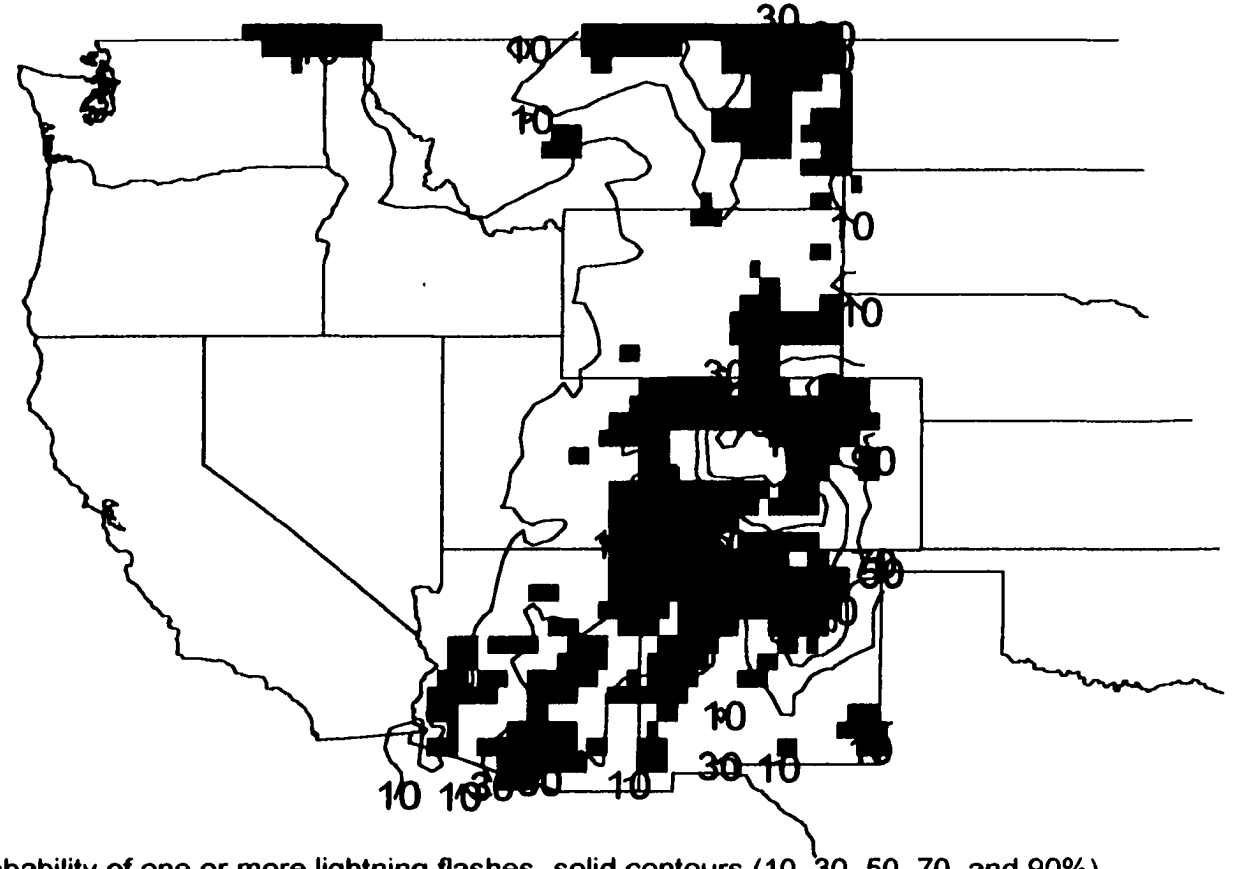

Fig. 5.11. Probability of one or more lightning flashes -solid contours (10, 30, 50, 70, and 90%) for 25 July 1999 and one or more lightning flashes per grid box detected from 00 to 03 UTC-solid color fills.

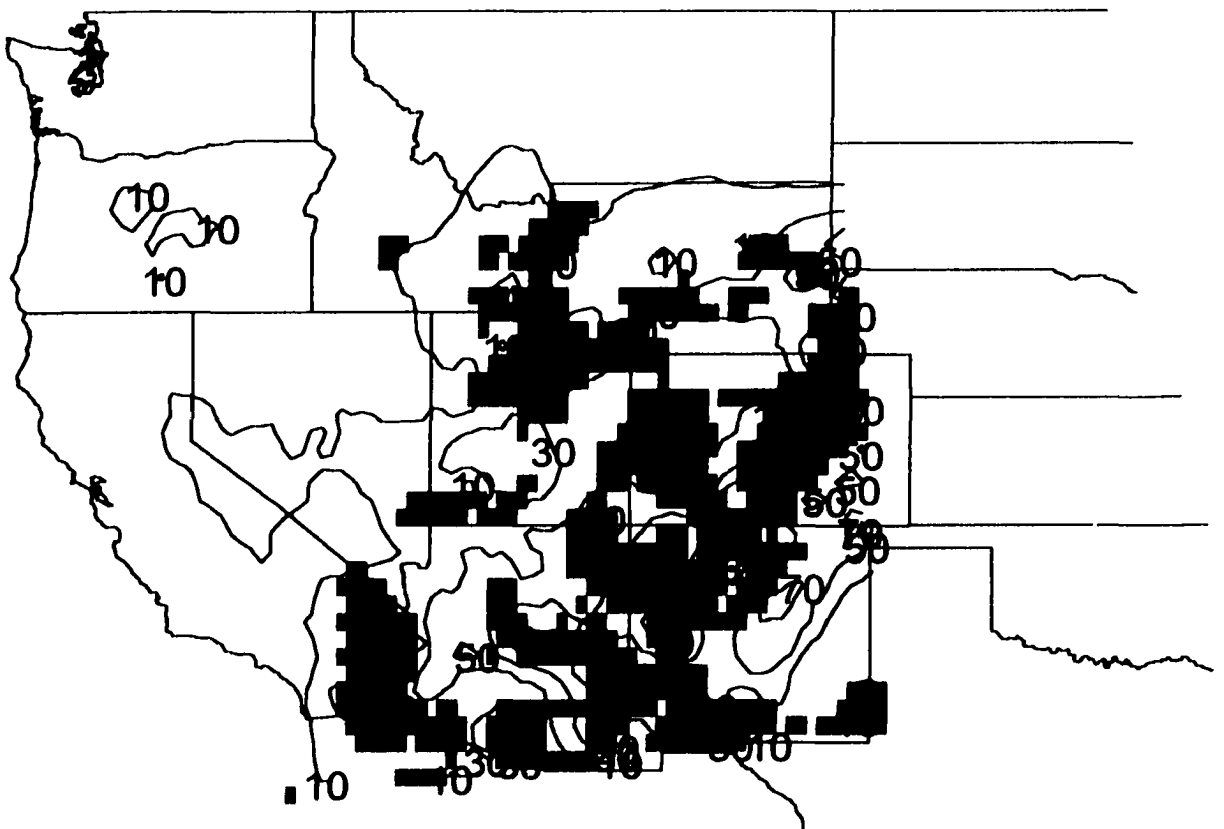

Fig. 5.12. Probability of one or more lightning flashes -solid contours (10, 30, 50, 70, and 90%) for 29 July 1999 and one or more lightning flashes per grid box detected from 00 to 03 UTC-solid color fills.

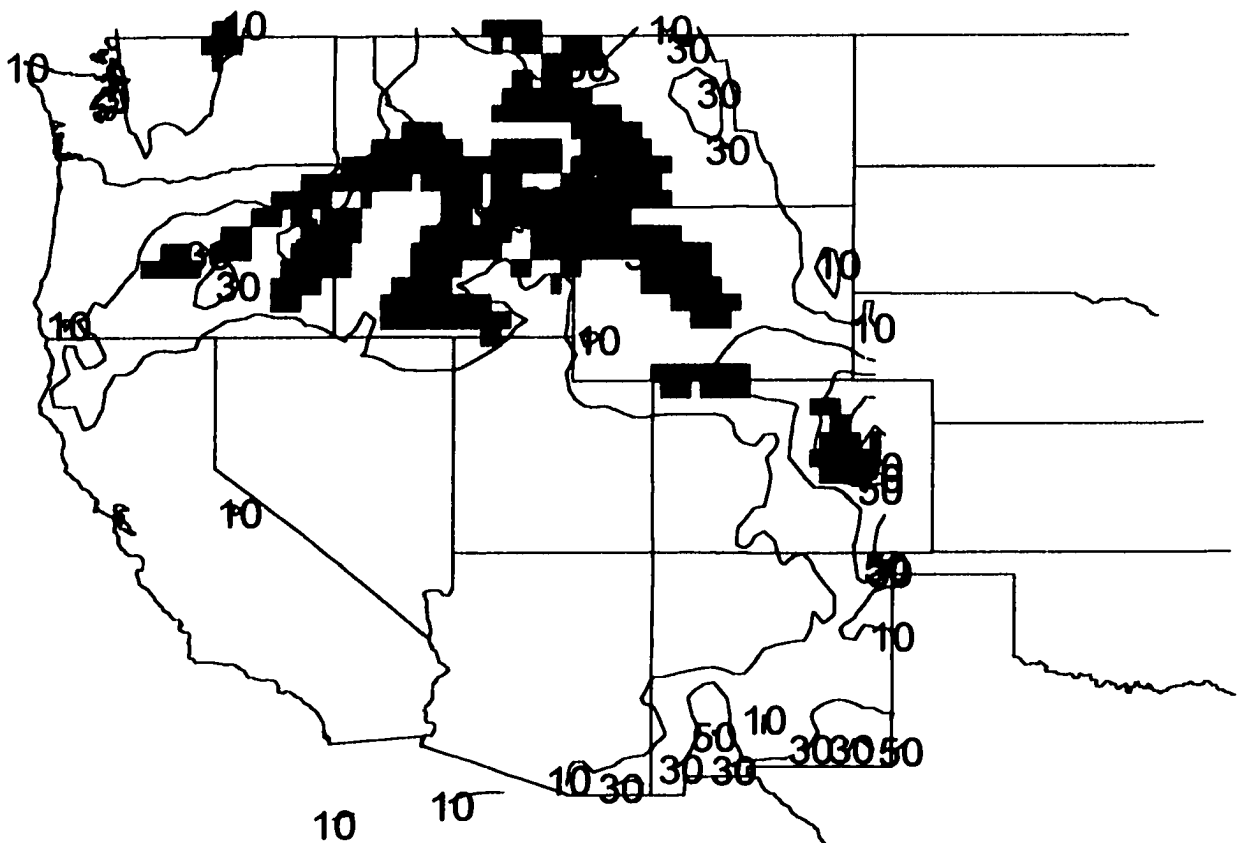

Fig. 5.13. Probability of one or more lightning flashes -solid contours (10, 30, 50, 70, and 90%) for 13 August 1999 and one or more lightning flashes per grid box detected from 00 to 03 UTC-solid color fills.

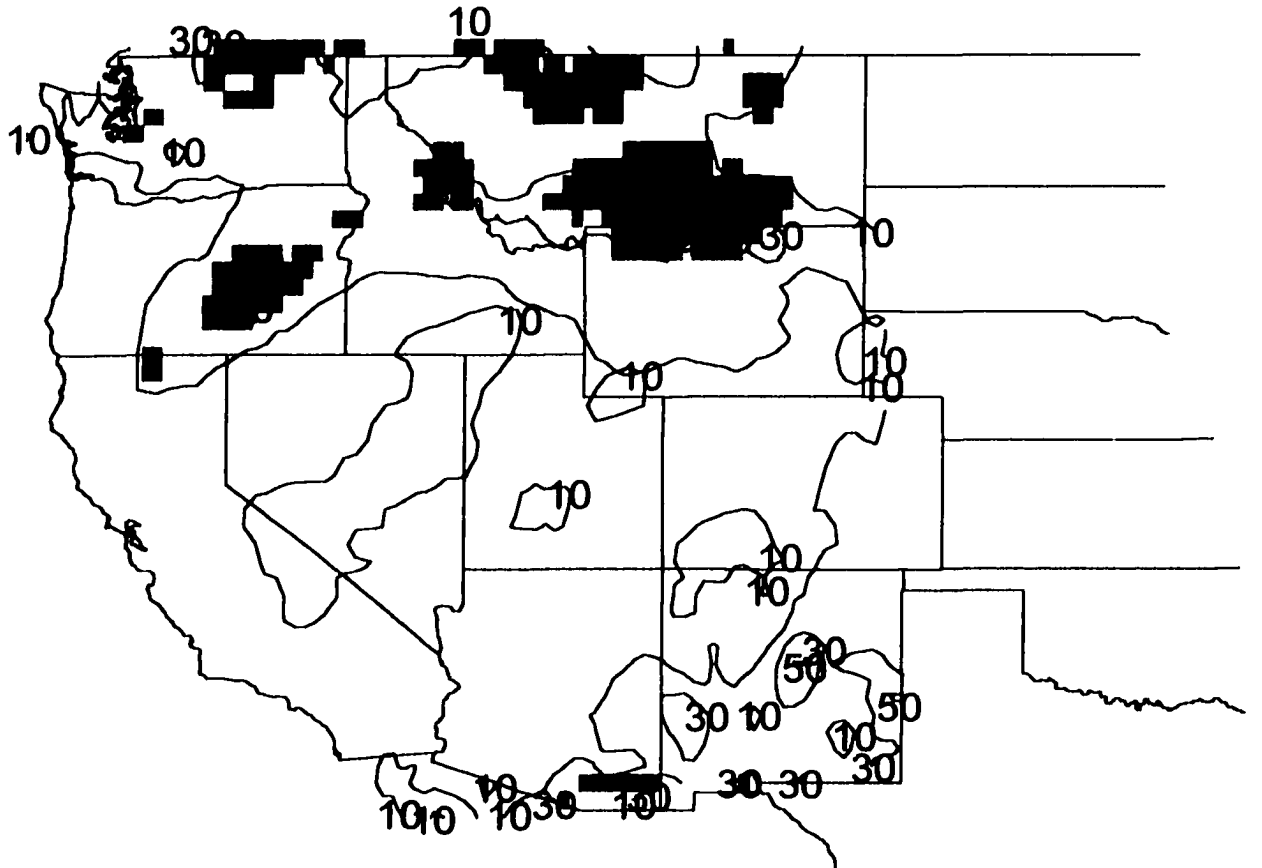
10
10
10

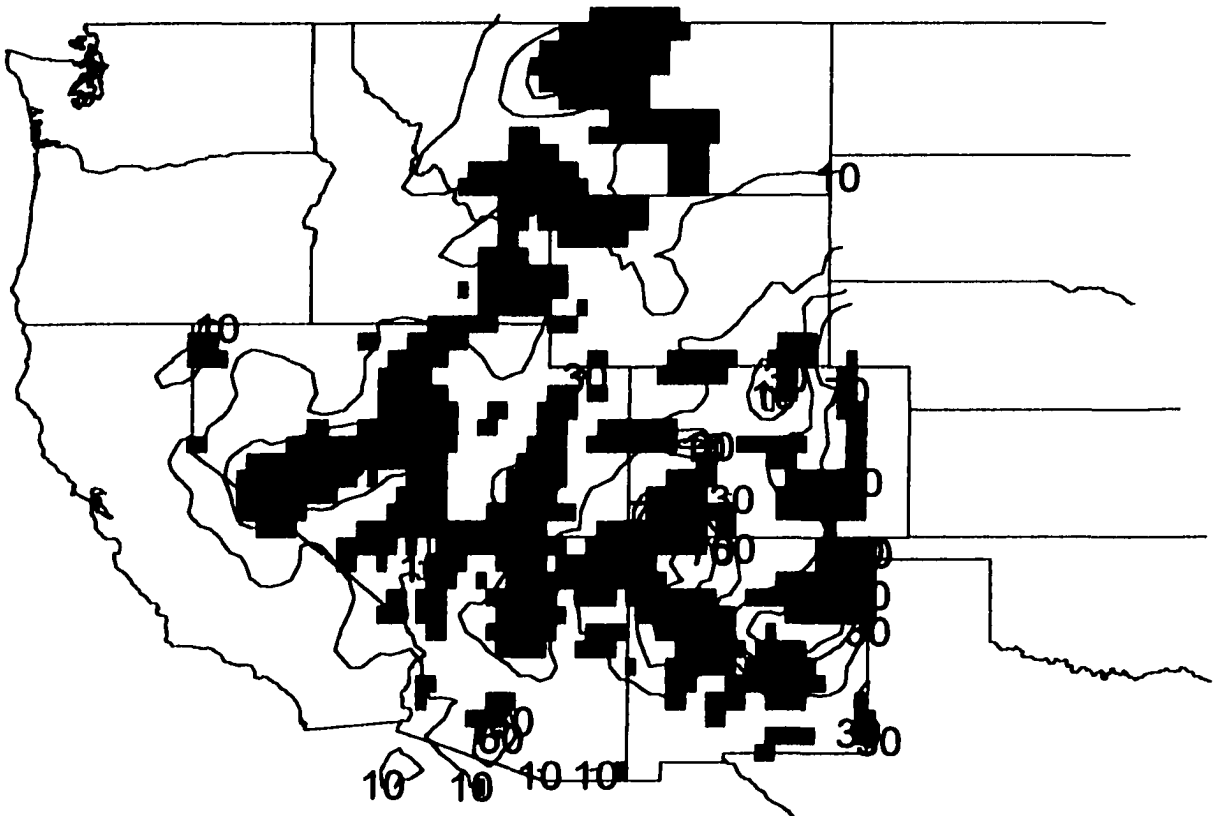

Fig. 5.15. Probability of one or more lightning flashes -solid contours (10, 30, 50, 70, and 90%) for 22 August 1999 and one or more lightning flashes per grid box detected from 00 to 03 UTC-solid color fills.

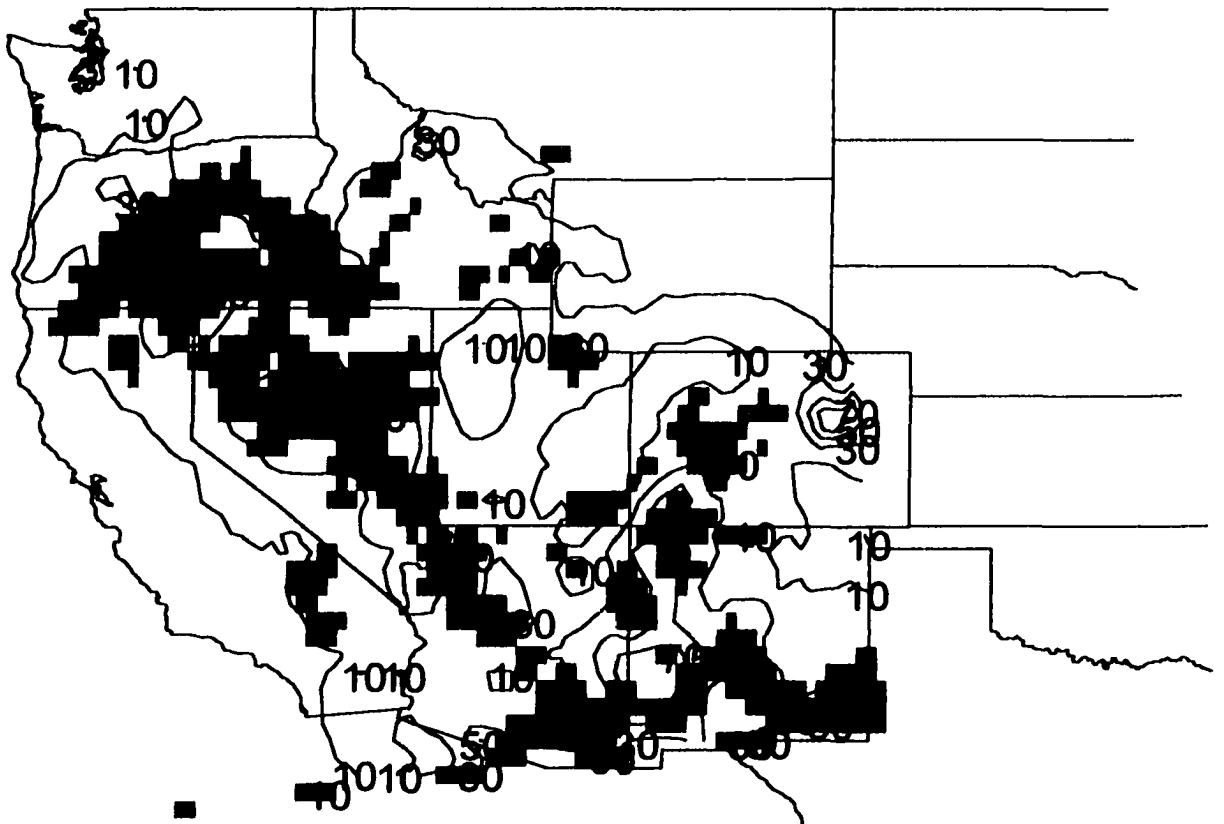
10
10
30
10
10
10
30
30
10
10
10

events. Conversely, it was rare that a forecast area of 10 percent or higher existed with no lightning observed in or near the area.

Inspection of individual days reveals the successes and failures of the technique. For example, the 10 percent forecast probability contour for 3 June 1999 shown in Fig. 5.1 captured the significant lightning across all sections of the western U.S. domain. Figure 5.2 for 8 June shows that the 10 percent contour captured the lightning across the northern half of the domain but there is an area of probabilities from 30 to 50 percent in southern Colorado and eastern New Mexico where no thunderstorms occurred from 00 to 03 UTC. Inspection of the data in this area indicated that the CAPE values that were analyzed represented surface air parcels that would have to be lifted over 200 mb through very dry air in the lower levels of the atmosphere to reach saturation (i.e., the LCL). It is likely that mixing with the dry air effectively eliminated the parcel buoyancy across this area. The forecast probabilities for 14 June 1999, as shown in Fig. 5.3, capture the significant convection that occurred. Figure 5.4 shows that the forecast probabilities of 10, 30, 50, 70 and 90% capture all of the significant convection for 17 June.

One case where a significant area of 10 to 30 percent forecast probabilities existed and no lightning occurred was for 23 June 1999 (Fig. 5.5). Only the extreme eastern section of the domain had lightning. It should be noted that a large area of thunderstorms occurred from 00 to 03 UTC from central and western Nebraska into western Kansas and extreme northeastern Colorado, immediately east of the area of greater than 50 percent probability in eastern Colorado and Wyoming. Figure 5.6, valid for 00 to 03 UTC on 28 June 1999, shows good agreement between the forecast

probabilities and the lightning with the exception of eastern Colorado. No thunderstorms were observed in eastern Colorado. The grid point data for that area indicates that it was analyzed as an area of MUCAPE (surface based) greater than 3500 J kg^{-1} and was not capped. Also, while the vertical motion field from the RUC 2 showed rising motion in the lowest levels, there was downward motion analyzed between 700 and 400 mb. This downward motion, along with cooling after 00 UTC, and lack of low level forcing, could have contributed to the absence of thunderstorms. The flow immediately off the surface was from the west at 10 to 20 m s^{-1}, which in that area of Colorado could have contributed to drying and downward motion, further decreasing the parcel buoyancy.

The independent case from 9 July is shown in Fig. 5.7. The forecast probabilities capture all of the significant activity during that time period. One area immediately off the coast of southern California has forecast probabilities from 10 to over 50 percent. Two main quantities appear to have produced this false alarm. First, even though the low levels were stable, the grid point data reveals that MUCAPE of approximately 100 to 150 J kg^{-1} was diagnosed just above 700 mb. Second, a very strong upper-level divergence center was analyzed off the coast with very strong upward motion analyzed from 700 to 400 mb over this area. Observational data did not support this center and may indicate an analysis problem.

For the five independent days shown in Figs. 5.8 through 5.12, there is generally very good agreement between the forecast probabilities and the lightning. Figure 5.13 for 13 August 1999 verifies well although there are forecast probabilities of 30 to 50 percent on the southern New Mexico border. When all lightning data is plotted for

the 00 to 03 UTC time period on 13 August, there was an extremely large area of thunderstorms in Mexico, immediately south of New Mexico (i.e., adjacent to, but outside the western U.S. grid used in this study). Figure 5.14 shows that across the northern half of the domain, the forecast probabilities verify well. There are several smaller areas across the southern half of the domain where the forecast probabilities were the order of 10 percent, yet no lightning was observed. Several areas above 30 percent probability are noted across central New Mexico on 14 August 1999. Similar to other days, these seem to be related primarily to high MUCAPE values which may or may not be real. The higher probabilities near 30 percent on the Arizona and New Mexico borders coincide with an area of lightning that was just on the U.S. border and extended southward into northern Mexico. The forecast probabilities for 22 August 1999 encompass all significant lightning (Fig. 5.15). Finally, the forecast probabilities verify well with the exception of eastern Colorado for the last independent day, 24 August 1999 (Fig. 5.16). Examination of model soundings in this area indicates the moisture was shallow, allowing it to mix out, thus decreasing the buoyancy.

As shown by the cases presented herein, the probabilities were closely related to the CAPE fields produced from the RUC 2 analyses. The RUC 2 occasionally exhibited unrealistically high CAPE values (as shown in Fig. 5.5) primarily over the higher elevations of east-central California, which produced errors in the forecasts. In these instances, the unrealistic CAPE values contributed in part to the production of forecast probabilities of 10 to sometimes 30 percent, which did not verify. Operationally, a quality control scheme would have to be developed to insure that these known

types of errors could be filtered out. Information on this error was relayed back to the RUC 2 developers, who were investigating the problem.

Figures 5.17, 5.18, and 5.19 provide insight into how the forecast probabilities perform compared with observed lightning. The median value (i.e., the 50th percentile) of the forecast probabilities are not subject to "outliers" and can provide a good measure of the value of the forecast. The box and wiskers plots in Figs 5.17-5.19 show the median, which is bounded by the upper (blue) and lower (red) quartile boxes. For each box, the "notched" intervals around the median (Velleman and Hoaglin (1981) indicate a difference in a location of the median at a 5% significance level (i.e., there is a 95% probability that the median is within the notched interval). The inter-quartile range extends 25 percent below to 25 percent above the median. Data that are separated from the upper/lower quartile by more than 1.5 times the inter-quartile range (the "whiskers") are considered outliers and are plotted as dots.

The box plots in Fig. 5.17 illustrate how the forecast probabilities can be interpreted. The median values for the forecast probabilities range below 5 percent when there are no observed flashes to over 25 percent when there are 1 to 9 flashes. The median values are over 30 percent for 10 to 99 flashes and above 40 percent for 100 to 999 flashes. Also, the probabilities are at, or below, 15 percent (shown by the dash-dotted line) over 75 percent of the time when no flashes are observed and above 15 percent over 75 percent of the time when flashes are observed.

Similar types of probability plots, along with the verifying lightning flashes, were produced for the forecast probability of 10 or more flashes and 100 or more flashes as shown in Figs. 5.18 and 5.19. As shown previously in Fig. 3.3, about one-

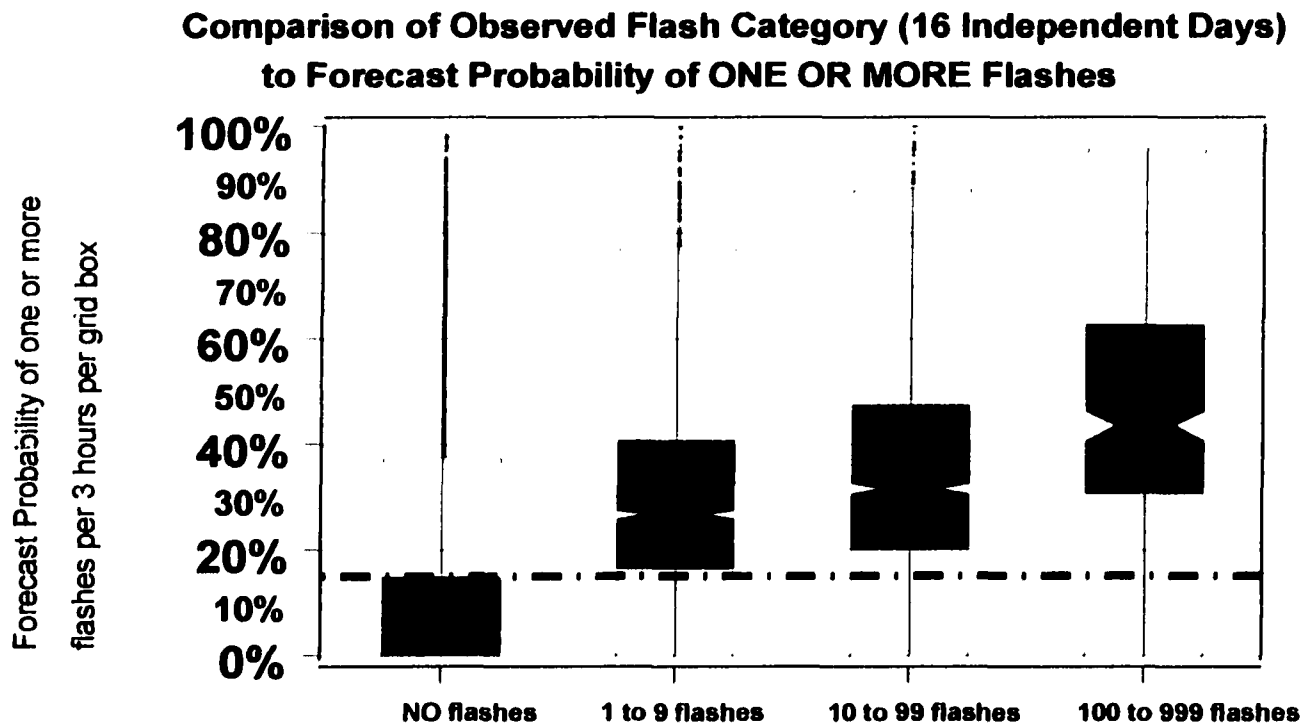

Fig. 5.17. Box and wiskers plot for total number of observed flashes per 3 hours per grid box versus forecast probability of one or more flashes. Median is between upper and lower (hatched) quartiles, 95% confidence (notched) interval around median, wiskers represent 1.5 times the interquartile range, and outliers are shown as dots. Dashed-dotted line is 15 % forecast probability (see text for discussion).

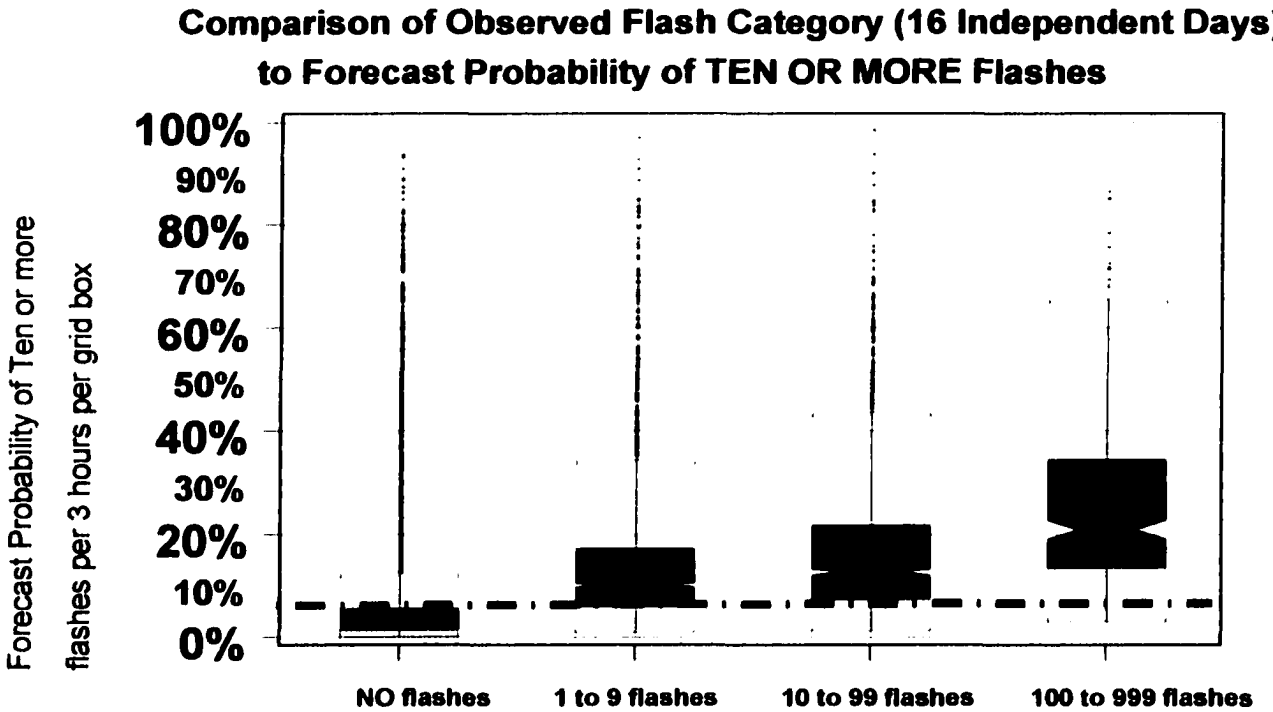

Fig. 5.18. Same as 5.17 except for forecast probability of 10 or more flashes. Dashed-dotted line is at 5 %.

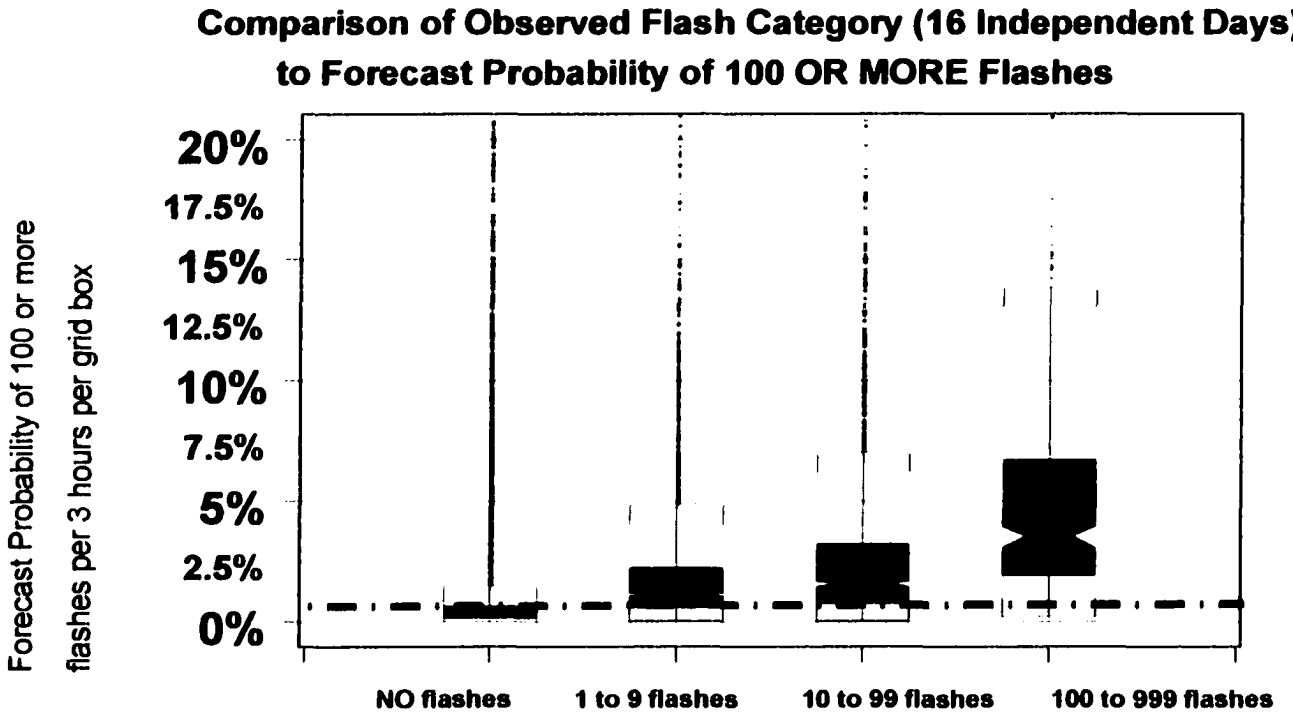

Fig. 5.19. Same as 5.17 except for forecast probability of 100 or more flashes. Dashed-dotted line is at 0.75 %. (Note: Y axis has changed to show forecasts from 0 to 20%)

half as many grid boxes report ten or more flashes as report one or more (i.e., 2191 grid boxes with 10 or more, versus 4835 grid boxes with one flash or more). The number of grid boxes reporting 100 or more flashes drops to less than one-tenth as many as are reported for one or more (355 versus 4835). Thus, for events that become less and less likely, corresponding forecast probabilities are also lower. In Fig. 5.18, the median value for the probability of ten or more is less than 5 percent when no flashes are reported, while it is above 12 percent when ten or more flashes are reported. Although a large change is not seen between forecast probabilities of 1 to 9 flashes and 10 to 99, the "notched" intervals around the medians for 1 to 9 and 10 to 99 flashes do not overlap, indicating a difference in the medians at a 5% significance level. When one hundred or more flashes are observed, the median of the forecast probability of ten or more flashes increases to 20 percent.

When specifically forecasting the probability of a rare event such as one hundred or more flashes (this occurred less than one percent of the time as shown in Fig. 3.3), Fig. 5.19 shows that, despite the lower probabilities, the median value of 3.5 for one hundred or more flashes is more than double the median value of 1.5 percent when 10 to 99 flashes are reported. The median for 100 or more flashes is ten times higher than the median value when no flashes are reported (0.3 compared to 3.5 percent).

Figures 5.20 and 5.21, from the same day as in Fig. 5.4 (i.e., 17 June), are typical examples of the forecast probabilities for 10 and 100 or more flashes, respectively. Viewing these probability forecasts for 10 and 100 or more flashes from the perspective of the location of the maximum probabilities shows that the forecasts are able to indicate the areas of high flash densities in many cases. The forecast probabilities

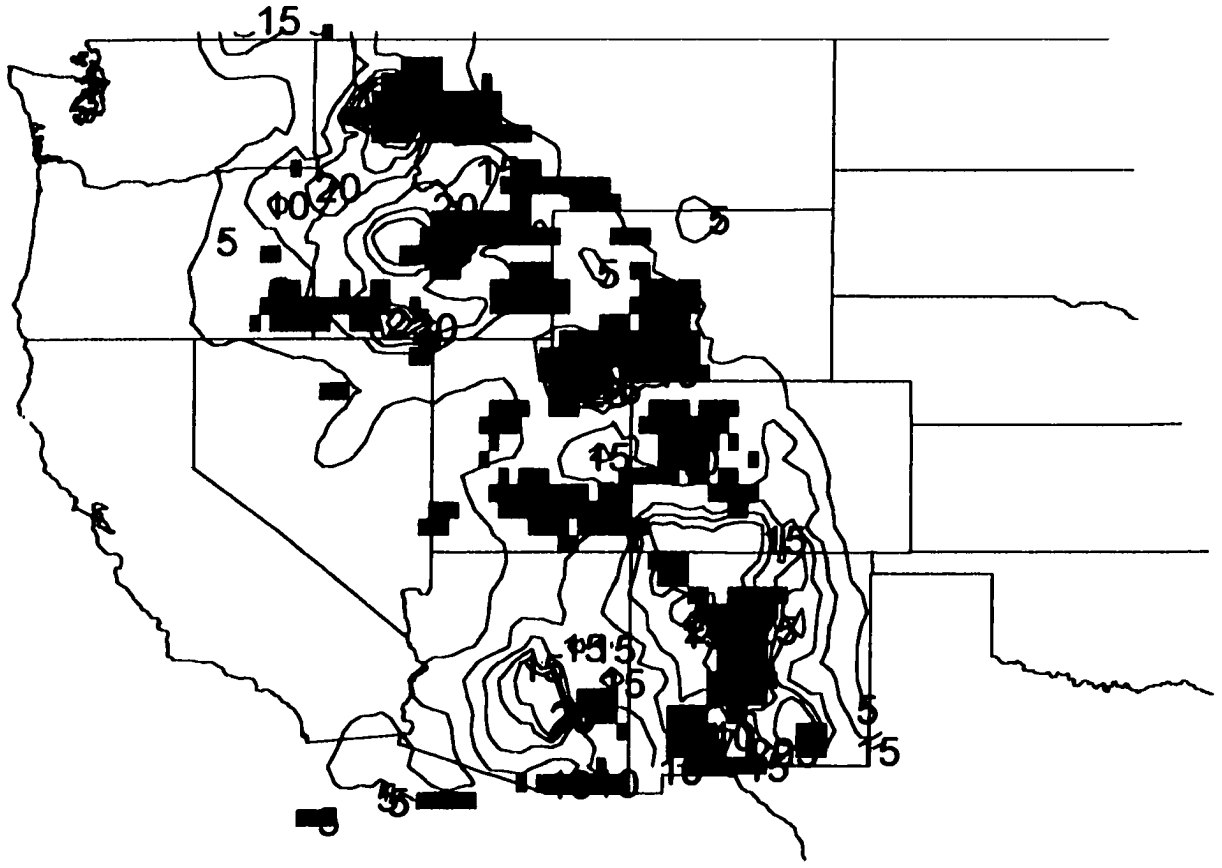

Fig. 5.20. Probability of 10 or more lightning flashes - solid contours (5, 10, 15, 20, 25%) for 17 June 1999 and ten or more lightning flashes per grid box detected from 00 to 03 UTC - solid color fills

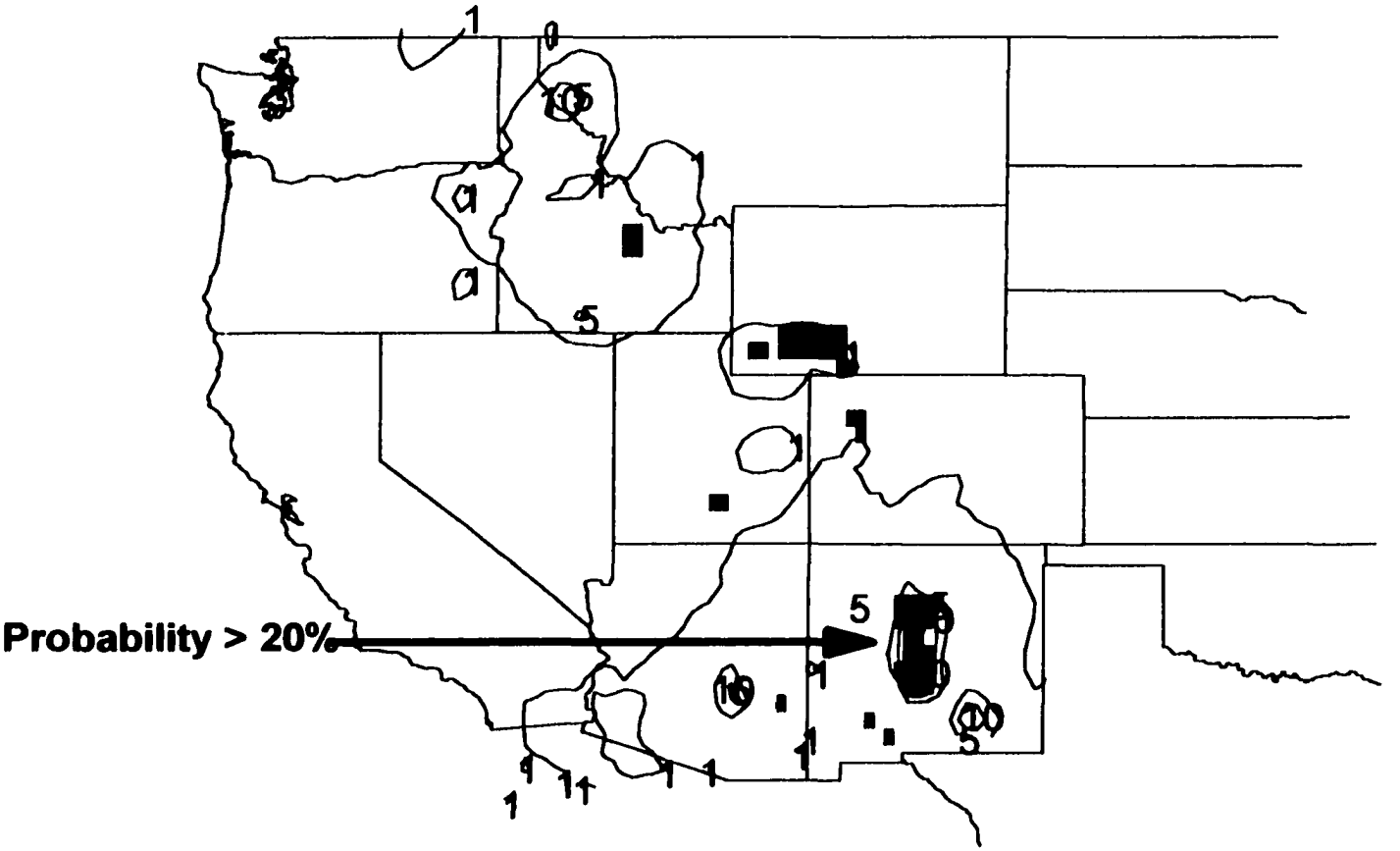

Fig. 5.21. Probability of 100 or more lightning flashes - solid contours (1, 5, 10, and 20%) for 17 June 1999 and 100 or more lightning flashes per grid box detected from 00 to 03 UTC - solid color fills

show an overall decrease in magnitude from the probability of one or more flashes as in Fig. 5.4, but the relatively higher probabilities on each plot are able to identify the locations of the higher flash densities. Fig. 5.21 illustrates how the forecast probabilities correctly forecast an area in central New Mexico of over 300 flashes per grid box.

To illustrate the value of the probabilities, a reliability diagram for the forecasts of one or more flashes was constructed (Fig. 5.22). Ten forecast probability groups were formed (0-9.99, 10-19.99, 20-29.99,.... and 90-100%). The percentage of times lightning occurred in a grid box for each of the 10 forecast groups was then calculated and plotted against the mid-point probability for each group (solid triangles). The logistic regression forecast probabilities yield good reliability for probabilities less than 70%. The slope of the least squares line, shown by the solid line and fit to the points indicated by solid triangles from 5 to 65 percent, also exhibits good reliability (through 65%). It is similar in slope to a line for a hypothetical forecast with perfect reliability (dashed line connecting points shown by solid diamonds). It also exhibits similar behavior to perfect prog output (Glahn et al. 1991) (i.e., slight under-forecasting at low probabilities, crossing the curve for perfect reliability near 20 percent (an average climatological value) and slight over-forecasting from 45 to 65 percent). The higher percentages (above 70%) show there is significant over-forecasting. The least-squares line that fits points from 5 through 95 percent changes dramatically when the higher (over-forecasting) values are included (dash-dotted line). However, because very few points are forecast and/or observed in this high range, it is felt that no firm conclusions can be reached with this limited data set.

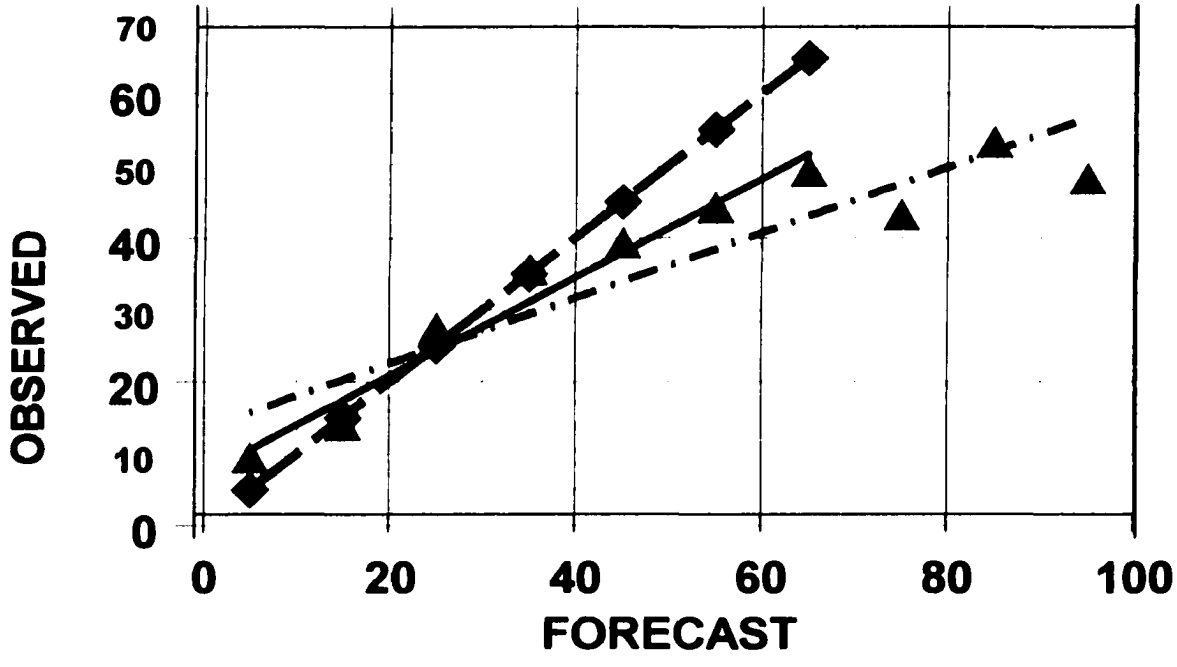

Fig. 5.22. Reliability diagram for all independent forecasts of one or more flashes (16 days). Logistic Regression -Solid triangles-mid point for each interval (0-9.99, 10-19.99,...90-99.99%). Solid line-least squares fit for 0 to 70%, and dashed-dotted line is least squares fit for all forecasts (0 to 100%). Perfect Forecast-Solid diamonds - dashed line.

To provide objective measures of the performance of the forecast probabilities, the percent improvement over the climatological probability (relative frequency) was computed from the half-Brier scores (see Appendix G). For the time period 00 to 03 UTC, the percent improvement over the climatological probability was 9 percent. For perspective, a 9 percent improvement for a three-hour forecast period appears to be comparable to the improvement over climatology of the 6 hour lightning probability forecasts from the AVN model and approximately equal to the percent improvement over climatology for the 24 hour NGM thunderstorm forecasts from the 00 UTC cycle (Hughes 2001). The 9 percent improvement is significant, because the percent improvement over climatology (as shown by Hughes for the AVN), drops as the length of the forecast interval decreases from 24 to 6 hours.

Other objective measures of the value of the lightning forecast probabilities (Appendix G) are the Probability of Detection (POD), False Alarm Rate (FAR), Critical Success Index (CSI) and Bias. These are shown in Table 5.1 and Fig. 5.23.

	POD	FAR	CSI	BIAS
10%	0.91	0.73	0.26	2.5
20%	0.72	0.65	0.31	2.1
30%	0.49	0.60	0.28	1.21
40%	0.31	0.56	0.22	0.73
50%	0.17	0.49	0.14	0.34

Table 5.1 Verification scores for forecast probabilities (10, 20, 30, 40, and 50%) of one or more flashes per grid box per three-hour period.

As Table 5.1 and Fig. 5.23 show, the CSI reaches a relative maximum (0.31) at around 20 percent forecast probability. The bias approaches 1.0 for a forecast probability between 30 and 40%. When compared to the SCAN extrapolative forecasts

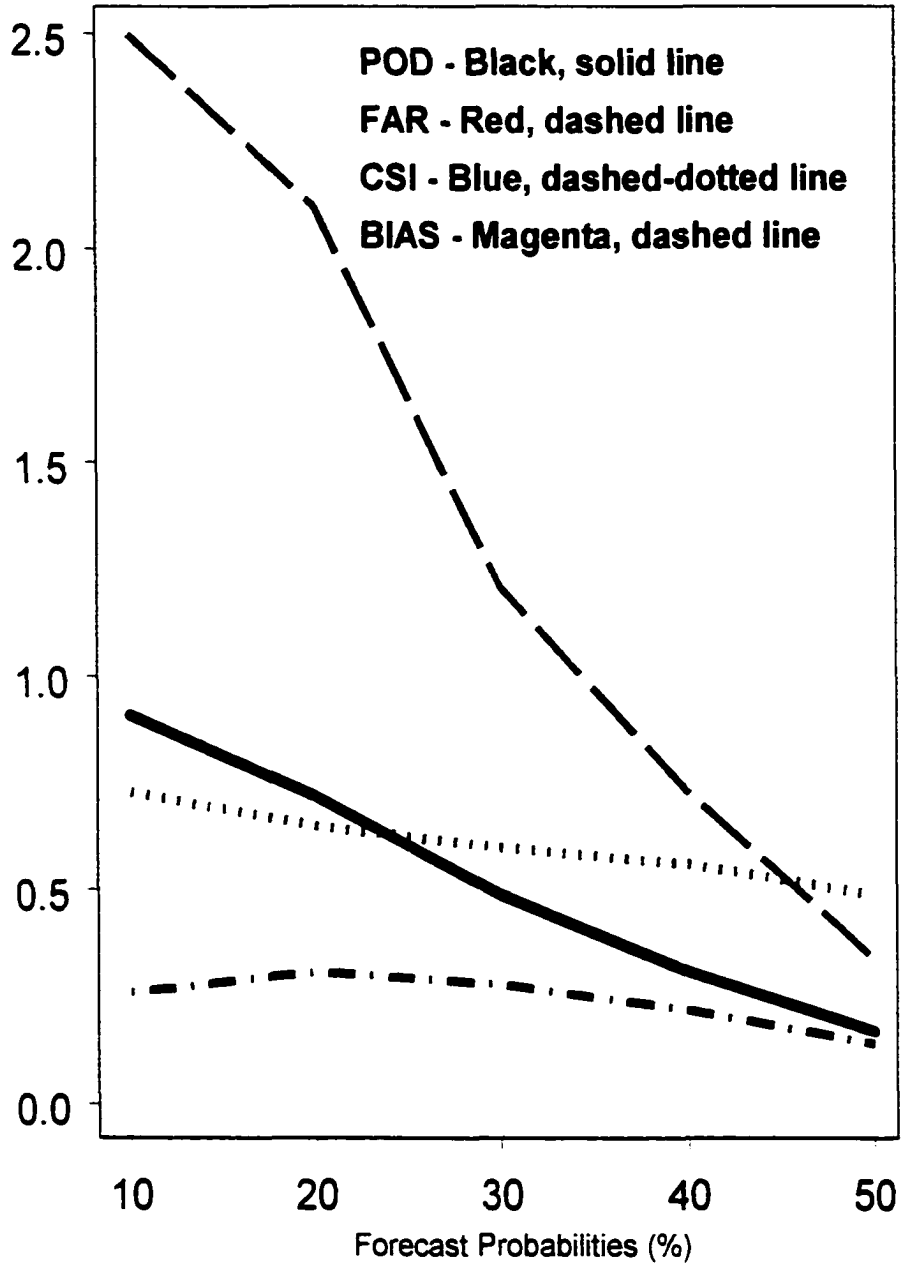

Fig. 5.23. POD, FAR, CSI and BIAS for independent data set (16 days). Probability of one or more flashes.

(Kitzmiller et al. 1999), the bias in this study is higher than those from the SCAN forecast, but the POD, FAR and CSI are similar to the verification scores from SCAN. The SCAN forecast scores, however, are from a dependent data sample, while the forecast skill scores in this study represent those from independent data. As in the case for most verification schemes, skill scores will not be as good when validated on independent data sets.

5.2 Conceptual Model for Storms That Produce Lightning

One way to visualize complex atmospheric processes is through a conceptual model that relates a series of observations to the phenomenon being studied. In this case, the model is used to relate quantities derived from thermodynamic parameters as well as the lightning climatology to the observed lightning flashes. Additionally, the model will be used to explain differences between cases of lightning versus no lightning (see Table 5.2) and cases of low numbers of flashes compared to a high number of flashes (Table 5.3).

5.2.1 Lightning Versus No Lightning Cases

A box and wiskers plot of the median values for the climatological probability of one or more flashes (Fig. 5.24) shows that the observed number of flashes in 1999 increases as the median climatological probability increases. The median probability doubles from 7 percent, when no flashes are observed, to 15 percent when one or more flashes occur. Similar differences are noted in the average length of time lightning is

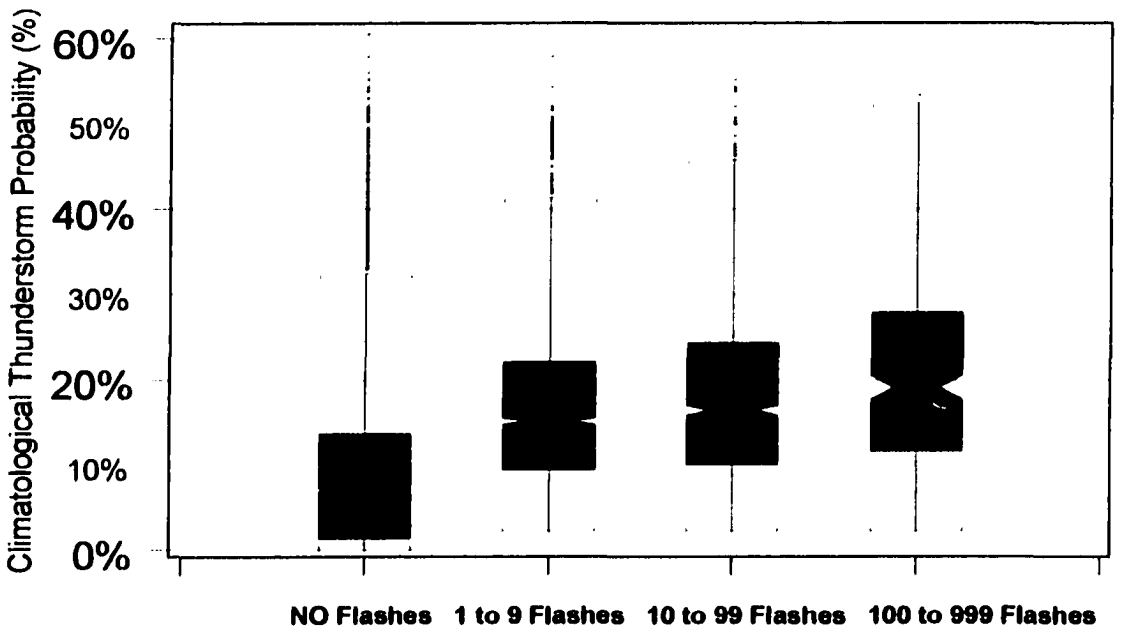

Fig. 5.24. Box and wiskers plot for climatological thunderstorm probability when each flash category (none, 1-9, 10-99, 100-999) is observed.

observed and the average number of flashes (Figs. 5.25, and 5.26). The median climatological length of time that lightning occurs is less than 10 minutes in the grid boxes when no thunderstorms were observed in June, July, and August of 1999 and approximately 20 minutes when lightning was observed during the same period. The median number of flashes from the lightning climatology is approximately 1 flash for the grid boxes where lightning flashes did not occur, and 2 or higher when one or more flashes were reported. These findings are partially attributed to the fact that storms are more likely if the underlying conditions (below the scale used in this study) are such that longer lived storms (with higher numbers of flashes) are climatologically favored. Also, because of storm cell interactions, Ziegler et al. (1991) have shown that the first storms to become electrically active can act on adjacent thunderstorm cells through microphysical particle interaction, as well as through electrical charge interactions to accelerate charging rates and produce more flashes. Once the initial storms develop, new thunderstorms may be more likely, because new storms have the potential to develop along the outflow boundaries of previous storms. Also, storms that last longer can produce a larger number of flashes simply because of their longevity.

The capping inversion, as measured by the convective inhibition (CIN), when strong enough, can act to inhibit convection. However, for both the time of day (00 to 03 UTC) and the time period of this study in the West, the most unstable parcel CIN (MUCIN if MUCAPE greater than 0) appeared to be weak for both lightning and non-lightning cases (Fig. 5.27). The median value of the MUCIN for all cases was close to

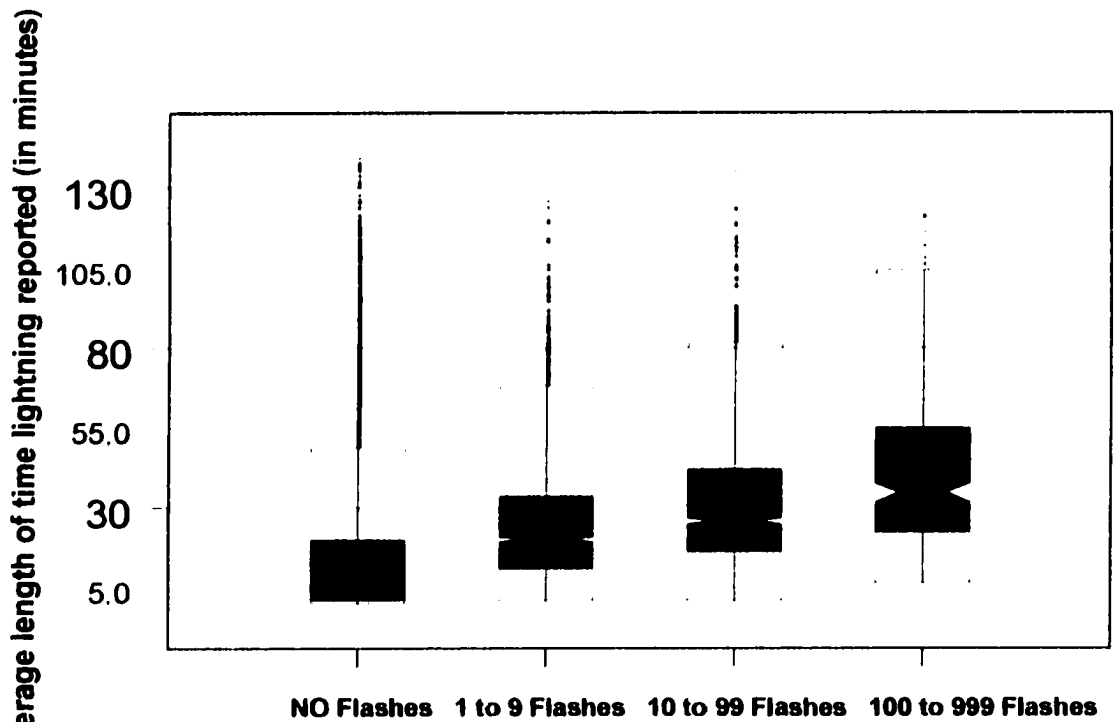

Fig. 5.25. Average length of time (minutes) that lightning is reported when each flash category (none, 1-9, 10-99, 100-999) is observed. From lightning climatology-number of 15 minute intervals with lightning divided by 12 and then converted to minutes (180 minutes maximum).

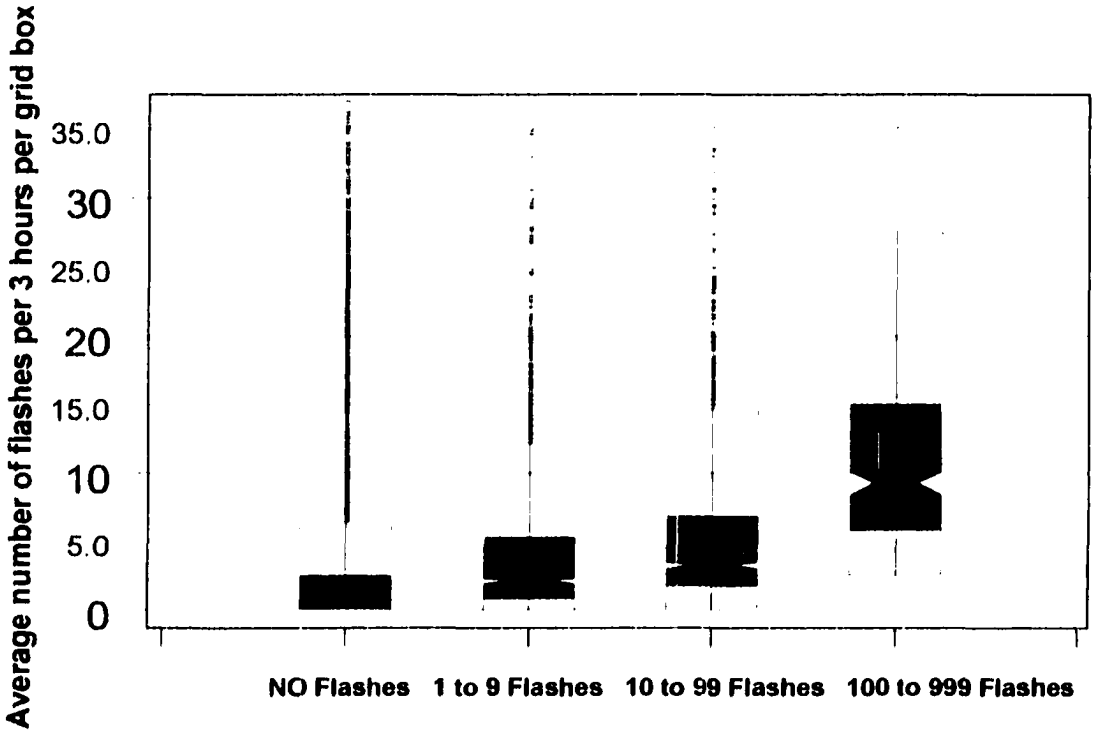

Fig. 5.26. Average number of flashes per grid box per 3 hours from lightning climatology when each flash category (none, 1-9, 10-99, 100-999) is observed.

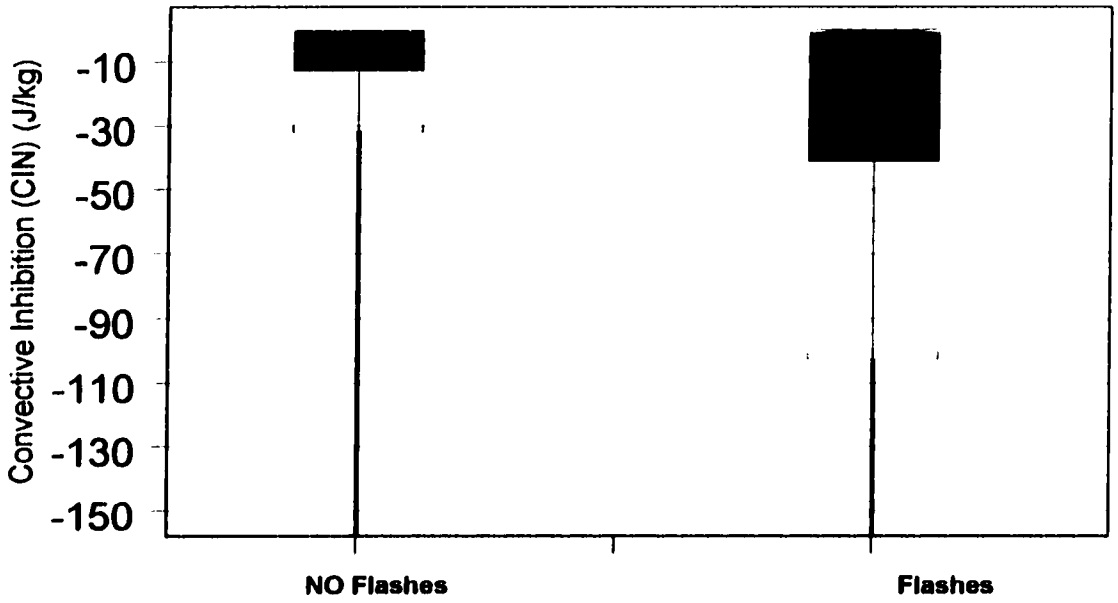

Fig. 5.27. Convective Inhibition (CIN) for no lightning/lightning cases when most unstable CAPE (MUCP) greater than 0 in 54 day developmental data set.

0 Jkg^{-1}. Also, the cap strength calculated using the most unstable parcel (not shown) was less than 1°C in over 75% of the cases.

Although the MUCIN was generally weak, the results showed that the CIN appeared slightly stronger when lightning occurred. No CIN was present in 48% of the cases with lightning and in 61% of the cases without lightning. In over 75 percent of the cases with lightning, it was less negative than approximately -40 Jkg^{-1} while it was less negative than -14 Jkg^{-1} in 75 percent of the cases without lightning. The mean value for the MUCIN with lightning was 33 Jkg^{-1} and 24 Jkg^{-1} when no lightning occurred. Figure 5.27 shows that when lightning is observed, there are grid boxes where the CIN may be slightly stronger than in the majority of the cases where no flashes are observed.

One explanation for this difference is that perhaps a weak capping inversion might favor convection because it serves to allow the lower-level temperature and moisture to increase, hence increasing the CAPE before convection breaks out. If moisture is shallow and parcels rise and continually mix with drier air above the boundary layer due to the absence of a restraining inversion, storms may not develop.

To evaluate any dependence of lightning on the vertical distribution of CAPE, each of the layer CAPE fields (CAPE from LFC to 0 °C, 0 to -5 °C, and so on) were examined. For example, there was a significant dependence of lightning frequency on the magnitude of the CAPE observed in the layer from -15 to -20 °C (Fig. 5.28). The median increased from approximately 80 J kg^{-1}, when no flashes were detected, to

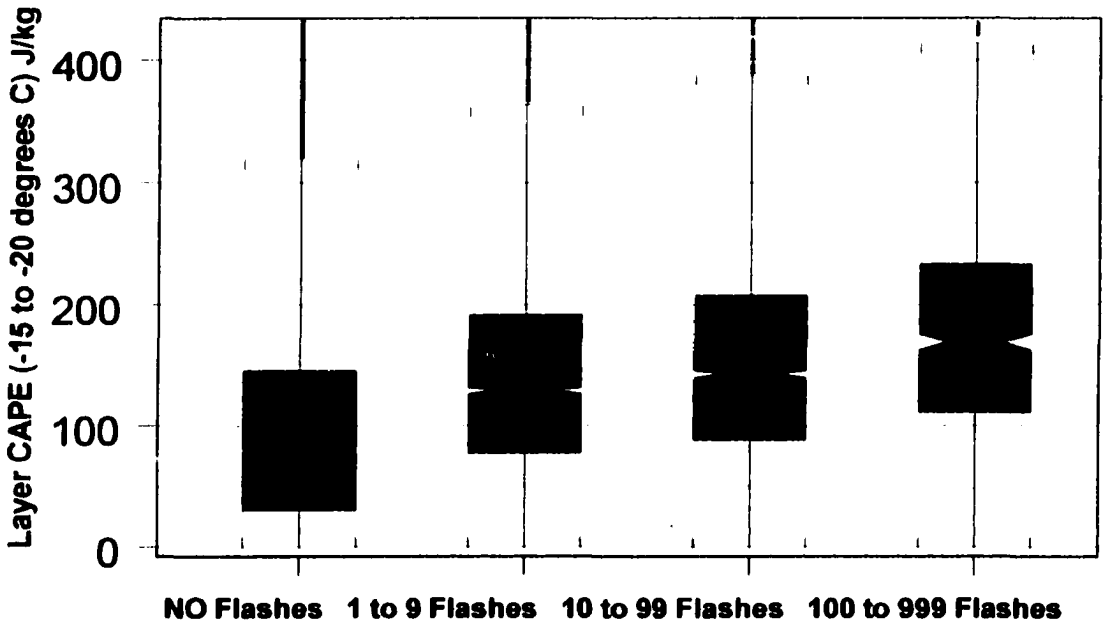

Fig. 5.28. LAYER CAPE (-15 to -20 degrees C) for cases when MUCP > 0 in 54 day developmental data set.

over 130 J kg^{-1} (over 50% higher), when one or more flashes occurred. Figure 5.29 shows that in cases when the most unstable CAPE was greater than zero and was present through at least the -20 °C level, the percentage of boxes reporting one or more flashes was between 98 and 99%. The highest percentage of grid boxes reporting one or more flashes (above 98%) occurred when CAPE was reported in the layers from -5 to -10, -10 to -15 and -15 to -20 °C.

Another method that combines the maximum information from each layer CAPE is to add the layers below -20 °C together to represent the layer from the LFC to -20 °C. When lightning is observed, the CAPE in the region from the LFC to -20 °C is greater than 500 J kg^{-1} (Fig. 5.30). It is less than 300 J kg^{-1} when no lightning occurs. Note that when a CAPE value doubles, the resulting updraft increases by approximately 1.4 or roughly 40%.

Thus the CAPE below and up to -20 °C appears critical in lightning development. This is consistent with the findings of Lhermitte and Krehbiel (1979) and others who reported that lightning activity began when the top of the radar echo of the storm grew to an altitude where the temperature was less than or equal to -20°C.

Previous investigators (Grosh 1977, Ludlam 1951) have found that a warmer cloud base, and clouds with a vertical extent greater than a minimum depth, are more likely when showers occur. These findings are likely to be important in the very early stages of precipitation formation within thunderstorms. Ludlam (1951), whose work examined rain showers, calculated a minimum cloud depth of 1500 to 1800 meters for

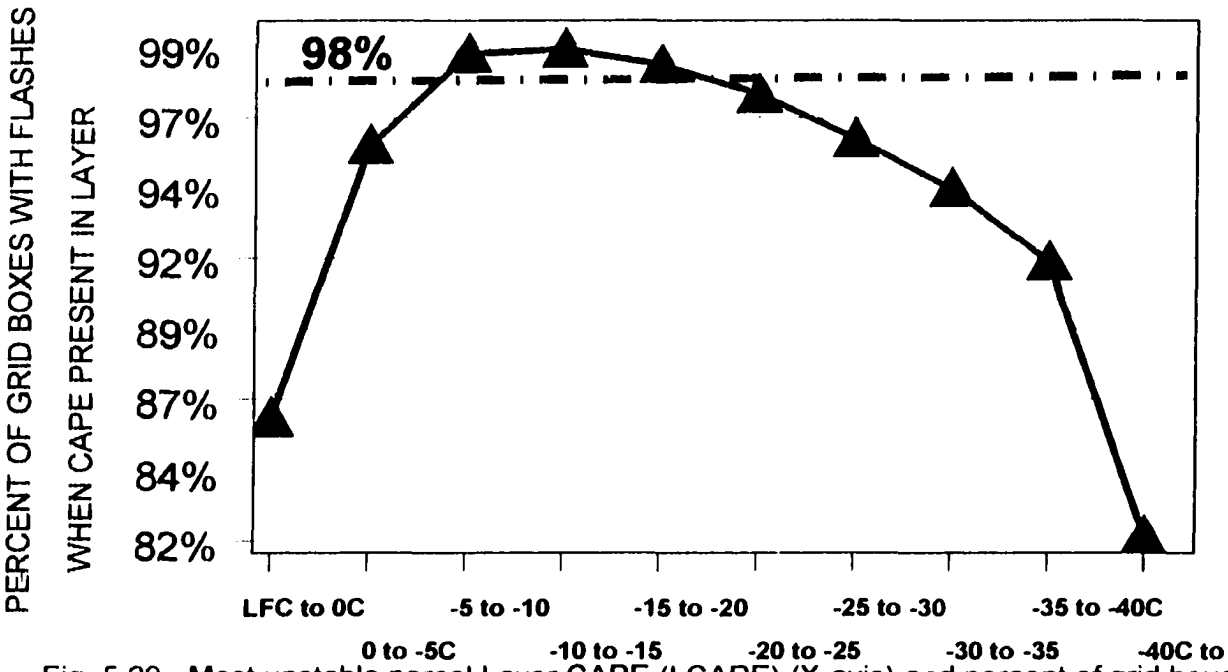

Fig. 5.29. Most unstable parcel Layer CAPE (LCAPE) (X-axis) and percent of grid boxes that have one or more flashes (Y-axis) for CAPE > 0 in the respective layer. Dashed-dotted line represents 98%.

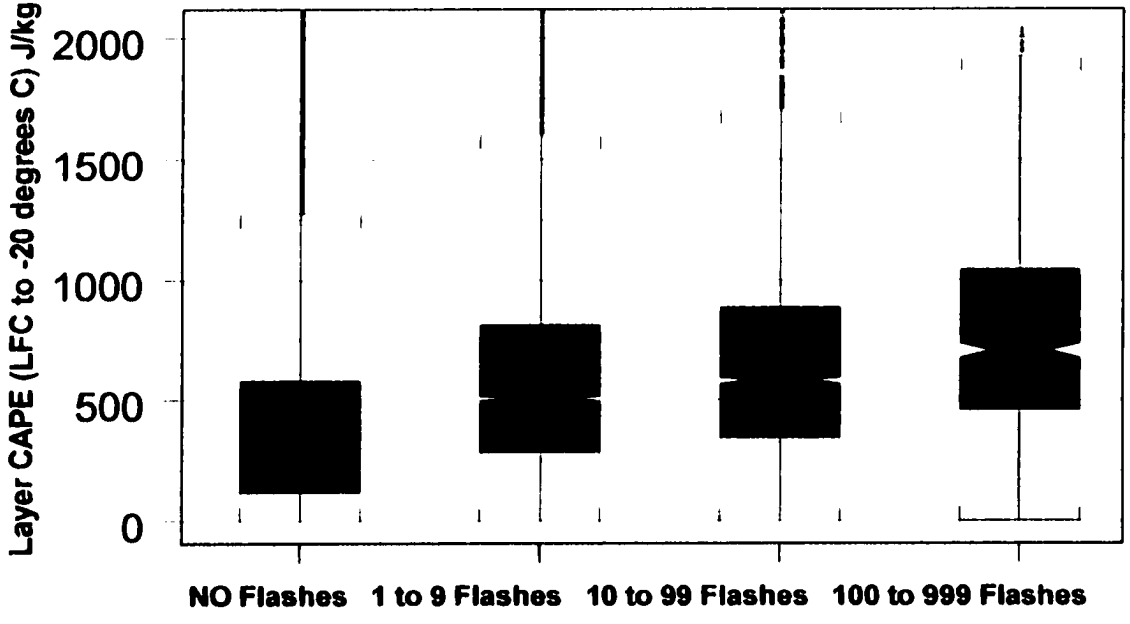

Fig. 5.30. LAYER CAPE (LFC to -20 degrees C) for cases when MUCP > 0 in 54 day developmental data set.

precipitation to occur via the coalescence process. He also predicted that if the cloud base temperature exceeded 8°C, showers could form even if the clouds did not grow to the freezing level. This was because the rain showers were able to develop through a coalescence process. This coalescence process should also be active in the lower levels of thunderstorms. Battan (1963), in a study of Arizona convection, noted that the liquid water content in a cloud at a given level increased as the cloud base temperature increased (cloud base altitude decreased). He came to the conclusion that the large cloud drops near the cloud base were growing by coalescence. Findings in this study (shown in Table 5.2 and Fig. 5.31) indicate that when lightning is reported, cloud depths (as measured from the LCL to the EL) are greater than 2500 meters. That is, when lightning is observed, there are no grid points where the computed cloud depth from the LCL to the EL is less than 2500 meters (including outliers). Conversely, there are grid points where the computed cloud depth is less than 2500 meters, and in all of those cases, no lightning occurs.

According to Grosh (1977), one of the two conditions that was more likely to produce thunderstorms was a cloud base temperature of approximately 10°C, leading to substantial updrafts at temperatures colder than 0°C. The other condition was that cloud tops were cold enough to have significant amounts of both ice and water. Holle and Maier (1982) found an increasing probability of lighting occurrence as storm height increased. This would also result in colder cloud top temperatures. In examining cloud systems with and without lightning in the tropics, Zipser (1994) proposed

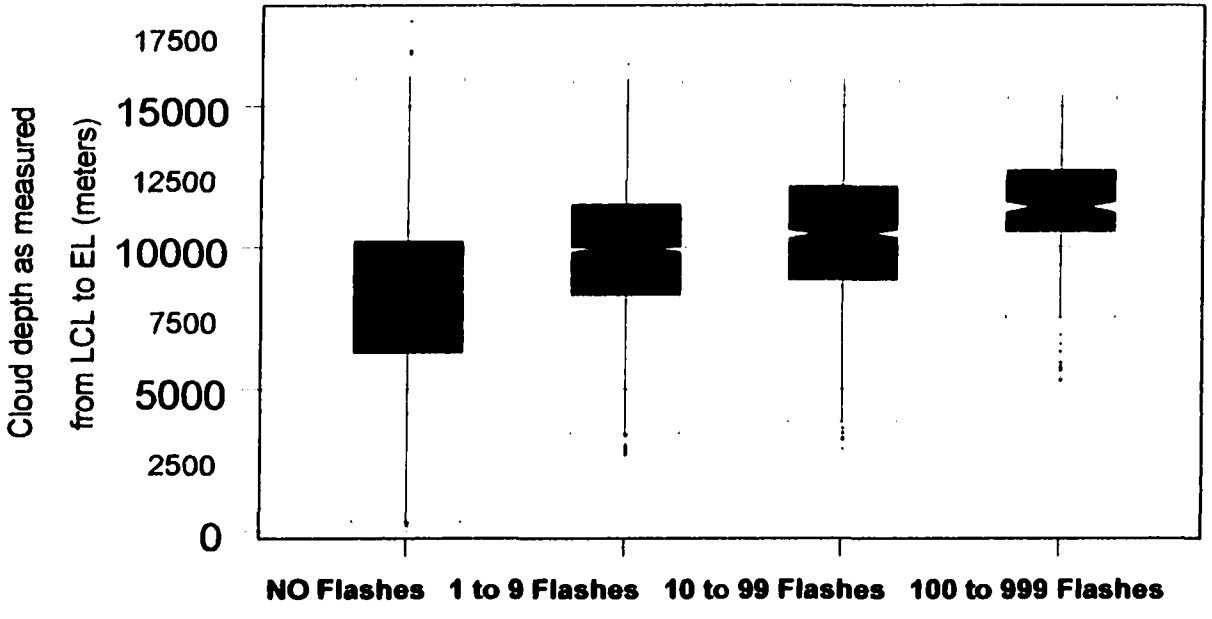

Fig. 5.31. Cloud Depth when MUCAPE >0 for grid boxes reporting NO flashes, 1-9, 10-99, 100-999.

that the difference was that the vertical velocity within the mixed-phase region (0 to -20°C) of convective cells was below a critical value estimated to be 6-7 m s^{-1} (mean updraft speed) or 10-12 m s^{-1} (peak updraft speed) during times when no lightning occurred. Based on aircraft penetrations and multi-parameter radar, electrification increased as reflectivity in the mixed-phase region increased to 40 dBZ or more. Cloud systems without lightning were missing one or both of the following: (1) large ice particles and (2) sufficient concentrations of supercooled liquid water. In this study, the median cloud base temperature (Fig. 5.32) ranges from near 4°C when no flashes occur to over 7°C when one or more flashes occur. This would support the argument that a warmer cloud base allows for a stronger updraft and higher liquid water content through the coalescence process.

The thunderstorm updraft perhaps plays the most important role in the storm electrification process. The updraft is key to the graupel-ice, noninductive charging mechanism. As stated by MacGorman and Rust (1998), "of the various types of non-inductive mechanisms that are possible, the graupel-ice mechanism is the only one thus far that detailed laboratory and modeling studies have suggested is capable of causing clouds to become electrified enough to be thunderstorms.... Furthermore, the observed dependence of graupel-ice charging on environmental parameters appears to explain qualitatively in almost all cases examined thus far why some storms are thunderstorms and others are not." They also went on to relate the noninductive mechanism and updraft to the environmental conditions: "...if the noninductive, graupel-ice

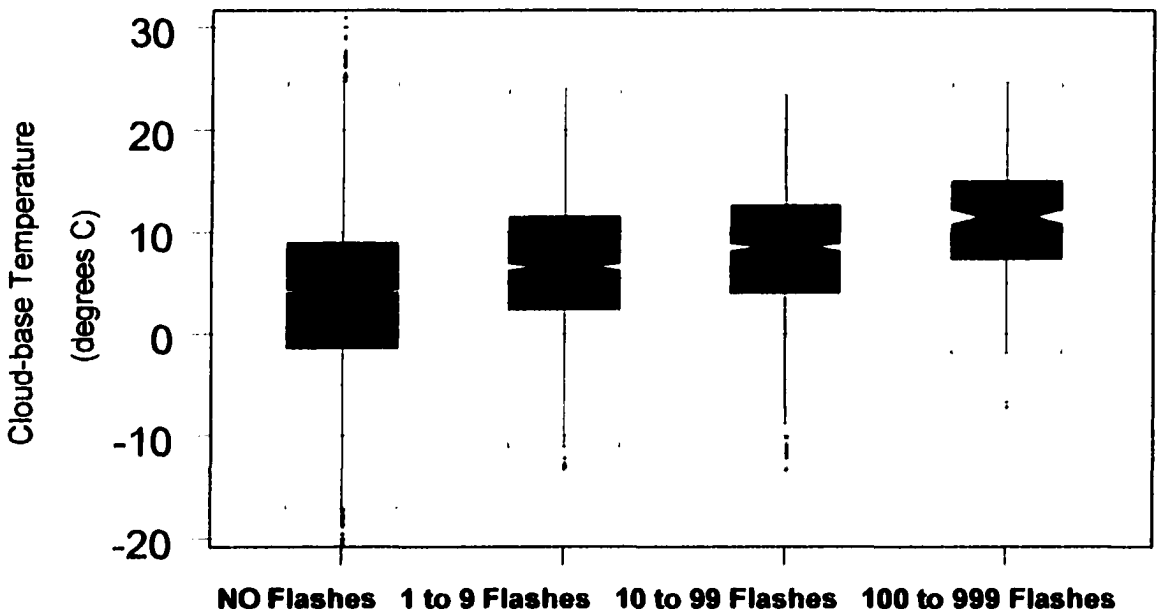

Fig. 5.32. Cloud-Base Temperature (with MUCAPE>0) for grid boxes reporting NO flashes, 1-9, 10-99, and 100-999.

mechanism is important to lightning production, as suggested by many of the studies..., then at least one factor that affects electrification and, hence, flash rates, is the number of graupel-ice interactions that occur under conditions favorable for electrification.....this depends on having sufficient concentrations of graupel, cloud ice, and supercooled cloud water particles simultaneously in the mixed-phase region. It also depends on....the residence time of graupel in the mixed-phase region.... These properties, in turn, are affected by the vertical and horizontal distribution of updraft speed, particularly above the lower boundary of the mixed phase region."

Parameter (median value)	No LTG N=35645	LTG N=4835
Lightning Climatology-Probability one or more flashes	< 7.5%	≥15%
Lightning Climatology-Storm duration	<10 minutes	≥20 minutes
Lightning Climatology-Average number of flashes	1	≥2
Cloud depth from LCL to EL	8000 meters	10000 meters
Cloud base temperature	4°C	>7°C
Normalized CAPE from LCL to EL	0.09 m s^{-2}	>0.13 m s^{-2}
Normalized CAPE from LCL to -20°C	0.062 m s^{-2}	>0.088 m s^{-2}
Potential/convective instability	>0	<0
Precipitable water	>0.55	0.7 inch
Equilibrium Level (EL) temperature	<-46°C	<-51°C

Table 5.2 Parameter differences between grid boxes without and with lightning. N=number of grid boxes with or without lightning

One measure of the updraft strength that is used extensively in this study is the most unstable CAPE (MUCAPE). The theoretical maximum updraft speed from parcel theory is the square-root of twice the CAPE. Blanchard (1998) recommended that Normalized CAPE (NCAPE) be used as a measure of the mean parcel buoyancy by making CAPE independent of the depth over which it occurs. Normalizing CAPE by dividing by the depth provides a convenient measure of the actual buoyant energy in terms directly related to acceleration per unit distance. Thus, at any given level, a parcel with a small value for NCAPE would have a lower vertical velocity compared to a parcel with larger value of NCAPE. If the total MUCAPE was the same, a parcel with smaller NCAPE would achieve the same vertical velocity as a parcel with larger NCAPE, but at a higher level. The NCAPE has been calculated from the LCL to the EL and from the LCL to the height of the -20°C environmental temperature.

The NCAPE from the LCL to the -20°C level was found to be an important discriminator between lightning and no lightning cases. For grid boxes where the most unstable CAPE was greater than zero, Fig. 5.33 shows a significant difference between NCAPE for cases of no lightning and those with one or more flashes. When lightning did not occur, the median value was 0.062 m s^{-2}, whereas it was 0.088 m s^{-2} or higher for all lightning categories (an increase of over 42%). This strongly supports the theory and observations that a strong updraft is needed in the mixed-phase region. The NCAPE for the entire depth of the storm (Fig. 5.34) also has a significant difference between the lightning and no lightning events. The NCAPE was less than 0.09 m

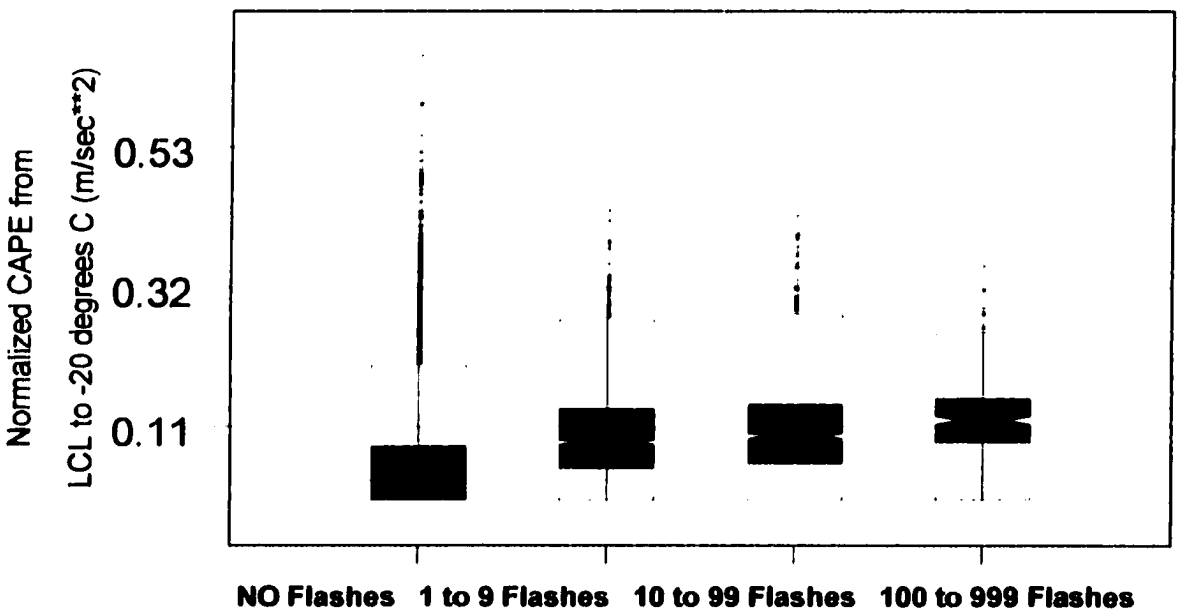

Fig. 5.33. Normalized CAPE from LCL to -20 degrees C (m/sec**2) for grid boxes reporting NO flashes, 1-9, 10-99, and 100-999 flashes.

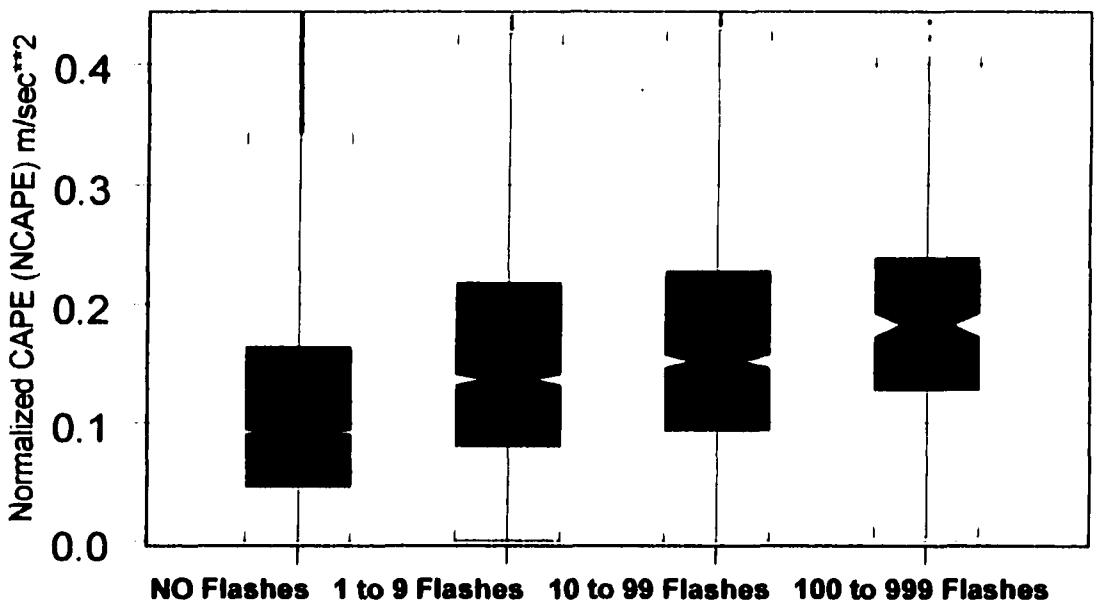

Fig. 5.34. Normalized CAPE (m/sec**2) for grid boxes reporting NO flashes, 1-9, 10-99, and 100-999 flashes.

s^{-2} for no lightning cases while it occur was close to 0.13 m s^{-2} (also an increase of over 40 percent).

While the maximum speed of the updraft is related to the CAPE, factors such as the liquid water (and ice) loadings and entrainment of dry air can act to reduce the speed of the updraft. If there is less CAPE per incremental vertical distance, there is a greater chance that the precipitation loadings and/or entrainment of dry air will have a measurable impact on reducing the updraft, and hence the chance of electrification.

The potential (or convective) instability (lapse rate of Theta-E) between 400 and 700 mb exhibits a distinct difference between grid boxes with no flashes and those with flashes. As the box plots in Fig. 5.35 show, the atmosphere is convectively stable for over 75% of the cases when no flashes are observed. Conversely, when lightning is observed, the atmosphere is convectively unstable for approximately 75% of the cases. This would imply steeper lapse rates and/or a sharp decrease of water-vapor mixing ratio with height. As long as Theta-E decreases with height, the lapse rates in the convectively unstable areas would also steepen when rising motion was also present.

The temperature at the equilibrium level (Fig. 5.36), using the most unstable parcel, is colder by nearly 5°C when lighting is observed. This relates to the second of the conditions listed by Grosh (1977): that cloud tops should be cold enough to have significant amounts of both ice and water. Finally, when lightning is observed, there are higher values of precipitable water present in the column of air. The median value of the precipitable water increases by 28 percent when lightning occurs (Fig. 5.37).

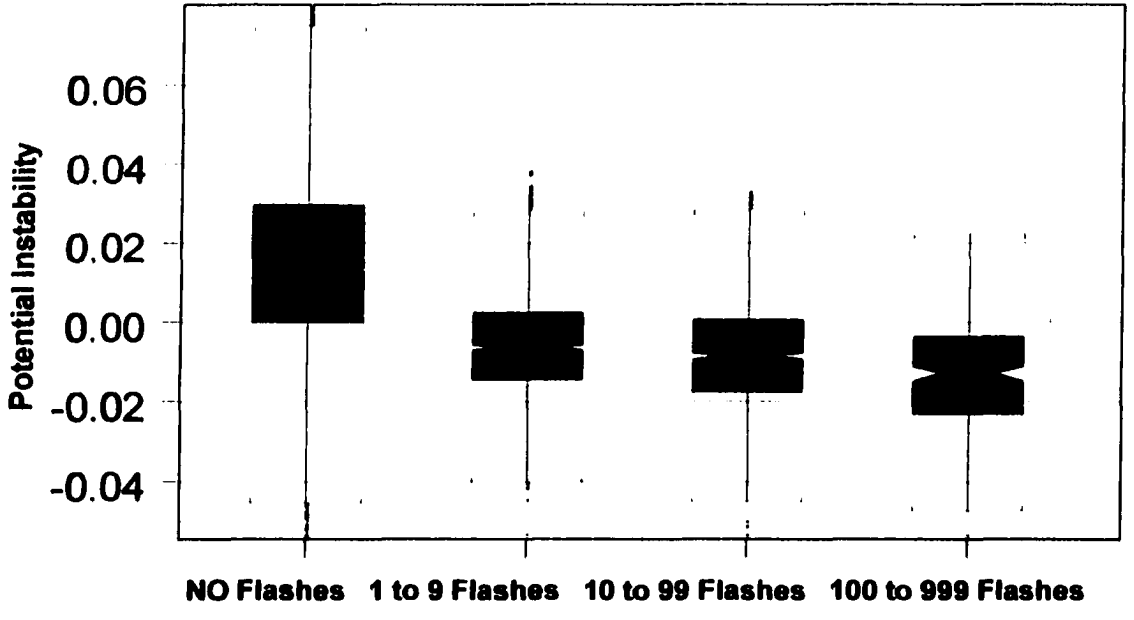

Fig. 5.35. Potential/convective Instability between 400 and 700 mb, for cases of NO flashes, 1-9, 10-99, and 100 to 999 flashes.

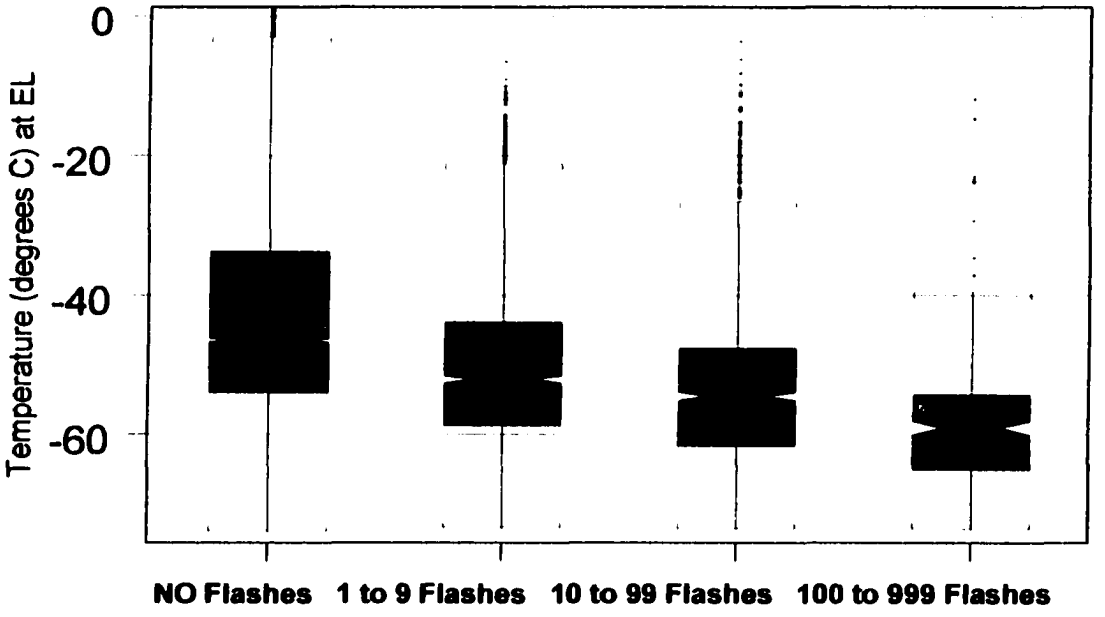

Fig. 5.36. Temperature (degrees C) at EL (for MUCAPE >0) for grid boxes reporting NO flashes, 1-9, 10-99 and 100 to 999.

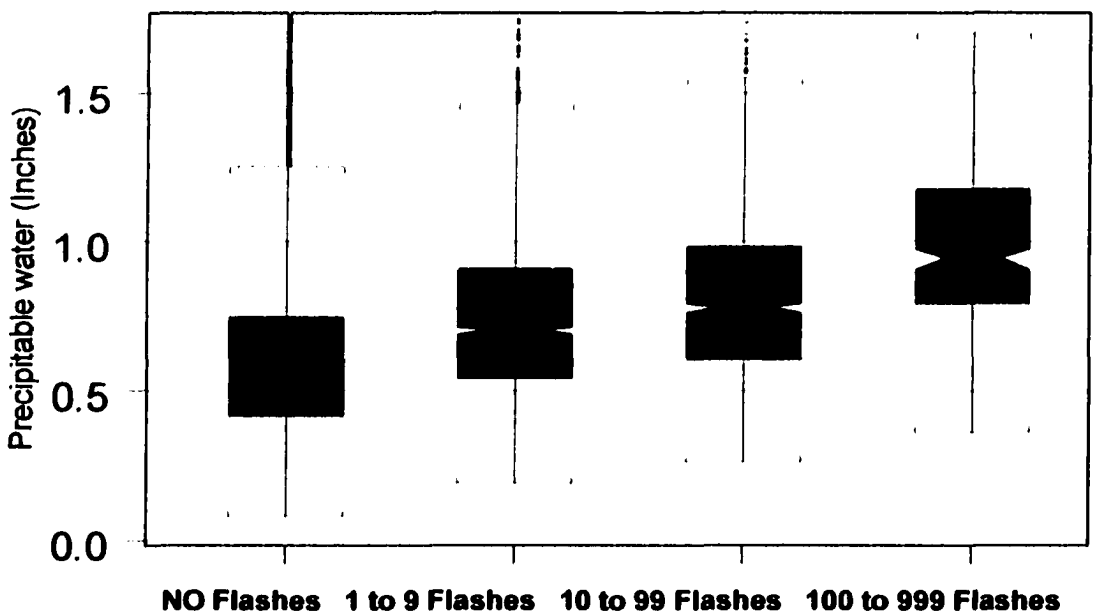

Fig. 5.37. Precipitable water (inches) for grid boxes reporting NO flashes, 1-9, 10-99 and 100 to 999 flashes.

5.2.2 Low Number of Flashes Versus High Numbers of Flashes

We now examine the cases where only low number of flashes are reported versus those cases where high numbers of flashes are reported. Three main groups of lightning flashes are identified in this study, 1 to 9, 10 to 99 and 100 to 999 (Log-base 10 scale). Results are shown in Table 5.3.

Parameter (median value)	1-9 Flashes LOW N=2644	10 to 99 Flashes MODERATE N=1836	100 to 999 Flashes HIGH N=355
Lightning Climatology-Probability one or more flashes	15%	>15%	>18%
Lightning Climatology-length of time lightning occurs	20 minutes	>25 minutes	>30 minutes
Lightning Climatology-Average number of flashes	2 flashes	3 flashes	9 flashes
Cloud depth from LCL to EL	>10000 meters	>11000 meters	>12000 meters
Cloud base temperature	>7°C	>8°C	> 11°C
Normalized CAPE-LCL to EL	>0.13 ms^{-2}	0.15 ms^{-2}	> 0.17 ms^{-2}
Normalized CAPE-LCL to -20°C	>0.088 ms^{-2}	>0.097 ms^{-2}	> 0.12 ms^{-2}
Potential/convective instability	-.007°Cmb^{-1}	-.009°Cmb^{-1}	-.012°Cmb^{-1}
Precipitable water	0.7 inch	>0.8 inch	>0.9 inch
Equilibrium Level (EL) temperature	<-51°C	-55°C	-60°C

Table 5.3. Parameter differences between grid boxes with low, moderate and high numbers of lightning flashes. N=number of flashes in each category.

The lightning climatologies (Table 5.3) for the probability of one or more flashes, length of time lightning occurs, and average number of flashes all show substantial increases from storms with low numbers of flashes to those storms with high numbers of flashes. When combined with the results shown in Table 5.2 for no flashes and one or more flashes, it is shown that there is substantial signal contained in the lightning climatologies concerning where storms preferentially form.

Lightning is more likely in areas where:

1) the climatological probability is relatively high
2) the climatological length (or percentage) of time lightning occurs is longer
3) the average number of flashes is higher

Also, storms with higher numbers of lightning flashes form in preferred regions.

We now examine the thermodynamic properties, variables such as cloud depth, cloud base temperature, normalized CAPE (and CAPE), and precipitable water all show significantly larger median values as the number of flashes increases from 1 to 9 through 100 to 999 flashes. As was the case for lightning versus no lightning, the normalized CAPE from the LCL to -20°C shows one of the largest changes, more than doubling from near 0.10 ms^{-2} to over 0.22 ms^{-2}. The potential/convective instability also increases as the number of flashes increases. The median temperature at the equilibrium level also steadily decreases (i.e., becomes colder) as the number of flashes increases. Baker et al. (1995) also reported that lightning frequency increased for colder cloud top temperatures.

At the start of this investigation, it was believed that at least some of the grid boxes with 100 or more flashes would be associated directly with a potential vorticity anomaly and a corresponding higher pressure (lower height) for the tropopause. Throughout this investigation, quite the opposite was found to be the case. In the West, none of the grid boxes with 100 or more flashes were in close proximity to a potential vorticity anomaly. The largest number of flashes were associated with a potential vorticity minimum of approximately 10^{-6} m^2 s^{-1} K kg^{-1}, as shown in Fig. 5.38. In addition, potential vorticity advection was examined. During the summer months across the western U.S. the median potential vorticity advection (not shown) was very near zero for both lightning and no lightning cases. Also, the tropopause was at its highest value with the median at approximately 175 mb, and all tropopause pressures were lower than 300 mb when 100 or more flashes were reported (Fig. 5.39). Similar results have been observed across the remainder of the country. The data would indicate that a while a potential vorticity anomaly can be associated with grid boxes with low to moderate numbers of flashes (and, correspondingly, a lower tropopause), possibly even providing enough lift to trigger a few flashes with marginal instability, the potential vorticity anomalies are not associated directly with the higher flash rates. Rather, storms that form in an environment with a high tropopause have the potential, given sufficient CAPE, to reach greater heights and hence very cold cloud top temperatures which could result in a large number of ice crystals, and correspondingly increase the number of flashes via the noninductive graupel-ice crystal

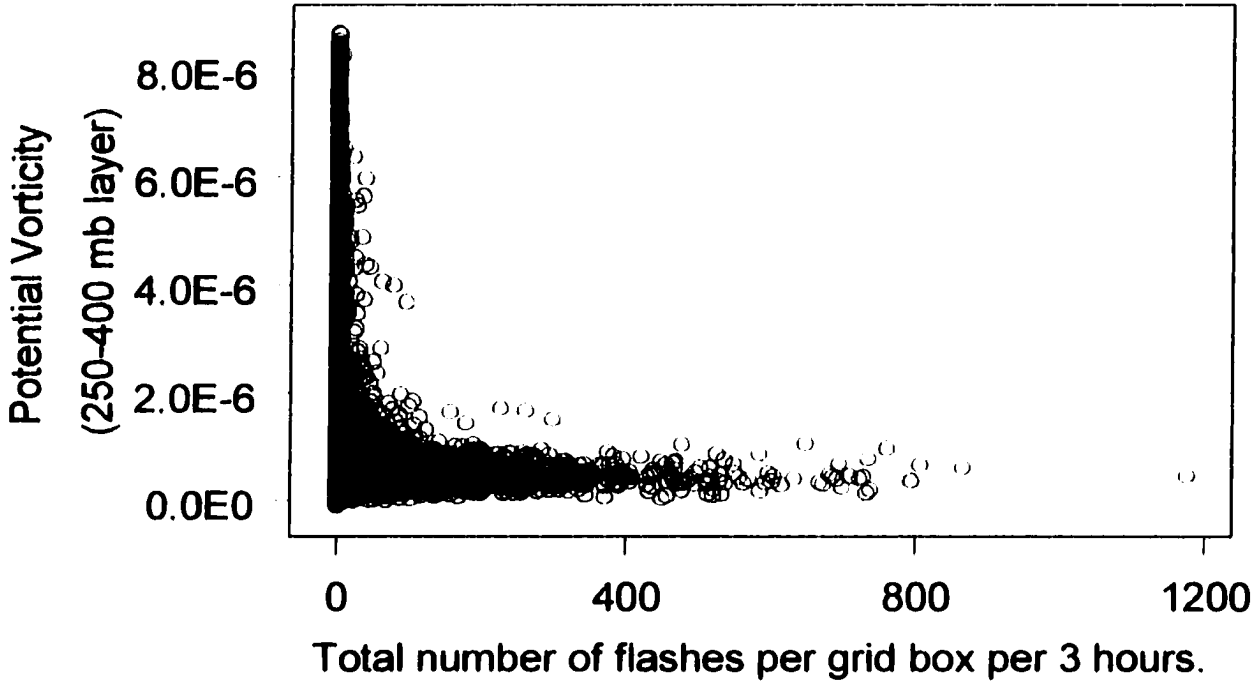

Fig. 5.38. Total number of flashes per grid box per 3 hours for the full 54 day development data set compared to potential vorticity.

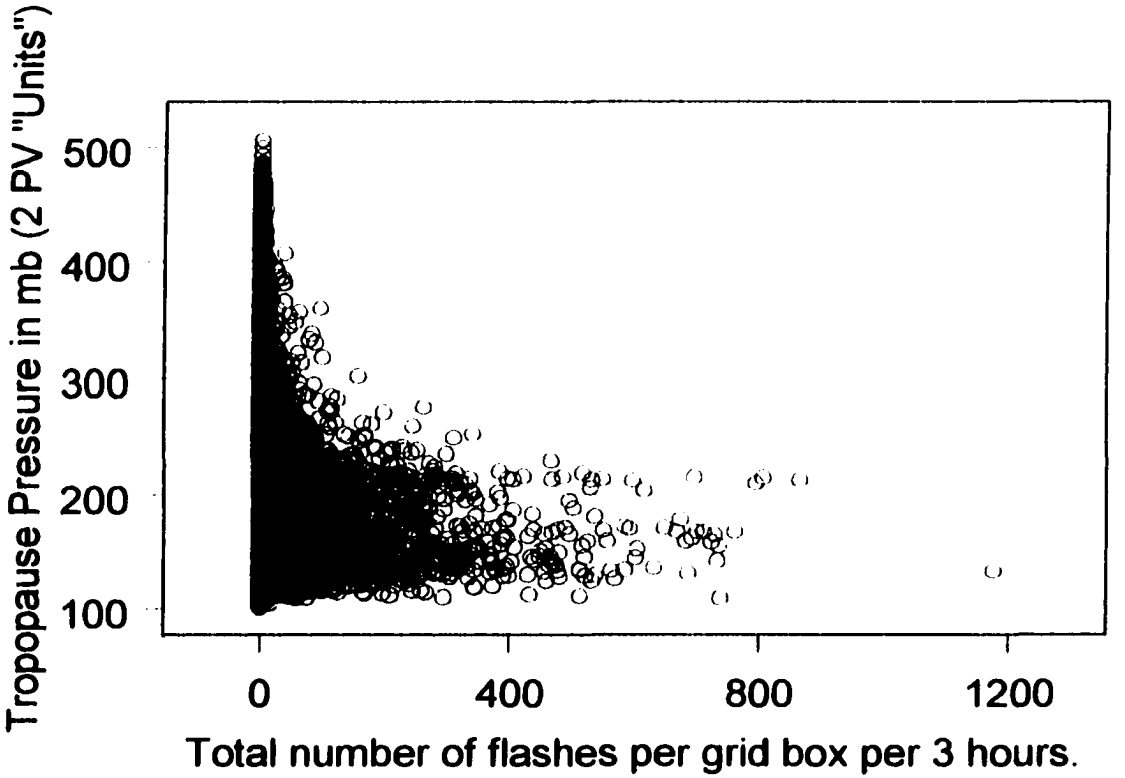

Fig. 5.39. Total number of flashes per grid box per 3 hours for the full 54 day development data set compared to the tropopause pressure (mb) using the 2 Potential Vorticity "Units" to define the tropopause.

mechanism. Also, since the storms are significantly far removed from any potential vorticity anomaly, the middle and upper level wind fields would not be as strong, resulting in slower moving storms when compared to the stronger wind fields associated with a potential vorticity anomaly. If a storm moves more slowly, it would be able to produce more flashes in a given grid box.

CHAPTER 6

Summary and Conclusions

The primary objective of this dissertation was to develop a prediction system that would produce three-hour grid point probability forecasts of cloud-to-ground lightning for the western United States. As shown in Chapter 5, probability forecasts for 1, 10, and 100 or more flashes were each able to capture most of the lightning events including significant events with large numbers of flashes. In practice, the predictive equations can be derived for any number of flashes (e.g., 30 flashes per three-hour period) or for any period of time (e.g., one-hour forecast period). This procedure is also capable of producing probabilities for specific types of lightning, such as the flashes that deliver positive charge to ground.

The lightning prediction system has bridged the gap that currently exists between extrapolative techniques (for lightning that is already occurring) and model forecasts (which are usually presented in increments of six hours after the model analysis time) by producing three-hour forecasts using the perfect prog method. The methodology developed in this dissertation allows for the future expansion of the forecasts to cover the central and eastern United States and to other seasons.

It has been shown in Appendix G, that even with the decreased grid size, shorter time interval of the forecasts, and other significant differences that are more difficult to quantify, these results represent a significant improvement over previous methods.

Another objective was to produce a set of lightning climatological predictors that contained sufficient detail to represent diurnal lightning trends as well as longer term trends such as the development of the Southwest Monsoon. An example of lightning relative frequency at a sample location in the West is shown in Appendix B (Figs B.2-B.4) to illustrate that the pentads used in the lightning climatology were able to capture both diurnal and intraseasonal trends.

In developing this predictive system, the analyses from the RUC 2 were used, but analyses or forecasts from other models could be used. The probability forecast equations were developed on a 40 by 40 km grid, but have the capacity to change to finer resolution grids. In order keep pace with changes in the models brought about by decreasing grid sizes, archived model data could be interpolated to the new (finer) grid mesh. Combining this with the lightning climatological predictors generated on the new grid mesh and using the methods developed herein, forecast probabilities can be developed to accommodate any grid resolution. Reap (1994a) was able to generate lightning forecasts associated with the land-sea breeze convergence zones over Florida using a 12 km resolution lightning grid by interpolating the NGM (grid spacing 150 km) predictors to the same grid as the lightning data.

This predictive system searches all levels (every 25 mb) in the vertical and determines which levels contribute the most information. It is not limited to just the surface and the standard pressure levels. For the 00 to 03 UTC period in the West and the months of June, July and August, the PCA statistical method was able to determine which predictors were important. These predictors were grouped such that a new predictor set with ten different and distinct physical processes could be ascer-

tained from more than 200 original predictors. The final ten predictors were uncorrelated even though there were many strong correlations among the original predictors. These ten predictors, illustrated in Fig. 4.3, are described in Tables 4.3 and 4.4.

In Chapter 2, a hypothesis was advanced as part of the conceptual three-dimensional thunderstorm model that proposed if thunderstorms formed where there was a source of (1) moisture, (2) instability, and (3) lift (i.e., lifting mechanisms), then the RUC 2 model contained sufficient information to evaluate these conditions and predict thunderstorm formation over the next three hours. The PCA identified ten groupings (predictors) out of the original 205 variables that explained approximately 60% of the variance in the original data. These ten rotated principal components were examined and, based on the most significant PC loadings, it was possible to identify a unique meteorological process for each of them. These ten new predictors, or "ingredients", when considered together, support the hypothesis that the RUC 2 analysis depicts the basic ingredients that directly relate to moisture, instability and lift.

It was also hypothesized that if the model analyses exhibited skill in forecasting thunderstorms (one or more flashes) in the short term (forecasts from zero to three hours) using the perfect prog approach, the analyses would also exhibit skill for the prediction of thunderstorms with high flash rates. As seen in Chapter 5, logistic regression was used to produce probability forecasts for the number of flashes per three-hour period above a certain pre-selected level (10 or more and 100 or more flashes). Although the forecast probabilities were not as high (climatology of high numbers of flashes was also low in the West), the methods and procedures developed were able to correctly locate important areas with high numbers of flashes.

In examining the original individual climatological and thermodynamic predictors, the lightning climatological predictors were able to show substantial differences between lightning and no lightning events as well as differences between low (1 to 9), moderate (10 to 99) and high (100 to 999) numbers of flashes per three-hour period for each grid box.

For lightning to occur, it was found that CAPE should extend to at least the -20 °C level in the environment. In addition, the CAPE below -20 °C should be large enough to support strong updrafts within the mixed-phase region of the cloud. Normalizing the CAPE (NCAPE) helped differentiate between CAPE profiles that were vastly different (i.e., "fat" and "skinny" CAPE) even though the total CAPE was the same. The difference between the no lightning and lightning cases was that the NCAPE was over 40% larger when lightning was observed. It was found that lightning was more likely in areas where (1) the layer from 700 to 400 mb was convectively (potentially) unstable, (2) the cloud depth from LCL to EL was above 10,000 meters, and (3) the cloud had a correspondingly cold EL temperature (colder than -50 °C) with warm cloud bases (above 7 °C). Furthermore, for progressively higher numbers of flashes (1 to 9, 10 to 99, and 100 to 999), the median cloud depth became larger, the cloud base temperature became warmer, the normalized CAPE from LCL to EL and LCL to -20 °C became larger, convective (potential) instability and precipitable water increased, and the EL temperature became colder.

Techniques and procedures were developed to produce predictive equations for lightning that can be applied to either observed gridded data (i.e., model analyses) or forecast data. Future work will include testing how well the equations perform on

3, 6, 9, and 12 hour forecasts from the RUC 2. Note that the RUC 2's 12-hour forecast from the 1200 UTC cycle, valid for the 12 to 15 hour time frame (00 to 03 UTC), can be continually updated during the day, using the 9-hour forecast from 1500 UTC, the 6-hour forecast from 1800 UTC, and the 3 hour forecast from 2100 UTC. In addition, these techniques could be applied to any forecast model for any time period.

If the procedures in this dissertation were automated in real-time, it is possible that a three-hour probability forecast would be ready by 15 minutes after the top of each hour by using the previous one or two-hour forecast valid at the time of the analysis. In addition, rather than waiting for the RUC 2 analyses, the one hour forecast from the previous hour's RUC 2 could be merged with the objectively analyzed surface data from the current hour. The surface analysis done by the is completed at the SPC by about 10 minutes after the hour, thus providing all necessary data to produce the forecast (e.g., for 00 to 03 UTC). Upon receipt of the RUC 2 analyses, updated forecasts using the analyses could be produced. It would also be possible to implement this on an hourly basis, with updated three-hour forecasts being produced each hour.

In Chapter 5, it was shown that in the West there were substantial differences in the thermodynamic environments for storms that had low numbers of flashes versus others that produced large numbers of flashes. Further investigations are needed to determine if these results will hold over the central and eastern U.S., where the available moisture is normally higher.

Additional developmental data from the 2000 and 2001 seasons should be incorporated into the procedures and tested. The initial developmental data set from 1999 was limited, and it is hoped that additional data will help reduce false alarms. Once the consistent problem of unrealistically high dew points over the mountains of east central California, along with other more isolated errors such as the one noted off the southern California coast have been corrected, the false alarms should further decrease when the procedures are rerun. For forecasts of events with a high number of flashes (i.e., greater than 100 flashes), a larger developmental data set that contains more events with a high number of flashes should lead to improved results.

With additional developmental data, it would also be possible to regionalize the predictive equations. In Chapter 5 an analysis of the variance explained by each of the ten predictive terms (RPCs) derived in the PCA showed distinct areas where each were more active. These areas could be used to form the basis of the regionalization.

Probabilistic forecasts for the other time periods (03 to 06 UTC,..., 21 to 00 UTC) can be developed using the procedures produced in this work. However, it is expected that there will be differences in the forecast equations, since not all the same processes are active during the entire 24 hour period (solar heating being just one example).

The forecast equations could also be evaluated using data from other models, including the Eta, and the newest model, the Weather Research and Forecasting (WRF) model. This would allow a common framework to be set up to compare forecasts from all three models (RUC 2, Eta and WRF), using the same forecast equations.

It is realized that in a 40 x 40 km grid box, there are often groups of storms within the grid box, rather than one isolated cell. It would be possible to apply these procedures to smaller scales. In the future, applications using additional years of archived lightning data would help to improve the lightning climatologies developed in this dissertation. The climatologies could, for example, use grids compatible with the national 4 km radar mosaics of reflectivity, echo tops, and vertically integrated liquid content (VIL). Finally, the same methodology applied here for probabilistic lightning forecasts could be used to derive probabilistic equations for hail, wind and/or tornadoes.

It is believed that the forecasts produced by the application of the procedures developed herein represent the start of improved lightning forecasts. It is hoped that these improvements in forecasts of lightning will help to reduce human and property losses nationwide.

REFERENCES

Baker, M.A., H.J. Christian, and J. Latham, 1995: A computational study of the relationships linking lightning frequency and other thundercloud parameters. *Q. J. R. Meteor. Soc.*, **121**, 1525-1548.

Battan, L.J., 1963: Relationship between cloud base and initial radar echo. *J. Appl. Meteor.*, **2**, 333-336.

Benjamin, S.G., J.M. Brown, K.J. Brundage, B.E. Schwartz, T.G. Smirnova, and T.L. Smith, 1998: RUC -2 - The Rapid Update Cycle Version 2. Technical Procedures Bulletin - draft. [Available on-line from http://maps.fsl.noaa.gov/ruc2.tpb.html.] Last revised 31 August 1998.

Benjamin, S.G., J.M. Brown, K.J. Brundage, D. Kim, B. Schwartz, T. Smirnova, and T.L. Smith, 1999: Aviation forecasts from the RUC-2. *Preprints, 8th Conf. on Aviation, Range, and Aerospace Meteorology*, Dallas, TX, Amer. Meteor. Soc., 486-490.

Blanchard, D.O., 1998: Assessing the vertical distribution of convective available potential energy. *Wea. Forecasting*, **13**, 870-877.

Bothwell, P.D., 2000: Forecasting dry thunderstorms as a part of fire weather outlooks at the Storm Prediction Center. *Preprints, Third Symposium on Fire and Forest Meteorology*, Long Beach, CA, Amer. Meteor. Soc., 76-79.

Bothwell, P.D., and J.A. Hart, 2000: *Evaluation of SPC Hourly Diagnostic Fields for the May 3rd Outbreak.* National Symposium on the Great Plains Tornado Outbreak of 3 May 1999. [Abstract available on-line from http://kkd.ou.edu/may3.htm]

Bower, J.B., 1993: NGM-based MOS thunderstorm and severe thunderstorm probability forecasts for the contiguous United States. NWS Technical Procedures Bulletin No. 407, NOAA, U.S. Department of Commerce, 16pp.

Brill, K.F., 1999: EMC eta model ICWF interface grib fields. [Available on-line from http://sgi62.wwb.noaa.gov:8080/ICWF/index.html.]

Brooks, H.E., 1999: Severe thunderstorm climatology [Available on-line from nssl.noaa.gov/hazard/data.html.]

Bryan, G.H., and J.M Fritsch, 2000: Moist Absolute Instability: The sixth static stability state, *Bull. Amer. Meteor. Soc.*, **81**, 1207-1230.

Cattell, R.B., 1952: *Factor Analysis*, Harper and Row, New York, NY.

Charba, J.P., 1977: An operational system for predicting thunderstorms two to six hours in advance. NOAA Technical Memorandum NWS TDL-64, National Oceanic and Atmospheric Administration, U.S. Department of Commerce, 24 pp.

Charba, J.P., 1984: Two-to-six hour probabilities of thunderstorm and severe local storms. NWS Technical Procedures Bulletin No. 342. National Oceanic and Atmospheric Administration, U.S. Department of Commerce, 14 pp.

Cummins, K.L, M.J. Murphy, E.A. Bardo, W.L. Hiscox, R.B. Pyle, and A.E. Pifer, 1998: A combined TOA/MDF technology upgrade of the U.S. National Lightning Detection Network. *J. Geo. Res.* **103.**, 9035-9044.

Curran, E.B., R.L. Holle, and R.E. López, 1997: Lightning fatalities, injuries and damage reports in the Unites States from 1959-1994, NOAA Tech. Memo. NWS SR-193, 64 pp.

desJardins, M.L., K.F. Brill, and S.S. Schotz, 1991: GEMPAK5, Part 1- GEMPAK5 Programmer's Guide Version 5.0. NASA Technical Memorandum 4261 Part 1.

Donaldson, R.J., Jr., R.M. Dyer, and J.J. Kraus, 1975: An objective evaluator of techniques for predicting severe weather events. *Preprints Ninth Conf. Severe Local Storms*, Norman, OK, Amer. Meteor. Soc., 321-326.

Doswell, C.A., III, 1987: The distinction between large-scale and mesoscale contribution to severe convection: A case study example. *Wea. Forecasting*, **2**, 3-16.

Douglas, M.W., R.A. Maddox, and K.W. Howard, 1993: The Mexican monsoon. *J. Climat.*, **6**, 1665-1677.

Fosdick, E.K., and A.I. Watson, 1995: Cloud-to-ground lightning patterns in New Mexico during the summer. *Nat. Wea. Dig.*, **19**, 17-24.

Fuquay, D.M., 1962: Mountain thunderstorms and forecast fires. *Weatherwise*, **15**, 149-153.

Glahn, H.R., 1985: Statistical weather forecasting. In *Probability, Statistics, and Decision Making in the Atmospheric Sciences*, A.H. Murphy and R.W. Katz, eds., Westview, Boulder, CO, pp 289-335.

Glahn, H.R., and D.A. Lowry, 1972: The use of Model Output Statistics (MOS) in objective weather forecasting. *J. Appl. Meteor.*, **11**, 1203-1211.

Glahn, H.R., A.H. Murphy, L.J. Wilson, and J.S. Jensenius, Jr., 1991: Lectures presented at the WMO training workshop on the interpretation of NWP products in terms of local weather phenomena and their verification, Programme on Short and Medium Range Weather Prediction Research, Wageningen, The Netherlands, 29 July-9 August 1991, PSMP NO. 34, WMO/TD NO. 421.

Grosh, R.C., 1977: Relationships between severe weather and echo tops in central Illinois. *Preprints, 10th Conf. On Severe Local Storms,* Amer. Meteor. Soc., 617-624.

Grell, G.A., 1993: Prognostic evaluation of assumptions used by cumulus parameterizations. *Mon. Wea. Rev.*, **121**, 764-787.

Harman, H.H., 1976: *Modern Factor Analysis.* The University of Chicago Press, Chicago, IL., 487 pp.

Holle, R.L., R.E. López, and E.B. Curran, 1999: Distributions of lightning-caused casualties and damages since 1959 in the United States. *Preprints, 11th Conf. on Applied Climatology*, Dallas, TX, Amer. Meteor. Soc., 363-370.

Holle, R.L., and M.W. Maier, 1982: Radar echo height related to cloud-ground lightning in south Florida. *Preprints, 12th Conf on Severe Local Storms*, San Antonio, TX., Amer. Meteor. Soc., 368-373.

Huffines, G.R., and R.E. Orville, 1999: Lightning ground flash density and thunderstorm duration in the continental United States: 1989-96. *J. Appl. Meteor.*, **38**, 1013-1019.

Hughes, K.K., 2001: Development of MOS thunderstorm and severe thunderstorm forecast equations with multiple data sources. *Preprints, 18th Conf. On Weather Analysis and Forecasting*, Ft. Lauderdale, FL, Amer. Meteor. Soc., 191-195.

Kithil, R., 1999: Annual USA lightning costs and losses., *11th International Conf. On Atmospheric Electricity*, Guntersville, AL.

Kitzmiller, D.H., M.A.Lilly, S.D.Vibert, 1999:The SCAN 0-3 Hour Rainfall and Lightning Forecast Algorithms. [Available on-line from http://www.nws.noaa.gov/tdl/radar/03h-doc.htm.]

Klein, W.H., B.M. Lewis, and I. Enger, 1959: Objective prediction of five-day mean temperature during winter. *J. Meteor.*, **16**, 672-682.

Lhermitte, R., and P.R.Krehbiel, 1979: Doppler radar and radio observations of thunderstorms, *IEEE Trans. On Geoscience Electron.*, **GE-17**, 162-171.

López, R.E., and R.L. Holle, 1986: Diurnal and spatial variability of lightning activity in northeastern Colorado and central Florida during the summer. *Mon. Wea. Rev.*, **114**, 1288-1312.

Ludlam, F.H., 1951: The production of showers by the coalescence of cloud droplets. *Q. J. R. Meteor. Soc.*, **77**, 401-417.

MacGorman, D.R., and W.D. Rust, 1989: An evaluation of the LLP and LPATS lightning ground strike mapping systems. *Preprints, 5th Int'l Conf. on Interactive Information and Processing Systems*, Amer. Meteor. Soc., 249-254.

MacGorman, D.R., and W.D Rust, 1998: *The Electrical Nature of Storms*. Oxford University Press, 422 pages.

Mathsoft Data Analysis Products Division, 1999: *S-Plus 2000*.

McNulty, R.P, 1983: A conceptual approach to thunderstorm forecasting. *Nat. Wea. Dig.*, **10**, 26-30.

Meisner, B.N., M.H. McCutchan, J.W. Benoit, B. Ly, and D. Albright, 1994: A lightning fire ignition assessment model. *Preprints, Symposium on the Global Electrical Circuit, Global Change and Meteorological Applications of Lightning Information*, Nashville, TN, Amer. Meteor. Soc., 368-373.

Newell, J.E., and D.G. Deaven, 1981: The LFM-II model–1980. NOAA Technical Memorandum NWS NMC-66, National Oceanic and Atmospheric Administration, U.S. Department of Commerce, 20 pp.

National Interagency Fire Center, cited 2000: Wildland fire statistics. [Available on-line from http://www.nifc.gov/stats/wildlandfirestats.html.]

Orville, R.E., and G.R. Huffines, 1999: Lightning ground flash measurements over the contiguous United States: 1995-97. *Mon. Wea. Rev.*, **127**, 2693-2703

Ramsey, G.S., and D.G. Higgins, 1986: Canadian forest fire statistics/Statistiques sur les incendies de foret au Canada 1981, 1982, 1983. Information report PI-X-49 E/F. Petawawa Natl. For. Inst., Can For. Ser., Chalk River, Ont.

Reap, R.M., 1972: An operational three-dimensional trajectory model. *J. Appl. Meteor.*, **11**, 1193-1202.

Reap, R.M., 1974: Thunderstorm and severe weather probabilities based on model output statistics. *Preprints Fifth Conf. on Forecasting and Analysis*, St. Louis, MO., Amer. Meteor. Soc., 266-269.

Reap, R.M., 1986a: Evaluation of cloud-to-ground lightning data from the western United States for the 1982-84 summer seasons, *J. Cli. App. Meteor.* **25**, 785-799.

Reap, R.M., 1986b: New 6-h thunderstorm probability forecasts for the West. NWS Technical Procedures Bulletin No. 362, NOAA, U.S. Department of Commerce, 8pp.

Reap, R.M., 1991: Climatological characteristics and objective prediction of thunderstorms over Alaska. *Wea. Forecasting*, **6**, 309-319.

Reap. R.M., 1994a: Analysis and prediction of lightning strike distributions associated with synoptic map types over Florida. *Mon. Wea. Rev.*, **122**, 1698-1715.

Reap, R.M., 1994b: 24-h NGM based probability and categorical forecasts of thunderstorms and severe local storms for the contiguous U.S. NWS Technical Procedures Bulletin No. 419, NOAA, U.S. Department of Commerce, 14pp.

Reap, R.M., and D.S. Foster, 1979: Automated 12-36 hour probability forecasts of thunderstorms and severe local storms. *J. Appl. Meteor.*, **18**, 1304-1315.

Richman, M.B., 1986: Rotation of principal components. *J. Climat.*, **6**, 293-335.

Richman, M.B., and X. Gong, 1997: Relationships between the definition of the hyperplane width to the fidelity of principal component loading patterns. *J. Climate*, **12**, 1557-1576.

Shuman, F.G., and J.B. Hovermale, 1968: An operational six-layer primitive equation model. *J. Appl. Meteor.*, **7**, 525-547.

Smith, S.B., J.T. Johnson, R.D. Roberts, S.M. Zubrick, and S.J. Weiss, 1998: The system for convection analysis and nowcasting (SCAN) 1997-1998 Field Test. *Preprints, 19th Conf. on Severe Local Storms.*, Minneapolis, MN, Amer. Meteor. Soc., 790-793.

Thompson, R.L. and R Edwards, 2000: A comparison of Rapid Update Cycle 2 (RUC-2) model soundings with observed soundings and supercell environments. *Preprints, 20th Conf on Severe Local Storms*, Orlando, FL., Amer. Meteor. Soc., 551-554.

Thurstone, L.L., 1947: *Multiple Factor Analysis.* The University of Chicago Press, Chicago, IL., 535 pp.

Velleman, P.F., and D.C. Hoaglin, 1981: *Applications, Basics, and Computing of Exploratory Data Analysis*, Duxbury Press, Boston, MA., 354 pp.

Wacker, R.S., and R.E. Orville, 1999: Changes in measured lightning flash count and return stroke peak current after the 1994 U.S. National Lightning Detection Network upgrade, 1, Observation, *J. Geo. Res.*, **104**, 2151-2157.

Wang, B., and X Xu, 1997: Northern hemisphere summer monsoon singularities and climatological intraseasonal oscillation. *J. Climat.*, **10**, 1071-1085.

Wilks, D.S., 1995: *Statistical Methods in the Atmospheric Sciences*. Academic Pess, San Diego, CA., 466 pp.

Ziegler, C.L., D.R. MacGorman, J.E. Dye, and P.S. Ray, 1991: A model evaluation of non-inductive graupel-ice charging in the early electrification of a mountain thunderstorm. *J. Geo. Res.*, **96**, 12, 833-55.

Zipser, E.J., 1994: Deep cumulonimbus cloud systems in the tropics with and without lightning. *Mon. Wea. Rev.*, **122**, 1837-1851.

APPENDIX A

The National Lightning Detection Network

Since the National Lightning Detection Network (NLDN) began providing real-time lightning data coverage to the contiguous United States in 1989, growing use of the NLDN data led to an increased demand for improving the location accuracy, percentage of lightning discharges detected, and estimates of the peak current for all strokes. This led to an upgrade of the NLDN that was completed in 1994. Most methods for locating cloud-to-ground (CG) lightning are based on either the gated wideband magnetic direction finder (MDF) or time-or arrival (TOA) methods. A new lightning location method for combining the MDF and TOA information is referred to as the improved accuracy from combined technology (IMPACT) method. The upgraded NLDN contains 59 TOA and 47 IMPACT sensors. The sensor locations are shown in Fig. 3.1. While the MDF and TOA sensor technologies each have strengths and weaknesses, the improved IMPACT sensors and location algorithm overcome many of the problems of either the MDF or TOA taken alone.

The gated, wideband magnetic direction finders, MDFs, were developed for locating CG lightning within a range of about 500 km. This system is designed to respond to the electromagnetic radiation field waveforms that are characteristic of the return strokes in the CG flashes. When such a field is detected, the magnetic direction is sampled just at the time of the initial field peak so that the direction vector pointed as closely as possible to the onset of the stroke and to the place where the

stroke hit the ground. The electric field was also sampled at this time to determine the stroke polarity. The MDFs require a minimum of two stations; however location errors are more uniformly distributed when there are at least three direction-finder stations located in a non-collinear arrangement. The location of the stroke can be determined by triangulation, and the peak current can be estimated from the measured peak field. (Cummins et al. 1998). If the flash is along or near the baseline between two sites, triangulated locations have large errors; hence range to the strike is calculated from the measured signal amplitudes by utilizing the 1 R dependence of amplitude on range. The largest sources of error in the MDFs are terrain features and man-made structures that reradiate lightning signals. Errors from these sources are called site errors (MacGorman and Rust 1998). These site location errors vary with azimuth, but typically are less than 5 km. These errors, which are not corrected in real-time, are eliminated by reprocessing the data off line before the data are archived. The site errors can be identified and corrected after sufficient lightning data (typically one to three months) have been accumulated (Cummins et al. 1998). These site errors are limited to the periods when the network is undergoing major changes, such as in 1994. Typically, the direction-finder systems detected 60-90% of the ground flashes (MacGorman and Rust 1998).

The time-of-arrival sensors for locating lightning are based on measurements of the time-of-arrival of a radio pulse at several stations that are precisely synchronized. Based on lightning generated radio signals propagating at close to the speed of light, a constant difference in the arrival time at two stations defines a hyperbola and multiple stations provide multiple hyperbolas whose intersections

define a source location. TOA methods can provide accurate locations at long ranges and systematic errors are usually minimal. For the newest TOA systems, the error in flash location is expected to be less than 1 km. Errors in lightning locations from TOA systems can be caused by anything that affects the determination of the time of the lightning signal, usually when the time is synchronized incorrectly. Radio noise from nearby thunderstorms can overload the station's processing capacity and in such cases the station is temporarily turned off. The TOA stations can also accept signals from both ground and cloud flashes which causes errors. To reduce this problem, the sensor gains were reduced and various waveform selection criteria were added. Sensor communication delays can also result from rain fade or data congestion during periods of high data rates, (e.g., when the lightning rate over the U.S. exceeds 35,000 to 50,000 flashes per hours). All data are reprocessed and corrected prior to being archived at GAI. The data used in this study are from archived, quality controlled lightning data. In the past, these systems sometimes detected less than 40 percent of the CG flashes (MacGorman and Rust 1989), but that problem has apparently been minimized or eliminated by increasing the bandwidth of the communication links.

When the network was upgraded in 1994, both the TOA sensors and IMPACT sensors were modified so that both sensor types detect CG flashes with similar sensitivity and discrimination. Due to an improved location algorithm in the IMPACT sensors that considers both timing and angle errors, these sensors overcame many of the problems inherent in either a MDF or TOA method taken alone. The IMPACT location algorithm operates in much the same manner as that for the MDFs except that in addition to stroke location, the time at which the return stroke begins at

the ground is also estimated. There is an additional term in the error function for each sensor that contributes precise timing information. As a part of the upgrade, the total number of NLDN sensors was reduced from over 130 to 106 because of an increase in the effective range of the sensors. The upgraded network was designed to detect 80 to 90% of the ground flashes (as shown in Fig. 3.2) and have a typical location error of 500 meters.

APPENDIX B

Determination of Lightning Climatologies

The following hypothetical case (illustrated in Table B.1) shows the degree of difficulty in constructing a lightning climatology for five day periods (pentads), using just 4 years of data. While the following example is for the computation of the average lightning relative frequency (per grid box per 3 hours), the same method was also applied to estimate the average for the (1) number of flashes, (2) percentage of flashes over all grid boxes that occurred in each grid box, and (3) percentage of the three-hour interval that lightning is observed (i.e., the number of 15 minute intervals with lightning, divided by 12). The following is a hypothetical example that illustrates the methodology for computing the relative frequency for one flash or more for one grid box.

Pentad			1	2	3	4	**5**	6	7	8	9		
Day ->	1	2	3	4	5	6	7	8	9	10	11	12	13
Year	t-6	t-5	t-4	t-3	t-2	t-1	t	t+1	t+2	t+3	t+4	t+5	t+6
1995	0	1	0	0	0	0	0	0	0	0	0	1	0
1996	0	1	0	0	1	0	0	0	0	0	0	1	0
1997	0	1	0	0	0	0	0	1	0	0	0	1	0
1998	0	1	1	0	0	0	0	0	0	0	1	1	0

Table B.1. Example for hypothetical pentad number 5 for a three-hour time period centered on day 7 (also identified as day "t"). One or more flashes is shown by 1 (0) = yes (no) one flash or more. Note: Pentad 1 includes days 1 through 5, Pentad 5 includes days 5 through 9, Pentad 9 includes days 9 through 13. When a pentad is referred to by a date, it is the center date of the pentad (e.g., June 2 pentad is comprised of the days from May 31, and June 1-4).

The relative frequencies for each daily pentad (pentads 1 through 9) are:

Pentad 1 = 0.30	Pentad 2 = 0.30	Pentad 3 = 0.10
Pentad 4 = 0.10	Pentad 5 = 0.10	Pentad 6 = 0.05
Pentad 7 = 0.10	Pentad 8 = 0.30	Pentad 9 = 0.25

As can be seen from the daily pentads, there is still considerable day-to-day variability even using pentads over 4 years (20 possible events). If the relative frequency from pentad 5 was used, surrounding days suggest this number could be underestimated by as much as 0.20 (e.g., 0.30 - 0.10) and conversely, it could be overestimated by 0.05 (e.g., 0.10 - 0.05).

However, since each of the daily pentads 1 through 9 contains at least one day (and hence, relative frequency value) that is in pentad 5, the simple solution is to compute an average relative frequency that is the average of all 9 pentads.

(0.30 + 0.30 + 0.10 + 0.10 + 0.10 + 0.05 + 0.10 + 0.30 + 0.25)/9=0.18

Each of the five days within the 9 daily pentads has a weight equal to that calculated for the pentad. This results in 13 days rather than 9 days being included and the previous equation, which (after expanding and rearranging terms) is shown to be:

Pentad 1 2 3 4 5 6 7 8 9

Day t-6 t-5 t-4 t-3 t-2 t-1 t t+1 t+2 t+3 t+4 t+5 t+6

0.2 *(.30+.30+.30+.30+.30
+.30+.30+.30+.30+.30
+.10+.10+.10+.10+.10
+.10+.10+.10+.10+.10
+.10+.10+.10+.10+.10
+.05+.05+.05+.05+.05
+.10+.10+.10+.10+.10
+.30+.30+.30+.30+.30
+.25+.25+.25+.25+.25)/9

$$L_t = 0.2 * (Lavg_{t-6} + 2*Lavg_{t-5} + 3*Lavg_{t-4} + 4*Lavg_{t-3} + 5*Lavg_{t-2} + 5*Lavg_{t-1} + 5*Lavg_t + 5*Lavg_{t+1} + 5*Lavg_{t+2} + 4*Lavg_{t+3} + 3*Lavg_{t+4} + 2*Lavg_{t+5} + Lavg_{t+6})/9$$

L_t is the average lightning relative frequency for the pentad centered on day t.

$Lavg_{t-n}$ is the average daily lightning relative frequency. It is found by adding all daily lightning relative frequencies for day t-n together and divided by total number of terms (1, 2, 3, 4, or 5).

For example: For day t-4 (3 days overlap),

$Lavg_{t-4} = (0.30 + 0.30 + 0.10)/4 = 0.175$
For day t (5 days overlap),
$Lavg_t = (0.10 + 0.10 + 0.10 + 0.05 + 0.10)/5 = 0.09$.

Multiplying each term on the right hand side of the equation for L_t by 0.2 gives:

$$L_t = (0.2*Lavg_{t-6} + 0.4*Lavg_{t-5} + 0.6*Lavg_{t-4} + 0.8*Lavg_{t-3} + Lavg_{t-2} + Lavg_{t-1} + Lavg_t + Lavg_{t+1} + Lavg_{t+2} + 0.8*Lavg_{t+3} + 0.6*Lavg_{t+4} + 0.4*Lavg_{t+5} + 0.2*Lavg_{t+6})/9$$

Figure B.1 illustrates this weighting scheme for each of the 13 days. This procedure is followed for each of the 73 contiguous pentads of the year. The average lightning relative frequency for the pentad centered on day t is assigned to each of the five days of that (contiguous) pentad. Thus every 5 days, a new average lightning relative frequency is computed and assigned to each day within the contiguous pentad. This has produced a climatology that is able to capture the growth and decay of the Southwest Monsoon. In addition, the 3 hourly intervals are able to capture the diurnal cycle. Examples of the daily cycle and the growth of the Southwest Monsoon for one location (point A in Fig. B.4) are shown in Figs. B.2 and B.3.

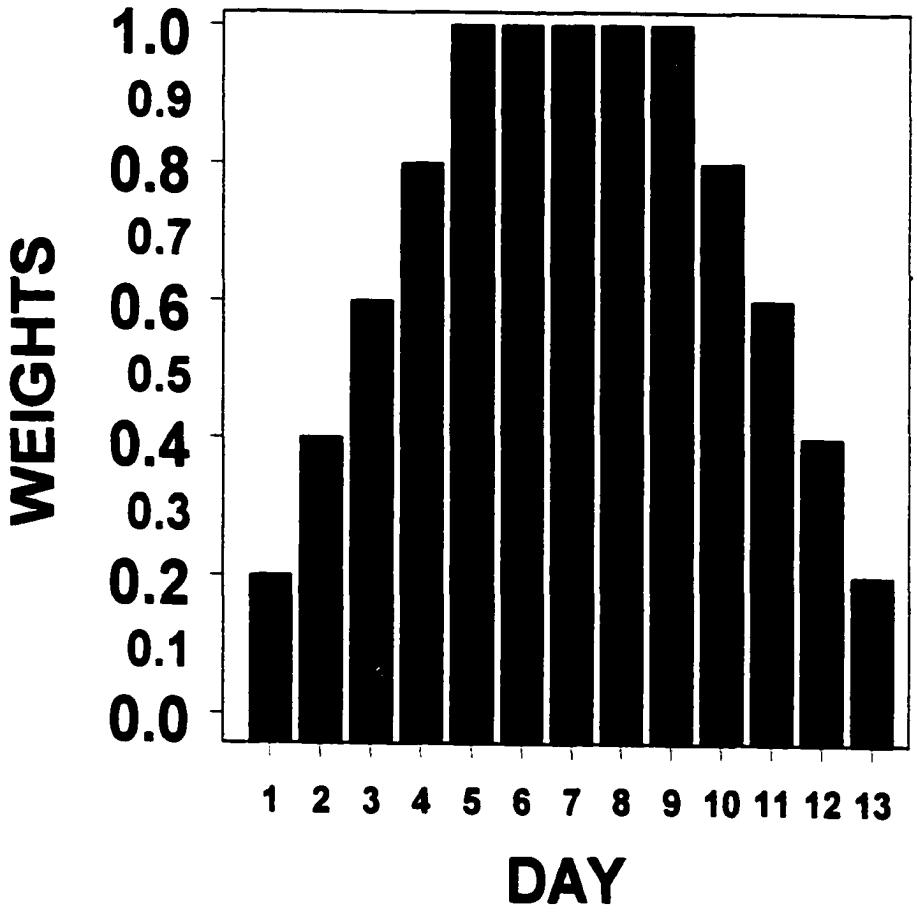

Fig. B.1. Example of weighting scheme applied for June 1 through June 13. Used in developing lightning climatology for June 7th pentad (Day 7).

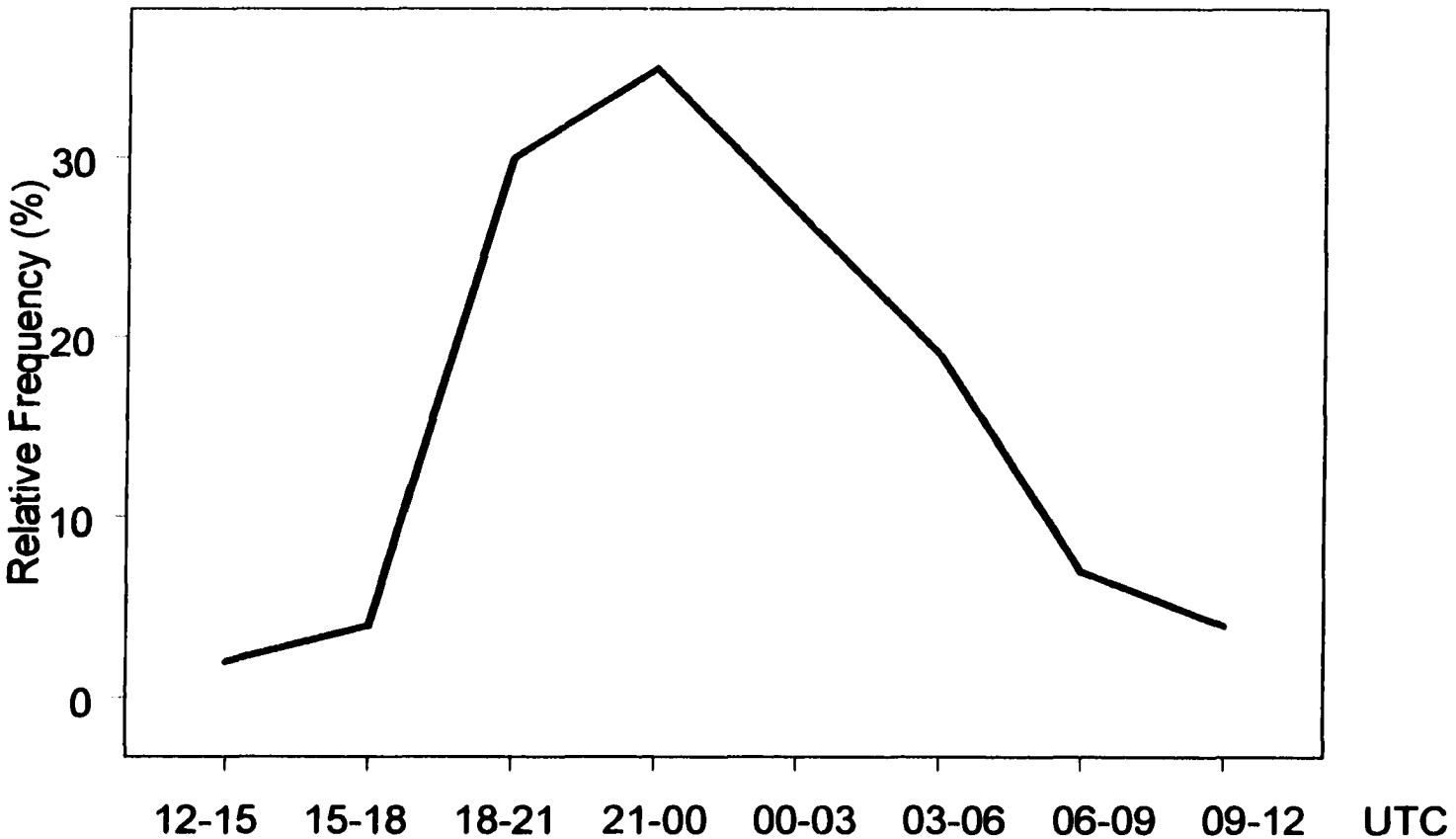

Fig. B.2. Lightning relative frequency for each three hour time period of the day for grid box located at point A in Fig. B.4.

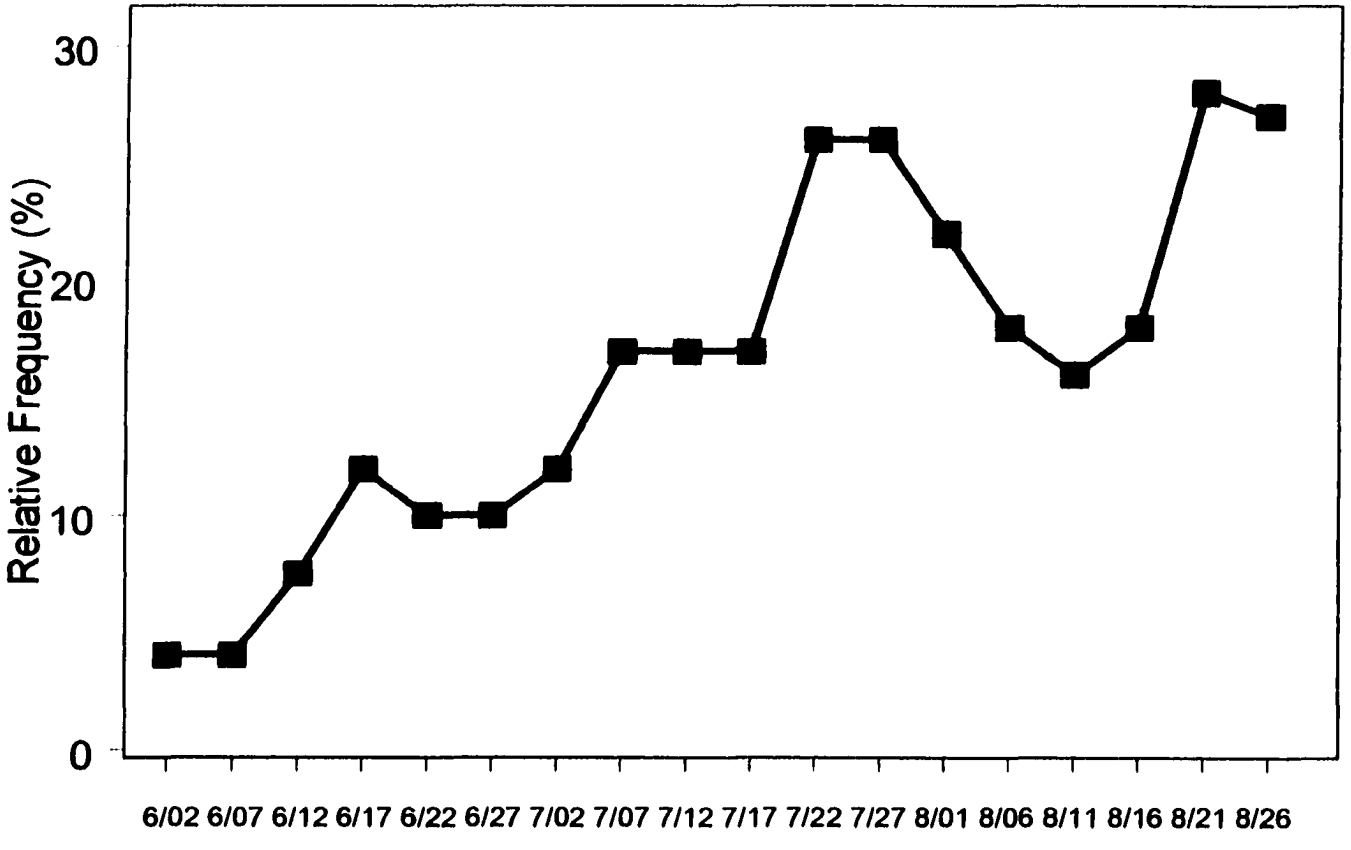

Fig. B.3 Pentad lightning relative frequency for 00 to 03 UTC for grid box located at point A in Fig. B.4.

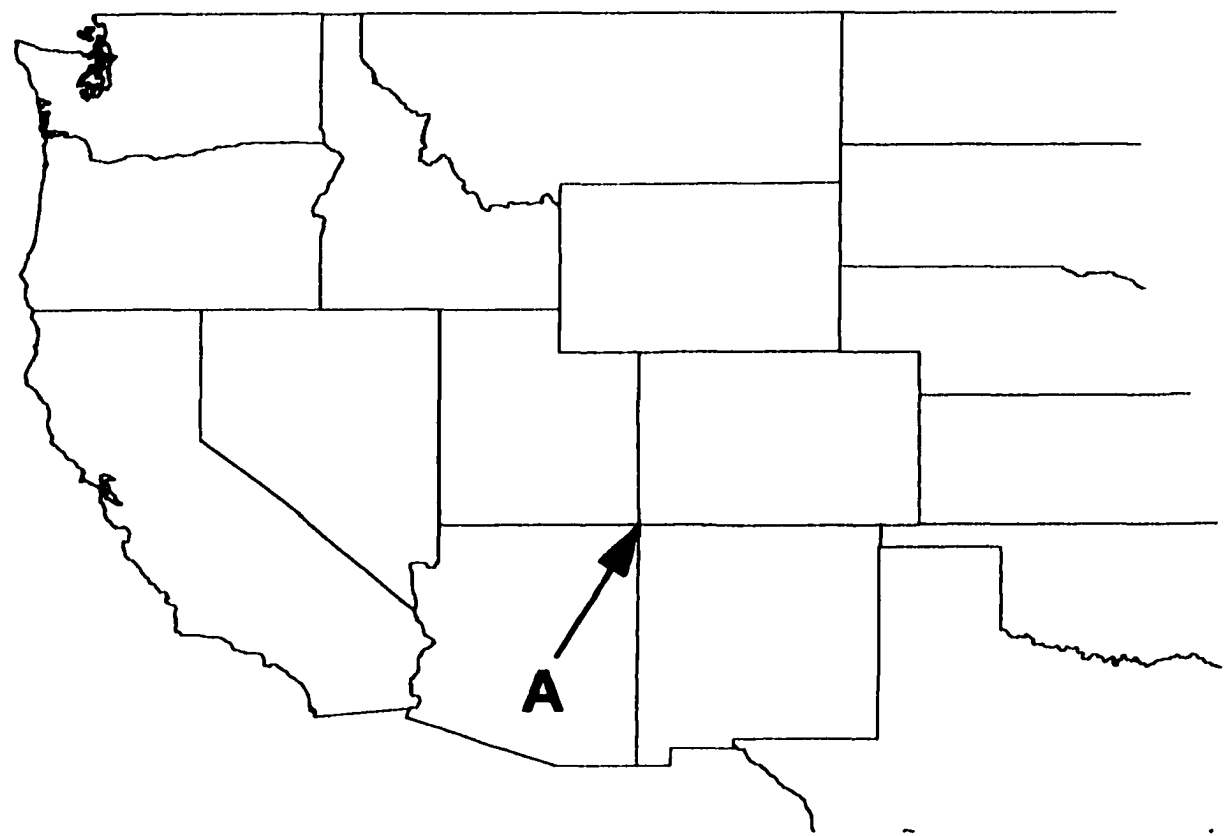

Fig. B.4. Point A (shown by arrow) is the location for the lightning climatologies in Figs. B.2 and B.3

APPENDIX C

Candidate Predictors

The parameters used as candidate predictors (except for the lightning climatology) have been derived from the RUC 2 temperature, moisture and wind fields using gridded surface and isobaric data in 25 mb vertical increments. Table C.1 includes a brief description of each parameter.

The GEneralized Meteorological PAcKage (GEMPAK), (desJardins et al., 1991), was used to compute many of the parameters. Additional software to compute parameters not available from GEMPAK was developed by Bothwell and Hart (Bothwell and Hart, 2000). The parameters, selected to represent moisture, instability, and lift, have been grouped into categories according to vertical level and physical processes strictly as an aid to presenting the large number of predictors. Currently the codes that generate these predictors are completed in approximately ten minutes on a HP J5000 UNIX workstation.

The following columns are listed in Table C.1.

1) Grid number
2) GEMPAK descriptor (1 to 4 characters)
3) Description of parameter
4) ID for vertical level of parameters. Figure 2.3 shows how these groups of parameters appear in the vertical, relative to a storm. For clarity, the fourth column in Table C.1 has a two-character ID that refers to one of the categories shown in Fig. 2.3.

The categories (as shown in Chapter 2, Fig. 2.3) are:

1) UL - **U**pper-**L**evel support
2) SR - wind **S**hear terms and/or storm **R**elative winds
3) AK - averages of vertical motion (**A**diabatic/**K**inematic)
4) TH - **TH**ermodynamics
5) LC - **L**ightning **C**limatology
6) TH/LC - best CAPE (**TH**ermodynamics)*Lightning Climatology
7) SD - **S**urface **D**ata
8) LL - **L**ower-**L**evel forcing
9) MU - **M**oist absolutely **U**nstable layer
10) LP - **L**apse **R**ates

Byran and Fritch (2000) have argued that a moist absolutely unstable layer, MAUL, can be created and maintained as mesoscale convective systems (MCSs) develop.

Abbreviations used in Table C.1:
Most Unstable Parcel (MUP), Most Unstable Parcel Level (MUPL), Lifted Index (LI), Equilibrium Level (EL), Lifted Condensation Level (LCL), Level of Free Convection (LFC), Mean Sea Level (MSL), Potential Vorticity (PV), Average (AVG)

In calculations involving the LFC, if no LFC (i.e., no CAPE), the LCL is substituted for calculations related to height of the LFC.
Moist and saturated geostrophic PV (all levels) are grouped under the ID of UL even though some levels extend below 500 mb.

Note: CAPE and Normalized CAPE from the LCL to the -20 °C level in the environment were calculated separately at a later time and added to the data set

Table C.1. Candidate predictors (1 to 208)

#	GEMPAK name	Description	General Category
1	K	K-grid point	SD
2	I	West to east grid point	SD
3	J	South to north grid point	SD
68	LMSL	Laplacian of mean sea level pressure	SD
69	PTND	Sfc pressure (altimeter) change-3hr	SD
70	LTND	Laplacian of sfc pressure change (3hr)	SD
71	LTHA	Laplacian of surface Theta	SD
72	PRES	Pressure at surface (altimeter based)	SD
73	ZMEG	Terrain upslope/downslope	SD
74	FRNT	Surface frontogenesis	SD
75	DQVC	Surface Q vector convergence	SD
76	PMSL	Mean sea level pressure	SD
77	RELH	Surface humidity	SD
78	MFCN	Surface moisture flux convergence	SD
79	WDIV	Surface wind divergence	SD
80	TWAD	Surface Theta-W advection	SD
81	RVRG	Surface relative vorticity	SD
186	LHGT	Laplacian of surface height field	SD
187	SMXR	Surface mixing ratio	SD
198	UWND	Surface U wind component	SD
199	VWND	Surface V wind component	SD
4	IOTF	LTG average number flashes	LC
5	ITFR	LTG spatial relative frequency	LC
6	IONE	Ltg relative frequency	LC
201	ITSM	LTG climo-% of 3hr pd ltg occurred	LC
204	BOTF	BECP * IOTF	TH/LC
205	BTFR	BECP * ITFR	TH/LC
206	BONE	BECP * IONE	TH/LC
207	BTSM	BECP * ITSM	TH/LC
46	FCRH	AVG humidity from LCL to LFC	LL
64	RHAV	AVG humidity from MUPL to LCL	LL
105	ASRH	AVG sub-cloud humidity	LL

109	MCAV	AVG moist flux convg (MUPL-LCL	LL
110	WCAV	AVG wind divergence (MUPL-LCL)	LL
111	TCAV	AVG Theta-W advection (MUPL-LCL)	LL
112	RCAV	AVG geostrophic rel vort (MUPL-LCL)	LL
113	LCAV	AVG frontogenesis (MUPL-LCL)	LL
114	LCAV	AVG Theta Laplacian (MUPL-LCL)	LL
115	HCAV	AVG height (pressure sfc) (MUPL-LCL)	LL
116	QCAV	AVG Q vect convergence (MUPL-LCL)	LL
117	MFAV	AVG moist flux convg (LCL-LFC)	LL
118	WFAV	AVG wind divergence (LCL-LFC)	LL
119	TFAV	AVG theta-W advection (LCL-LFC)	LL
120	RFAV	AVG geostrophic rel vort (LCL-LFC)	LL
121	LFAV	AVG frontogenesis (LCL-LFC)	LL
122	LFAV	AVG Theta Laplacian (LCL-LFC)	LL
123	HFAV	AVG height Laplacian (LCL-LFC)	LL
124	QFAV	AVG Q vect convergence (LCL-LFC)	LL
132	AWLC	AVG ageostrophic wind (MUPL-LCL)	LL
133	AWLF	AVG ageostrophic wind (LCL to LFC)	LL
134	VUAV	Change-ageostrohic shear (LCL-400 mb)	LL
135	GUAV	Gradient vertical motion (LCL-400 mb)	LL
136	VLAV	Change-ageostrophic shear (LCL-LFC)	LL
137	GLAV	Gradient vertical motion (LCL to LFC)	LL
188	MXTE	Theta-E at MUPL	LL
7	MLIM	Most negative LI (MUP) from any level	TH
8	MLIO	Pressure level of MLIM	TH
9	MLIH	Height of MLIM	TH
11	MELP	Pressure of the EL using the MUP	TH
12	MELH	Height of the EL using the MUP	TH
13	MELT	Temperature (°C) of the EL	TH
14	CDPM	Cloud depth(meters) from LCL to EL	TH
15	FCDP	Depth LCL to LFC (when LFC present)	TH
16	MLPP	Originating pressure level of MUP	TH
17	MBST	Lift (mb) for MUP to reach saturation	TH
18	MMPP	Pressure (mb) Max Parcel Level (MPL)	TH
19	MMPH	Height (meters) of MPL	TH
20	NCAP	Normalized Most Unstable CAPE ($m\ s^{-2}$)	TH
21	BECP	Best CAPE-best-50 mb avg or level above	TH
22	BECN	Convective Inhibition (CIN) for BECP	TH
23	EMCP	Elevated most unstable CAPE above cap	TH
24	EMCN	CIN for EMCP	TH
25	UUCP	Unstable and uncapped CAPE	TH
26	MUCP	Most Unstable CAPE (MUCAPE)	TH
27	MUCN	CIN-most unstable CAPE (MUCAPE)	TH
28	MULI	LI for most unstable parcel at 500 mb	TH
29	MLF0	Layer CAPE (LFC to 0 °C)	TH
30	MM05	Layer CAPE (0 to -5 °C)	TH
31	MM10	Layer CAPE (-5 to -10 °C)	TH
32	MM15	Layer CAPE (-10 to -15 °C)	TH
33	MM20	Layer CAPE (-15 to -20°C)	TH
34	MM25	Layer CAPE (-20 to -25 °C)	TH
35	MM30	Layer CAPE (-25 to -30 °C)	TH

36	MM35	Layer CAPE (-30 to -35 °C)	TH
37	MM40	Layer CAPE (-35 to -40 °C)	TH
38	MM4E	Layer CAPE (-40 °C to EL)	TH
39	MLCT	Cloud base (LCL) temperature (°C)	TH
40	MH10	Height (meters-MSL) of -10 °C	TH
43	MH20	Height (meters-MSL) of -20 °C	TH
50	MUCF	Most unstable CAPE from LCL to LFC	TH
53	MCAP	Capping inversion for MUP (°C)	TH
54	LMCN	Laplacian of CIN	TH
55	EFDF	Diff(meters) EL to freezing level	TH
56	EWDF	Diff(meters) EL to wet-bulb zero	TH
57	WBZH	Height of wet-bulb zero (meters-MSL)	TH
58	FZLH	Height of freezing level (meters-MSL)	TH
59	DNCP	Downdraft CAPE ($J\ kg^{-1}$)	TH
60	TEDF	Theta-E difference mid-levels to sfc	TH
61	MXMX	Mixing ratio for MUP	TH
62	QTRN	MXMX * storm rel inflow at MUPL	TH
63	XTRN	MXMX * wind speed at MUPL	TH
82	MLCH	Cloud base height (meters-msl) for MUP	TH
83	MLFH	Height of LFC for MUP	TH
106	INPW	Inches of precipitable water	TH
189	MULP	Laplacian of most unstable CAPE	TH
190	THEL	Laplacian of Theta-E from MUPL	TH
191	TRPK	Temp (°K) at tropopause ("2 PV" units)	TH
192	TRPT	Isentropic surface (°K) of tropopause	TH
195	MCNP	Pressure level of capping inversion	TH
196	MLCP	Pressure level of LCL for MUP	TH
197	MLFP	Pressure level of LFC for MUP	TH
200	NCIN	Normalized CIN ($m\ s^{-2}$)	TH
202	CTOT	Layer CAPE from LFC to -20 °C	TH
203	CZ20	Layer CAPE from 0 to -20 °C	TH
208	BMCR	Ratio BECP to MUCP (0 IF MUCP=0)	TH
41	ELSU	U shear component from EL to LCL	SR
42	ELSV	V shear component from EL to LCL	SR
44	FCSU	U shear component from LCL to LFC	SR
45	FCSV	V shear component from LCL to LFC	SR
84	UPMW	Sfc to 6 km pressure-weighted U comp	SR
85	VPMW	Sfc to 6 km pressure-weighted V comp	SR
86	UCBL	Cloud-bearing layer U mean wind comp	SR
87	VCBL	Cloud-bearing layer V mean wind comp	SR
88	U3SV	Surface to 3 km U shear component	SR
89	V3SV	Surface to 3 km V shear component	SR
90	U6SV	Surface to 6 km U shear component	SR
91	V6SV	Surface to 6 km V shear component	SR
92	ULSV	Low level to 6 km U shear component	SR
93	VLSV	Low level to 6 km V shear component	SR
94	BRNS	Bulk Richardson Number Shear ($m^2\ s^{-2}$)	SR
95	USSR	Surface to 2 km storm rel. U wind comp	SR
96	VSSR	Surface to 2 km storm rel. V wind comp	SR
97	U4SR	4 to 6 km storm rel U wind comp	SR
98	V4SR	4 to 6 km storm rel V wind comp	SR

99	U9SR	9 to 11 km storm rel U wind comp	SR
100	V9SR	9 to 11 km storm rel V wind comp	SR
101	UASR	Anvil level storm rel U wind comp	SR
102	VASR	Anvil level storm rel V wind comp	SR
103	UMXP	U wind component at MUPL	SR
104	VMXP	V wind component at MUPL	SR
125	INFL	Storm relative inflow (magnitude)	SR
126	OTFL	Storm relative outflow (magnitude)	SR
179	SH38	300 to 850 mb speed shear	SR
48	VKCL	Kinematic vertical velocity at LFC	AK
49	VVCL	Adiabatic vertical velocity at LCL	AK
51	VKFL	Kinematic vertical velocity at LFC	AK
52	VVFL	Adiabatic vertical velocity at LFC	AK
108	VVAV	AVG adiabatic vert vel (LCL-400 mb)	AK
127	VVLC	AVG adiabatic vert vel (MUPL-LCL)	AK
128	VKLC	AVG kinematic vert vel (MUPL-LCL)	AK
129	VVLF	AVG adiabatic vert vel (LCL-LFC)	AK
130	VKLF	AVG kinematic vert vel (LCL-LFC)	AK
131	VKAV	AVG kinematic vert vel (LCL-400mb)	AK
66	TELP	Moist Absolutely Unstable Layer	MU
67	MMBD	Depth of MAUL (mb)	MU
47	FCTL	Theta difference MUPL to LFC	LR
65	THLA	Theta difference from MUPL to LCL	LR
107	LLLR	Lower level lapse rate-sfc to 3 km	LR
138	LP78	Theta-change/press diff 700 to 850 mb	LR
139	LC78	LP78 * AVG converg 700 to 850 mb	LR
140	SL78	Sat Theta-E/press diff 700 to 850 mb	LR
141	ML78	Theta-E/pressure diff 700 to 850 mb	LR
144	LP67	Theta-change/press diff 600 to 700 mb	LR
145	LC67	LP67 * AVG converg 600 to 700 mb	LR
146	SL67	Sat Theta-E/press diff 600-700 mb	LR
147	ML67	Theta-E/press diff 600 to 700 mb	LR
152	LP56	Theta-change/press diff 500 to 600 mb	LR
153	LC56	LP56 * AVG converg 500 to 600 mb	LR
154	SL56	Sat Theta-E/pressure diff 500-600 mb	LR
155	ML56	Theta-E/pressure diff 500 to 600 mb	LR
158	TL75	Temperature diff-700 to 500 mb (°C)	LR
159	LPS4	Theta-change/press diff 400 mb to sfc	LR
160	LP48	Theta-change/press diff 400 to 850 mb	LR
161	LP47	Theta-change/press diff 400 to 700 mb	LR
162	LP45	Theta-change/press diff 400 to 500 mb	LR
163	LC47	LP56 * AVG converg 500 to 600 mb	LR
164	LC45	LP45 * AVG converg 400 to 500 mb	LR
165	SLS4	Sat Theta-E/press diff 400 mb to sfc	LR
166	SL48	Sat Theta-E/press diff 400 to 850 mb	LR
167	SL47	Sat Theta-E/press diff 400 to 700 mb	LR
168	SL45	Sat Theta-E/press diff 400 to 500 mb	LR
169	MLS4	Theta-E/press diff 400 mb to sfc	LR

170	ML48	Theta-E/press diff 400 to 800 mb	LR
171	ML47	Theta-E/press diff 400 to 700 mb	LR
172	ML45	Theta-E/press diff 400 to 500 mb	LR
173	SP45	Sat Geostrophic PV-400 to 500 mb	LR
174	MP45	Moist Geostrophic PV-400 to 500 mb	LR
175	SP34	Sat Geostrophic PV-300 to 400 mb	LR
176	MP34	Moist Geostrophic PV-300 to 400 mb	LR
10	TRPP	Tropopause (as defined by 2 PV units)	UL
142	SP78	Sat Geostrophic PV-700 to 850 mb	UL
143	MP78	Moist Geostrophic PV-700 to 850 mb	UL
148	SP67	Sat Geostrophic PV-600 to 700 mb	UL
149	MP67	Moist Geostrophic PV-600 to 700 mb	UL
150	H5HT	500 mb height field (meters)	UL
151	H5LP	Laplacian of 500 mb height field	UL
156	SP56	Sat Geostrophic PV-500 to 600 mb	UL
157	MP56	Moist Geostrophic PV-500 to 600 mb	UL
177	UREL	300 mb U wind component	UL
178	VREL	300 mv V wind component	UL
180	AUDV	AVG upr-lvl divergence (250 to 400 mb)	UL
181	AUAW	Mag ageostrophic wind (250 to 400mb)	UL
182	PVOR	Potential vorticity(PV) (250 to 400 mb)	UL
183	PVAV	PV advection by 300 mb wind	UL
184	SP23	Sat Geostrophic PV 200 to 300 mb	UL
185	MP23	Moist Geostrophic PV 200 to 300 mb	UL
193	TRPU	U wind component at tropopause level	UL
194	TRPV	V wind component at tropopause level	UL

APPENDIX D

Predictor Correlations and Stepwise Regression

In order to gain a better understanding of which individual terms may be most strongly related to the occurrence of lightning as well as the total number of lightning flashes, the Pearson product-moment correlation coefficient (r_{xy}) was computed between the binary predictand, FONE (0 for no flashes, 1 for one or more flashes), and each of the 208 candidate predictors listed in Appendix C. The correlation was also computed between the total number of flashes, TOTF, and each of the 208 candidate predictors. The correlation coefficient is limited in that it can be strongly affected by outliers in the data and is not robust to deviations from linearity in the relationship. A high correlation between any two variables does not imply that one necessarily causes the other (or vice versa), nor does it provide any explanation about the relationship between the two variables. While "x" does not cause "y", the higher the correlation, if "x" occurs, it is more likely that "y" will also occur. Table D.1 lists the correlation coefficients between each of the 208 parameters and the occurrence (FONE=1) or non-occurrence (FONE=0) of lightning. The table is in descending order (using absolute values) from the parameter with the highest correlation to the lowest correlation. From Table D.1, it can be seen that the probability of one or more flashes is most correlated with the climatological lightning relative frequency and the percentage of the time that lightning occurred (from the lightning climatology). However, the strength of the relationships (0.33 and 0.31) is weak, suggesting the relationships may be more non-linear and/or subject to outliers in the data. No single parameter is highly associated with lightning.

In Table D.2, the predictor with the highest correlation to the total number of flashes, TOTF, is the product of the Best CAPE and the climatological average number of flashes (i.e., BOTF=BECP*IOTF). As mentioned in Chapter 4, it is interesting to note that the top 17 most correlated parameters are the same in both lists (Table D.1 (FONE) and Table D.2 (TOTF)), although the order of parameters is slightly different.

Stepwise regression was performed using the binary predictand (FONE) which represented the occurrence or non-occurrence of lightning as well as the total number of flashes per three hours (TOTF). The results of the stepwise regression was discussed in Chapter 4. Table D.3 is the complete listing of the predictor order selected by stepwise regression for all 208 variables in the case of each predictand (FONE, and TOTF).

IONE	0.326	VVCL	0.180	MH10	0.134	EMCP	0.075	LTND	0.028
ITSM	0.314	CZ20	0.179	MM40	0.133	MP23	0.075	TWAD	0.028
ML47	0.298	MCAV	0.179	LP48	0.129	VREL	0.070	FCTL	0.027
BONE	0.292	LP78	0.179	UWND	0.128	LTHA	0.070	SP56	0.027
BTSM	0.277	RHAV	0.178	FZLH	0.127	ML78	0.069	VLSV	0.026
ML48	0.262	VVLF	0.177	MM4E	0.126	TRPV	0.069	ZMEG	0.025
CDPM	0.262	MM10	0.177	TRPP	0.126	NCIN	0.068	SL48	0.025
SMXR	0.261	VKLC	0.176	MLF0	0.123	SL47	0.065	MFAV	0.025
WBZH	0.254	ASRH	0.176	TRPT	0.120	LP67	0.061	VPMW	0.024
BECP	0.251	MM20	0.175	MCAP	0.120	VSSR	0.061	VCBL	0.024
IOTF	0.246	INFL	0.174	UMXP	0.118	TCAV	0.059	FCDP	0.024
INPW	0.245	WCAV	0.173	FCAV	0.117	ECAV	0.058	HFAV	0.023
ITFR	0.238	MLS4	0.173	MCNP	0.115	SL56	0.057	LC45	0.021
MLCT	0.234	CTOT	0.172	MLCP	0.115	PVAV	0.056	USSR	0.021
BTFR	0.234	VVAV	0.170	MMBD	0.113	PVOR	0.056	VUAV	0.021
MXMX	0.232	VVFL	0.170	U9SR	0.113	MUCF	0.055	SP78	0.019
BOTF	0.228	MLFH	0.169	PMSL	0.111	EMCN	0.054	BRNS	0.018
BECN	0.228	ML67	0.168	MLPP	0.111	RCAV	0.054	VLAV	0.018
MBST	0.221	LP45	0.164	THLA	0.109	SP45	0.052	LC47	0.017
MELH	0.211	LLLR	0.163	H5HT	0.108	TL75	0.052	RFAV	0.017
FCRH	0.209	MM25	0.160	TELP	0.107	FRNT	0.049	LMCN	0.016
VKAV	0.207	MUCP	0.160	MFCN	0.106	PTND	0.049	LFAV	0.014
EFDF	0.204	AUDV	0.158	SLS4	0.104	AWLF	0.047	LC56	0.014
EWDF	0.204	UPMW	0.153	MLFP	0.101	LCAV	0.047	MULP	0.013
MLCH	0.202	UCBL	0.153	PRES	0.101	LP47	0.047	VWND	0.013
RELH	0.200	MM05	0.152	MP67	0.097	SP67	0.043	V9SR	0.013
LPS4	0.200	MH20	0.150	U4SR	0.094	VMXP	0.043	WFAV	0.011
MELP	0.199	MM30	0.150	SL67	0.091	THEL	0.042	V3SV	0.010
BMCR	0.198	LC78	0.148	U6SV	0.090	ELSU	0.041	LP56	0.009
MULI	0.196	XTRN	0.142	UASR	0.089	U3SV	0.039	LMSL	0.009
MXTE	0.196	MLIM	0.142	SH38	0.087	MP34	0.038	FFAV	0.009
MELT	0.194	J	0.142	ELSV	0.086	V6SV	0.037	LHGT	0.008
GUAV	0.192	K	0.141	MP45	0.084	V4SR	0.034	H5LP	0.008
VKCL	0.191	UREL	0.140	SL45	0.083	DNCP	0.033	FCSV	0.008
MMPH	0.190	MM35	0.139	QTRN	0.082	AWLC	0.033	TFAV	0.007
VKLF	0.188	VVLC	0.139	WDIV	0.082	LC67	0.032	DQVC	0.005
ML56	0.188	UUCP	0.139	MLI0	0.082	FCSU	0.032	OTFL	0.005
I	0.188	TRPK	0.136	MLIH	0.080	SP34	0.030	QFAV	0.004
MM15	0.185	MMPP	0.136	MUCN	0.080	MP78	0.030	QCAV	0.003
GLAV	0.185	MP56	0.136	SL78	0.078	RVRG	0.030	AUAW	0.002
ML45	0.184	TRPU	0.135	ULSV	0.078	TEDF	0.029		
VKFL	0.182	NCAP	0.135	SP23	0.076	VASR	0.029		

Table D.1. Correlation between binary predictand (FONE = 0 for no flashes,1 for one or more flashes) and the 208 parameters (highest to lowest correlation).

BOTF	0.319	MM30	0.103	LP48	0.078	VMXP	0.039	VASR	0.018
BTFR	0.305	MLF0	0.100	MCNP	0.077	BRNS	0.038	ELSU	0.018
IOTF	0.275	MBST	0.099	MFCN	0.077	V4SR	0.038	VREL	0.018
BTSM	0.256	MM35	0.098	MLCP	0.077	FCTL	0.037	U3SV	0.017
ITFR	0.249	RELH	0.098	J	0.076	MP45	0.036	RVRG	0.016
BONE	0.241	MM4E	0.097	VVLC	0.076	UASR	0.036	SP45	0.016
BECP	0.210	VKLF	0.096	K	0.075	SL78	0.035	LC45	0.016
ITSM	0.205	VKCL	0.096	ML56	0.075	SL67	0.035	TRPV	0.015
SMXR	0.174	MM40	0.096	TRPU	0.072	MUCF	0.035	THEL	0.013
INPW	0.172	MLIM	0.095	UREL	0.072	VSSR	0.033	OTFL	0.013
IONE	0.165	MH20	0.095	MMPP	0.070	ULSV	0.033	MLPP	0.013
ML47	0.157	VKFL	0.094	PMSL	0.069	FRNT	0.032	SL48	0.012
MXMX	0.155	GLAV	0.093	MLIH	0.068	MP78	0.032	VWND	0.012
CDPM	0.148	I	0.093	MLFH	0.066	SP67	0.032	QCAV	0.012
MLCT	0.148	TRPK	0.093	THLA	0.066	FCDP	0.029	ELSV	0.011
ML48	0.140	VKLC	0.093	MLI0	0.065	LC67	0.029	QFAV	0.009
WBZH	0.130	GUAV	0.093	H5HT	0.064	HFAV	0.029	LHGT	0.009
MELH	0.129	LLLR	0.092	UMXP	0.064	EMCN	0.029	LC56	0.009
BMCR	0.128	NCAP	0.092	LC78	0.064	SL47	0.029	DNCP	0.009
MXTE	0.128	UUCP	0.092	MLFP	0.061	VUAV	0.028	USSR	0.009
VKAV	0.127	VVCL	0.092	TELP	0.060	SL56	0.027	MFAV	0.008
XTRN	0.126	VVLF	0.092	SP23	0.056	LMSL	0.027	AUAW	0.007
EFDF	0.124	MLCH	0.091	FCAV	0.055	MP34	0.027	FCSV	0.007
EWDF	0.124	UPMW	0.091	U9SR	0.055	NCIN	0.027	VLSV	0.007
ML67	0.120	UCBL	0.091	MP23	0.055	VLAV	0.026	PVAV	0.006
MELP	0.118	WCAV	0.090	EMCP	0.055	SP56	0.026	LP67	0.006
CTOT	0.117	VVFL	0.089	HCAV	0.054	LTHA	0.025	V6SV	0.005
CZ20	0.116	TRPP	0.088	MUCN	0.053	RFAV	0.025	TL75	0.005
MELT	0.116	MH10	0.088	MP56	0.052	VPMW	0.025	WFAV	0.004
MM15	0.115	AUDV	0.087	RCAV	0.050	VCBL	0.025	H5LP	0.004
MM10	0.115	LP78	0.085	WDIV	0.049	AWLF	0.025	LMCN	0.004
MUCP	0.113	MCAP	0.085	TEDF	0.049	SP34	0.025	LTND	0.003
MCAV	0.112	TRPT	0.084	PVOR	0.046	TFAV	0.025	SP78	0.003
MLS4	0.112	RHAV	0.084	U6SV	0.044	LFAV	0.023	LC47	0.002
MULI	0.112	ML45	0.083	LP47	0.044	FCSU	0.023	PRES	0.002
MM20	0.111	FCRH	0.082	TCAV	0.043	V9SR	0.023	V3SV	0.002
VVAV	0.110	ASRH	0.082	SLS4	0.042	LP56	0.022	MULP	0.001
MMPH	0.109	LP45	0.081	LCAV	0.041	AWLC	0.022	ZMEG	0.001
LPS4	0.109	UWND	0.081	SH38	0.040	SL45	0.022	FFAV	0.001
BECN	0.106	FZLH	0.080	U4SR	0.040	PTND	0.021	DQVC	0.000
MM25	0.105	INFL	0.079	ML78	0.039	QTRN	0.019		
MM05	0.104	MP67	0.079	MMBD	0.039	TWAD	0.018		

Table D.2. Correlation between total number of flashes (TOTF) and the 208 parameters (highest to lowest correlation).

	FONE	TOTF		FONE	TOTF		FONE	TOTF		FONE	TOTF
1	IONE	BOTF	61	MM05	H5HT	121	SLS4	ITFR	181	ML48	TRPU
2	INPW	VKAV	62	MM30	FZLH	122	WDIV	V3SV	182	AUAW	MMPP
3	VKCL	BTSM	63	MLIM	MM05	123	SP23	J	183	VUAV	VLSV
4	LP78	IOTF	64	CDPM	MM30	124	MP67	MUCP	184	TRPT	VPMW
5	ML47	BECP	65	THEL	LP67	125	MP23	MH10	185	MH20	MLCP
6	BONE	LC67	66	LTHA	MLIM	126	UASR	MELT	186	BTFR	HCAV
7	MFCN	LP78	67	MP56	MLFP	127	MLF0	XTRN	187	VVLC	RCAV
8	AUDV	ML47	68	MP34	MP78	128	MULI	CZ20	188	MLIH	LHGT
9	LC67	MFCN	69	THEL	I	129	LP47	BTFR	189	MLIO	H5LP
10	MLCH	MCAP	70	HFAV	NCAP	130	LHGT	MH20	190	MLPP	ML48
11	TL75	PTND	71	LFAV	MM35	131	LC78	LP47	191	MUCF	ML78
12	SMXR	ONE	72	LMCN	MMBD	132	NCIN	TL75	192	XTRN	MULP
13	MCAV	DNCP	73	MCNP	TELP	133	V6SV	BMCR	193	MLFH	MULI
14	U4SR	MBST	74	TFAV	ULSV	134	MUCP	FCSU	194	CTOT	FCAV
15	PMSL	MM15	75	WFAV	UMXP	135	MMPH	TWAD	195	MM15	MUCF
16	SL78	TEDF	76	TCAV	UWND	136	NCAP	VVCL	196	CZ20	VSSR
17	WBZH	ZMEG	77	MELP	U6SV	137	MXMX	LFAV	197	LPS4	MLCH
18	I	MCAV	78	U3SV	V4SR	138	MMBD	VKFL	198	PTND	U3SV
19	ML45	WCAV	79	VASR	VASR	139	SP56	VVFL	199	EFDF	MMPH
20	FCSU	PMSL	80	U9SR	V9SR	140	SL48	SP78	200	NCIN	SP23
21	MFAV	VWND	81	FCSV	INFL	141	SL56	TRPT	201	LP68	SL48
22	UCBL	VMXP	82	UREL	SH38	142	VVFL	TRPP	202	ELSU	LP48
23	LMSL	VLAV	83	V4SR	USSR	143	VVFL	TRPK	203	ML67	SP34
24	LCAV	ITSM	84	ULSV	UCBL	144	VKLF	MLF0	204	ML56	FRNT
25	H5LP	ONE	85	MM40	VKLC	145	RFAV	CTOT	206	K	K
26	ELSV	LCAV	86	TRPP	UASR	146	FFAV	MLCT	207	EWDF	EFDF
27	TRPV	THLA	87	QTRN	U9SR	147	MELH	LC56	208	VPMW	VCBL
28	WCAV	PVAV	88	OTFL	LTND	148	MMPP	MLPP			
29	VKAV	TCAV	89	V9SR	ML67	149	ITSM	FCDP			
30	ZMEG	TFAV	90	USSR	LC78	150	MUCN	SLS4			
31	VKFL	MFAV	91	U6SV	QCAV	151	TWAD	MXTE			
32	LC47	SL78	92	UWND	SP56	152	AWLF	MCNP			
33	MLCT	UREL	93	BRNS	MM25	153	AWLC	CDPM			
34	MH10	SL56	94	MCAP	MM20	154	SP45	MELP			
35	PRES	BRNS	95	MLFP	LMSL	155	QCAV	MM40			
36	H5HT	TRPV	96	UMXP	LTHA	156	QFAV	MM4E			
37	MLCP	U4SR	97	RELH	RELH	157	THLA	LPS4			
38	SL47	ELSV	98	RHAV	HFAV	158	MXTE	MLIH			
39	FZLH	DQVC	99	ASRH	RFAV	159	UUCP	SP67			
40	MELT	THEL	100	LLLR	VREL	160	LP45	ML10			
41	MLS4	LMCN	101	VKLC	FCSV	161	VVAV	ASRH			
42	PVOR	EMCN	102	BECM	SMXR	162	LC45	RHAV			
43	MP78	FCTL	103	SP67	MELH	163	LC56	VVAV			
44	RVRG	MLFH	104	GUAV	EWDF	164	VCBL	MP34			
45	EMCN	BECN	105	FRNT	SL67	165	SP78	RVRG			
46	FCTL	EMCP	106	MULP	MXMX	166	FCRH	MP56			
47	LTND	QTRN	107	GLAV	GUAV	167	TELP	SP45			
48	DQVC	MLS4	108	DNCP	GLAV	168	MP45	MP45			
49	MBST	FCRH	109	VVCL	MUCN	169	SP34	SL45			
50	BMCR	MM10	110	FCAV	UUCP	170	VSSR	VVLF			
51	VWND	AUAW	111	VLAV	ELSU	171	PVAV	VKCL			
52	VMXP	WDIV	112	BOTF	FFAV	172	ITFR	MP67			
53	SH38	VVLC	113	BTSM	AWLF	173	RCAV	VUAV			
54	J	WFAV	114	INFL	AWLC	174	HCAV	LP45			
55	IOTF	SLS4	115	MM20	MP23	175	MM10	QFAV			
56	SL67	ITFL	116	MM25	PVOR	176	MM4E	V6SV			
57	VLSV	LPS6	117	LP67	LC45	177	FCDP	ML45			
58	VREL	WBZH	118	LPS6	AUDV	178	V3SV	ML56			
59	BECP	INPW	119	SL45	VKAV	179	MM35	LC47			
60	EMCP	PRES	120	TEDF	LLLR	180	ML78	NCIN			

Table D.3. Results from stepwise regression for 208 predictors and two predictands. 1) FONE-binary predictand – 0 for no flashes, 1 for one or more and 2) TOTF-total number of flashes

APPENDIX E

Principal Component Analysis

The principal component analysis (PCA) in Chapter 4 begins with the computation of the scaled data matrix, **[Z]**, and the correlation matrix, **[R]**, from the data matrix $\mathbf{[X]}=\{x_{ij}: i=1,...,89115; j=1,..., 205\}$ where i indexes the grid points and j indexes the parameters.

The scaled data matrix **[Z]** is computed from the original data matrix **[X]** as:

$$\mathbf{[Z]} = \mathbf{[D]}^{-1}(\mathbf{[X]} - 1/n\mathbf{[1][X]}) \quad .$$

where $1/n\mathbf{[1][X]}$ is the mean of **[X]**, **[1]** is the matrix whose elements are all equal to 1, and $\mathbf{[D]}^{-1}$ is the diagonal matrix whose elements are the reciprocals of the sample standard deviations of the 205 parameters on the diagonal of **[D]**.

The correlation matrix **[R]** can be computed from the scaled data matrix by

$$\mathbf{[R]} = (1/(n-1))\mathbf{[Z]}^{T}\mathbf{[Z]} \quad .$$

The correlation matrix is used rather than the variance-covariance matrix because of the large difference in the magnitude of the parameters. If the data were not scaled (i.e., normalized to lie between plus and minus 1), the terms with the smaller variance might be incorrectly excluded. For example, because the variance of a set of 500 mb heights would normally be many times larger than the variance of a set of vertical velocity

values, the PCA covariance matrix would be dominated by the 500 mb heights.

Using the principal component model (Richman 1986), the matrix **[Z]** is related to the principal component scores **[F]** and the principal component loadings **[A]** by:

$$[Z] = [F][A]^T \quad .$$

Later in this appendix, this equation is rewritten to solve for the scores, **[F]**. These scores will serve as the predictors in the regression in place of the original 205 parameters.

In order to calculate the scores, the PC loadings, **[A]**, must first be computed. The principal component weights or loadings, **[A]**, are computed from the matrix of the eigenvectors, **[E]**, and the diagonal matrix, **[Λ]**, the elements of which are the descending eigenvalues, Λ, of the correlation matrix **[R]**

$$[A] = [E][\Lambda]^{1/2} \quad .$$

The eigenvectors **[E]** and eigenvalues, Λ, are calculated from the symmetric correlation matrix **[R]**.

The PC model, $[Z] = [F][A]^T$, can be rewritten, solving for the principal component scores [F] as:

$$[F] = [Z][A]\,([A]^T[A]\,)^{-1} \quad .$$

Mathematically, there are as many eigenvectors as there are original variables if there are no linearly dependent variables. In this study, there were 205 original variables as grid point coordinates K, I, and J were excluded since they remained fixed. A plot of the eigenvalues (as shown previously in Fig. 4.2) illustrates graphically how the number of eigenvectors to be retained can be determined. The plot in Fig. 4.2, is called a scree graph, named after the pattern or slope that loose rock, called scree, forms along a hill side. Several methods exist to determine how many PCs should be retained, with the scree graph being one of these methods. The purpose of the scree graph is to separate the steeply sloping portion of the plot (signal and noise) from the portion where the slope is much less (noise). A break in the slope appears after the first ten eigenvalues. For the first part of the analysis, the goal of data reduction would be achieved by reducing the number of variables from 205 to 10. However, if the procedure were to stop at this point, there is the possibility that different physical processes could be included in the first PC (since it explains the maximum variance), making the physical interpretation

misleading. Unrotated solutions exhibit four characteristics that hamper their utility to isolate individual modes of variation (Richman 1986). These four characteristics are (1) the inaccurate portrayal of the physical relationships embedded within the input matrix, (2) the PCs dependence on the shape of the domain, and/or (3) the size of a smaller subdomain, plus (4) inability to physically interpret the results even with large sample sizes.

Since one of the goals of this dissertation was the physical interpretation of the underlying order, an orthogonal (varimax) rotation, or linear transformation, was applied to the first 10 loadings. Tests were also conducted applying the rotation to the first 12, 14, and 16 PCs. Minimal differences were noted in the results as the first 10 rotated PC loadings were nearly identical in each of the cases. Increasing the number of terms that were rotated from 10 to 16 accounted for minimal data compression (i.e., 58% of the original variance represented by the 10 terms versus 69% for 16 terms). Therefore, only 10 terms were rotated since this was where a distinct "break" in the scree plot occurred and little additional variance was explained in terms 11 through 16. In addition to the varimax orthogonal rotation, two other transformations were attempted (oblique rotation (oblimin) and Procrustes) with no significant differences in the loadings. Thus the results from the original orthogonal (varimax) rotation of 10 terms were used to interpret the RPC terms. The scores computed from these PC loadings were used in the logistic regression (see

Appendix F).

As discussed earlier, the first ten loadings were deemed important because of the distinct break in the slope of the scree graph after 10 loadings. According to the review article on rotation of principal components by Richman (1986), Thurstone (1947) first applied the term "simple structure" to the transformed (rotated) solution to help ensure that the results could be easily interpretable. The conditions for simple structure can be shown by a series of graphic plots of each pair of the columns of the rotated PCs. According to Thurstone, simple structure is met when the pair-wise plots show 1) a large concentration of points in two radial streaks, 2) a large number of points at or near the origin and 3) only a small number of points off the two radial streaks. The pair-wise plots of all PC loadings shown in Fig. E.1 illustrate fairly strong simple structure as defined by Thurstone.

Not all PC loadings are included when it comes to physically interpreting the PCs. Richman and Gong (1997) have addressed the problem of how to correctly estimate a "cutoff" for the loadings, such that only the important ones are retained for the physical interpretation of the PC. In their paper, they recommend a correlation-based PC loading cutoff value of plus or minus 0.2 to 0.35 (i.e., loadings that fall closer to zero than that can be ignored). Also, they recommend that, for small sized data sets, the value should be increased slightly. Since the present study contained only one season of data, cutoffs of 0.3 and 0.4 were tested. The cutoff of

0.4 was found to provide better simple structure and the results (eliminating loadings smaller than plus or minus 0.4) are shown in Table E.1 and Fig. E.2. The loadings (and their values) that were retained for each of the 10 rotated PCs are shown in Table B.2. In this manner, the RPCs and the different underlying physical processes were uniquely identified. The rotated PCs (RPCs) were renamed according to the largest coefficients in each of the PCs (Chapter 4).

The 10 scores computed from the scaled data matrix and the RPCs became the predictors for the logistic regression. The development scores **[F]** used in the logistic regression were computed from the scaled data matrix **[Z]** and the rotated principal component loadings **[A]** as previously shown. The independent scores **[F]** were computed from the scaled independent matrix and the rotated principal component loadings from the development matrix **[A]**. These scores were used in the logistic regression (Chapter 4) to develop and test the lightning probability forecasts.

The principal component analysis (PCA) techniques in this work used the statistical software package, S-Plus 2000, developed by Mathsoft (now Insightful Corporation) (1999).

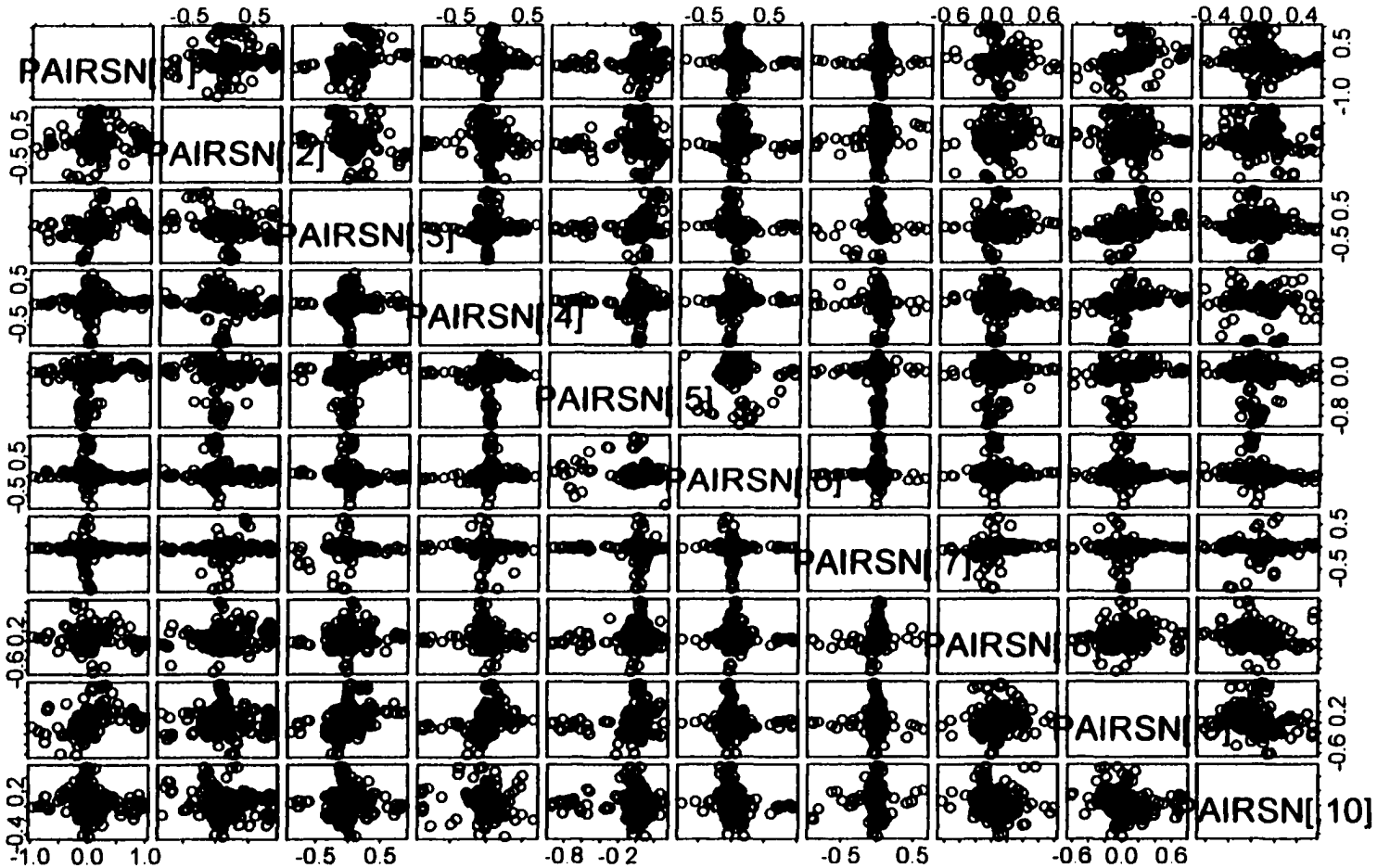

Fig. E.1. Pair-wise plot for 10 rotated PCs using all loadings

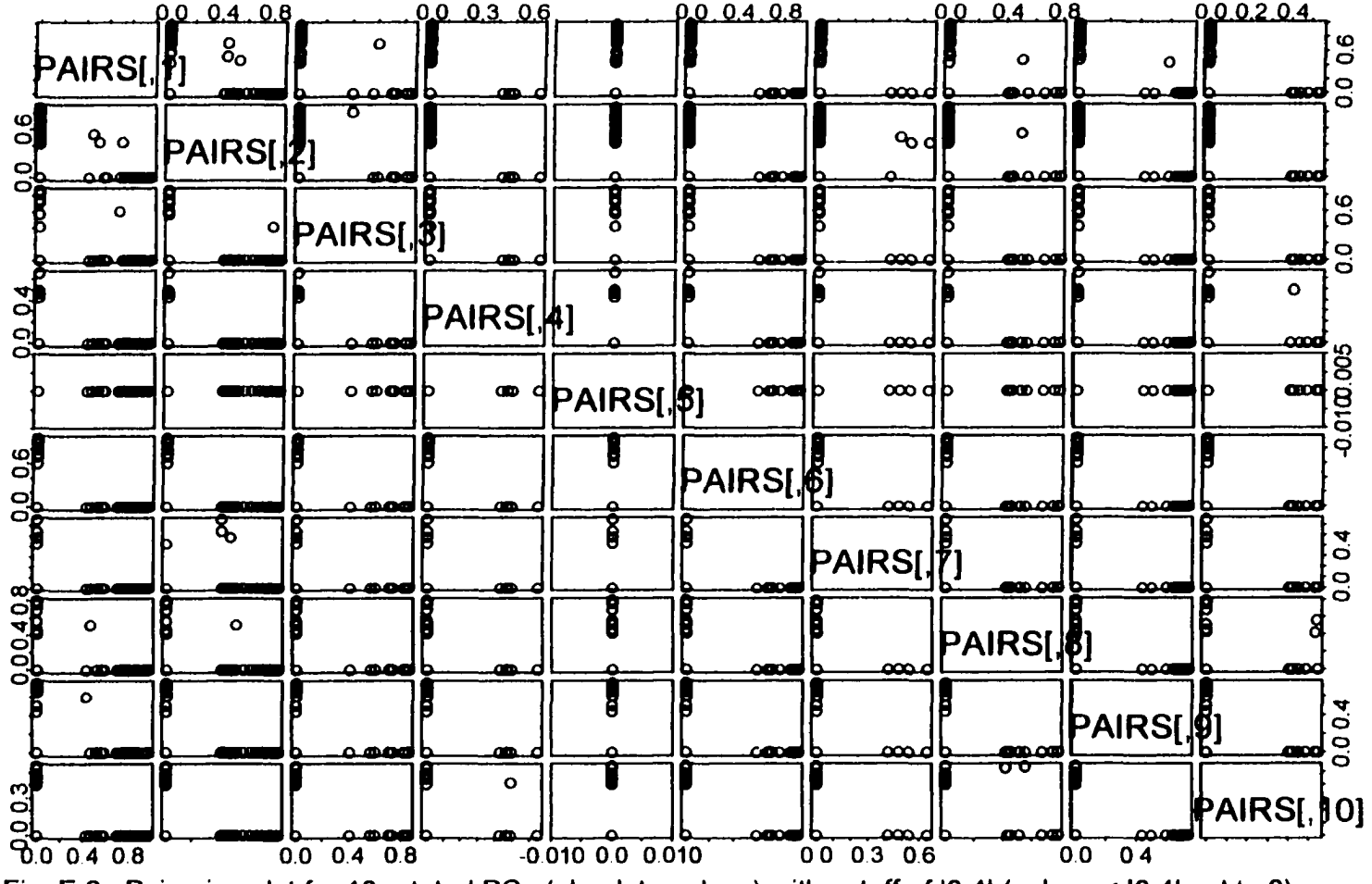

Fig. E.2. Pair-wise plot for 10 rotated PCs (absolute values) with cutoff of |0.4| (values < |0.4| set to 0).

TERM 1		TERM 2		TERM 3		TERM 5		TERM 7(cont)	
MM30	0.97	LP48	0.87	MH20	0.85	INFL	-0.52	HFAV	-0.89
MM35	0.97	SL47	0.85	TRPT	0.83	QTRN	-0.54	RFAV	-0.90
MM25	0.97	SL48	0.85	MH10	0.82	V4SR	-0.54	HCAV	-0.91
NCAP	0.97	ASRH	0.82	H5HT	0.73	OTFL	-0.54	RCAV	-0.91
MUCP	0.97	RHAV	0.82	FZLH	0.73	UCBL	-0.61	TERM 8	
MM40	0.96	LP47	0.81	WBZH	0.71	UPMW	-0.61	FCDP	0.78
MM20	0.95	MLCP	0.80	MXTE	0.60	VSSR	-0.62	MCAP	0.75
CZ20	0.94	MCNP	0.80	LP45	0.57	BRNS	-0.63	FCTL	0.68
MM15	0.93	LPS4	0.80	LP47	0.41	U4SR	-0.69	PRES	0.56
CTOT	0.93	SLS4	0.79	MELH	0.40	SH38	-0.70	MLCT	0.51
UUCP	0.93	MLFP	0.78	MP34	-0.61	UASR	-0.74	FCSU	0.45
MM10	0.89	RELH	0.77	SP34	-0.65	ELSU	-0.75	THLA	0.43
MM4E	0.88	SL56	0.77	TRPK	-0.74	U9SR	-0.76	MLPP	0.42
TEDF	0.88	SL67	0.75	MP23	-0.77	U3SV	-0.81	LP78	0.40
EMCP	0.85	SL78	0.75	PVOR	-0.77	TRPU	-0.83	LLLR	-0.51
MM05	0.84	LP67	0.70	SP23	-0.77	UREL	-0.85	EMCN	-0.53
EWDF	0.83	LP56	0.65	TRPP	-0.87	ULSV	-0.92	MUCN	-0.64
EFDF	0.83	FCRH	0.60	TERM 4		U6SV	-0.94	TERM 9	
CDPM	0.80	MLCT	0.54	MCAV	0.65	TERM 6		BTSM	0.74
MELH	0.77	PMSL	0.53	LC47	0.49	V6SV	0.94	BONE	0.73
MLF0	0.74	LP78	0.51	FCAV	0.49	VLSV	0.93	BTFR	0.70
MXMX	0.72	SL45	0.50	MFCN	0.47	VREL	0.92	BOTF	0.69
MXTE	0.70	SP78	0.49	LC56	0.43	TRPV	0.88	ITSM	0.69
MMPH	0.58	MLI0	0.48	GUAV	0.40	ELSV	0.79	IOTF	0.66
MLIH	0.57	MXMX	0.44	LCAV	-0.41	V3SV	0.73	IONE	0.65
SMXR	0.52	SMXR	0.44	WDIV	-0.49	VASR	0.72	ITFR	0.64
MLCT	0.47	OTFL	0.43	LC78	-0.62	V9SR	0.71	BECP	0.59
BECP	0.43	INPW	0.43	VVLC	-0.78	VCBL	0.69	BMCR	0.50
MLFP	0.40	SP56	0.43	WCAV	-0.81	VPMW	0.69	BECN	0.44
MLFH	-0.41	SP67	0.42	VVFL	-0.87	V4SR	0.60	ML56	-0.40
ML78	-0.44	H5HT	-0.40	VKLC	-0.87	VSSR	-0.43	ML67	-0.45
ML48	-0.48	MLIH	-0.44	VKFL	-0.88	U4SR	-0.55	ML48	-0.60
MLI0	-0.52	FZLH	-0.49	VVCL	-0.88	USSR	-0.76	ML47	-0.61
THEL	-0.68	MLFH	-0.67	VVLF	-0.89	TERM 7		TERM 10	
MULP	-0.70	LLLR	-0.68	VKCL	-0.89	SP67	0.65	VKAV	0.54
MELP	-0.73	DNCP	-0.71	VKLF	-0.89	SP56	0.54	PRES	0.54
MLS4	-0.74	MBST	-0.74			SP78	0.48	MLPP	0.53
MELT	-0.75	MLCH	-0.78			MP67	0.42	WFAV	0.48
MULI	-0.85	TL75	-0.82			MP34	-0.48	VVAV	0.45
MLIM	-0.96					LMSL	-0.56	LC47	0.42
						MP45	-0.63	ML45	0.40
						H5LP	-0.81	MFAV	-0.40
								AUDV	-0.43

Table E.1. PC loadings for (absolute value) of cutoff at or above 0.4

APPENDIX F

Multiple Logistic Regression

Logistic regression used in Chapter 4 has, as input, the binary predictand FONE, which is 1 for one or more flashes and 0 otherwise. The ten PC scores (X_1 to X_{10}) computed from the PCA (Chapter 4 and Appendix E) are the predictands. Using the statistical package, S-Plus 2000, developed by Mathsoft (now Insightful Corporation (1999)), a generalized linear model (glm) is used to derive the predictive equation of the form :

$$Y = \exp[Z]/(1 + \exp[Z]) \quad \text{,where}$$

$$Z=\beta_0 + \beta_1X_1 + \beta_2X_2 + \beta_3X_3 + \beta_4X_4 + \beta_5X_5 + \beta_6X_6 + \beta_7X_7 + \beta_8X_8 + \beta_9X_9 + \beta_{10}X_{10}.$$

The maximum likelihood estimates of the coefficients (β_N) are produced by an interatively reweighted least squares approach.

Using the developmental PC scores (X_N) as an example, the S-shaped graph, bounded by 0 and 1 on the Y-axis, is shown in Fig. F.1. Substituting in the coefficients derived from the logistic regression in the previous equation for Z gives:

$$Z = -2.24 + 0.37X_1 + 0.23X_2 + 0.28X_3 + 0.46X_4 - 0.28X_5 + 0.33X_6 - 0.01X_7 +$$

$$0.03X_8 + 0.86X_9 + 0.51X_{10} \quad .$$

X_1 = CAPE
X_2 = Lapse rates/relative humidity
X_3 = Upper-level potential vorticity, saturated and moist geostrophic potential vorticity (above 400 mb), tropopause pressure, temperature, 500 mb height, height of 0, -10, and -20 °C, WBZ
X_4 = Low level forcing and vertical velocity through LFC
X_5 = U wind components, shear and storm relative terms
X_6 = V wind components, shear and storm relative terms
X_7 = Mid-level saturated geostrophic potential vorticity (below 400 mb), mid and low level cyclonic circulation.
X_8 = Convective Inhibition/Capping inversion
X_9 = Best CAPE*LTG Climo, LTG Climo, potential instability
X_{10} = Forcing from LCL to LFC, mid-level vertical velocity, upper- level divergence, pressure at most unstable parcel level

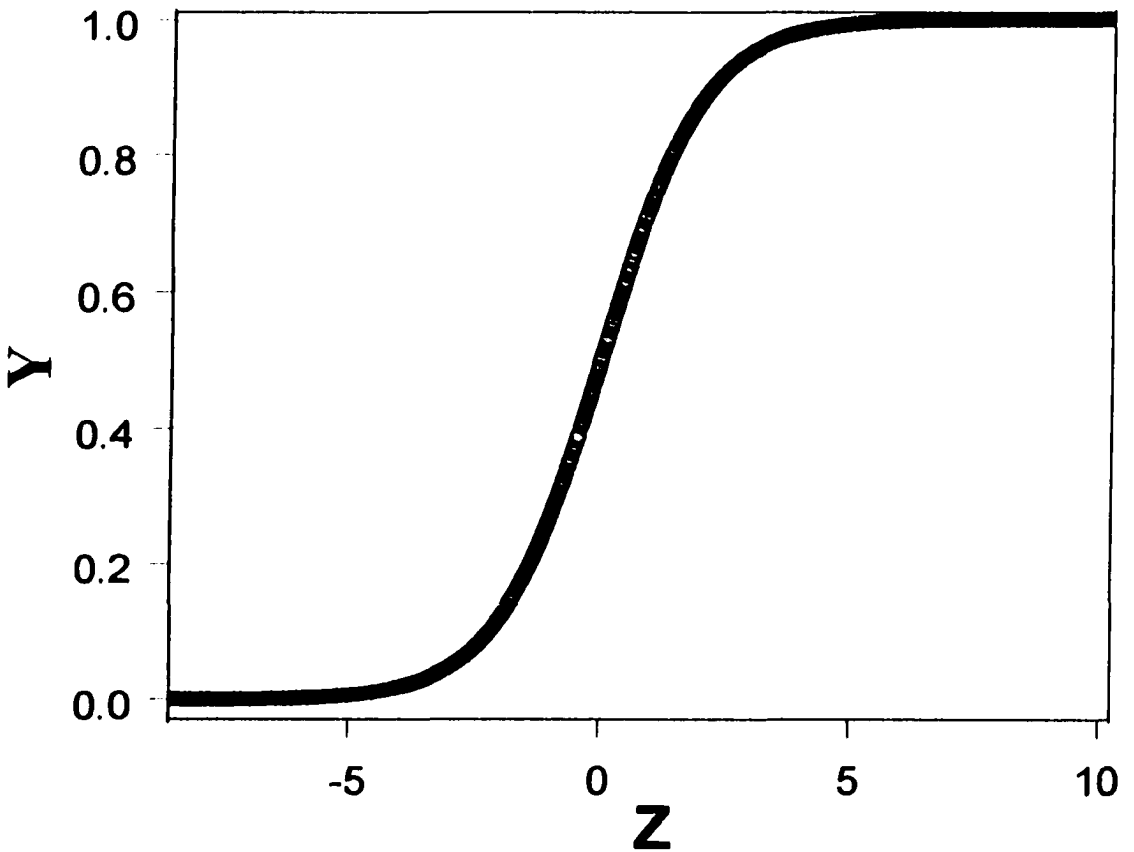

Fig. F.1. Example of response of predictand (Y) from logistic regression. Z is defined in Appendix F. Data is from developmental sample.

APPENDIX G

Measures of Forecast Skill and Accuracy

Several methods have been used over the past decades to verify probabilistic thunderstorm forecasts. These include the probability of detection (POD), the false-alarm rate (FAR), critical success index (CSI) or threat score (TS), the bias, and the Brier skill score (SS) (also called the half-Brier score). Each of these terms is defined in Table G.1. Figure G.1 is an example of the 2 X 2 contingency table that is used in the definition of the terms in Table G.1.

FORECAST	OBSERVED YES	OBSERVED NO
YES	a	b
NO	c	d

Fig. G.1. Contingency table (2 X 2). Each letter (a, b, c, and d) represents a possible combinations of forecast/event pairs.

POD = a / (a + c)

FAR = b / (a + b)

CSI = TS = a / (a + b + c)

Bias = (a + b) / (a + c)

$$BS = 1/n \sum_{k=1}^{n} (y_k - o_k)^2.$$

where the index k denotes a numbering of the n forecast/event pairs. The probability is y_k and the observation, o_k, is 1 if the event occurs and 0 if it does not occur.

$SS = 1 - BS / BS_{ref}$. where BS_{ref} is the lightning climatology (pentads).

Table G.1. Summary of terms used to assess forecast skill and accuracy.

This study has referred to previous work by Reap (1986), Charba (1984), and Hughes (2001). Each of these have used some or all of these measures of skill and accuracy. However, it is impossible to precisely compare their results to those cited in this study for the following reasons. These various measures of performance are affected by: (1) the size (area) of the grid box, (2) time interval of the forecast (3, 6, 12, or 24 hours), (3) whether the predictand is 1 or more flashes or 2 or more flashes, (4) using MDR data to verify a thunderstorm versus lightning data, (5) changes in the detection efficiency, and to a lesser degree, accuracy of flash location, (6) different geographic regions of the country, (7) dependent versus independent data verified, (8) lightning climatological predictors a function of season, month, or pentad, (9) forecasts valid at different times of the day, and (10) large scale model data (predictors) interpolated to grid versus calculated at grid point. While each of these reasons can make a direct comparison difficult, estimates of differences caused by the first two (size of grid box and length of forecast) can help make any comparisons more meaningful.

In the first hypothetical example, initially 16 adjacent grid boxes, 80 km on each side are accounted for by contingency table on the left of Fig. G.2. If the dimensions of the original 16 boxes are cut in half, there are 64 boxes, each 40 km on a side that are accounted for by the contingency table on the right of Fig. G.2.

To approximate how CSI changes with decreasing the size (area) of the box, assume for every full-size box (80 km) with lightning, that 25, 50, and 75%, respectively, of the smaller boxes (40 km) had lightning.

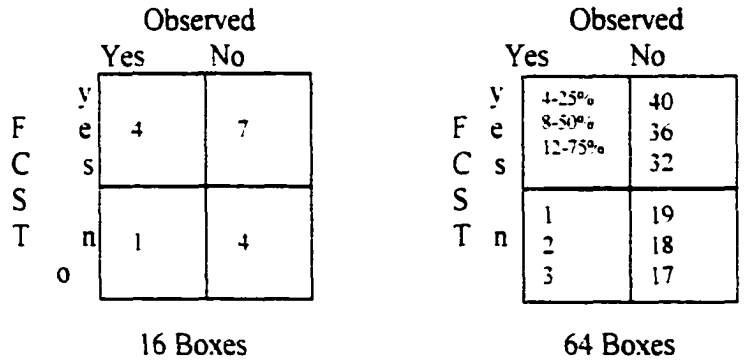

Fig. G.2. Contingency tables for 16 grid boxes each 80 km per side (left), and for when the dimensions are cut in half (the area of the box is one-quarter), producing 64 grid boxes (each 40 km per side) (right).

Original CSI = 4 / (4 + 7 + 1) = 33.3%.

CSI for box ¼ original area with 25% of new boxes having flashes
(actual case if there is only one flash in each original box (80 km on a side), the flash can only be assigned to one box)
CSI = 4 / (4 + 40 + 2) = 8.7%

CSI for box ¼ original area with 50% of new boxes having flashes
CSI = 8 / (8 + 36 + 2) = 17.4%

CSI for box ¼ original area with 75% of new boxes having flashes
CSI = 12 / (12 + 32 + 3) = 26.7%

Thus, while the original CSI is 33.3%, much lower CSIs can be expected (8.8 to 26.7% in this hypothetical example) when the dimensions are cut in half (area is one-quarter).

The second example is for cases involving different lengths of time that the forecast is valid. A 3-hour and 24-hour forecast are compared in Fig. G.3. Thus, for a hypothetical case where the forecast probability is 30% for both a 3-hour and 24-hour forecast. Normally, when fewer flashes are reported over a shorter time ($1/8^{th}$ of the time), the hypothetical CSI drops from 0.83 to 0.33.

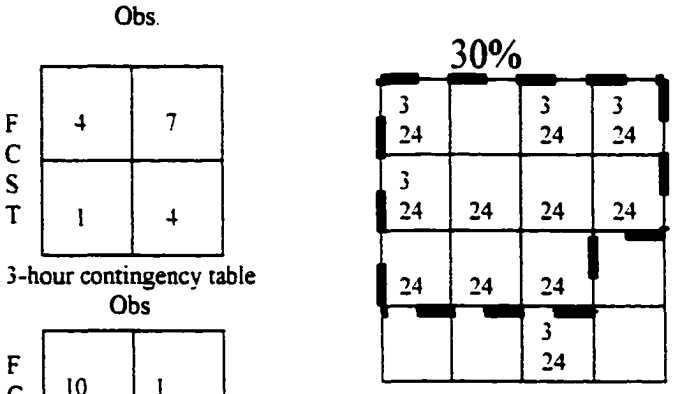

Example with 16 total grid boxes (4 boxes by 4 boxes). Grid boxes reporting one or more flashes per time interval as follows: Boxes denoted by 3 have one or more flashes in a 3-hour period. Boxes denoted by 24 have one or more flashes in a 24-hour period. Thick dashed line encloses a 30% probability forecast.

For the 3- hour period, CSI = 4/(4+7+1) = 0.33
For the 24-hour period, CSI = 10/(10+1+1) = 0.83

Fig. G.3. Contingency tables for two different time periods and hypothetical grid boxes reporting one or more flashes per time interval (as shown) as evaluated for 30% forecast probability.

Figure G.4 shows that if the boxes with one or more flashes were not included, approximately 20% of the data would be thrown away. Grid boxes with only one flash are the most common. When lightning occurs, one or more flashes were reported nearly twice as often as two or more flashes (19% versus 9%). With the exception of Hughes (2001), all other climatologies were developed with using 2 flashes or more (prior to the network upgrade in 1994). If all other factors were held constant, the skill score would be expected to improve when verification changed from two to one flashes. This is because the Brier score for observed lightning (in the numerator of the skill score) would improve (become smaller) as all one flash events

would now be counted as correct forecasts. These results would further complicate any comparison with previously reported scores.

Skill scores, through the half-Brier score measure, can also produce different results, depending on the lightning climatology that is used as a reference. Since the reference climatology is in the denominator of the Brier score, if the pentad climatology more accurately represented the intraseasonal change in lightning in the West compared to a monthly lightning climatology, the skill scores could be affected even if all the forecast probabilities in the numerator were identical. In effect, a more representative (pentad) climatology (BS_{ref} closer to 0) would produce a lower skill score because the smaller Brier score in the denominator would result in a lower skill score. Also, a monthly climatology that was less representative would have a higher Brier score and hence a higher skill score, even if the numerator was identical.

Therefore, while the numbers in this study at first do not appear dramatically different from that of previous work (see Fig. 2.1), it has been shown that as a result of the decreased grid size and shorter time interval used here (as well as other factors), the verification scores presented in Chapter 5 represent a significant improvement over previous methods.

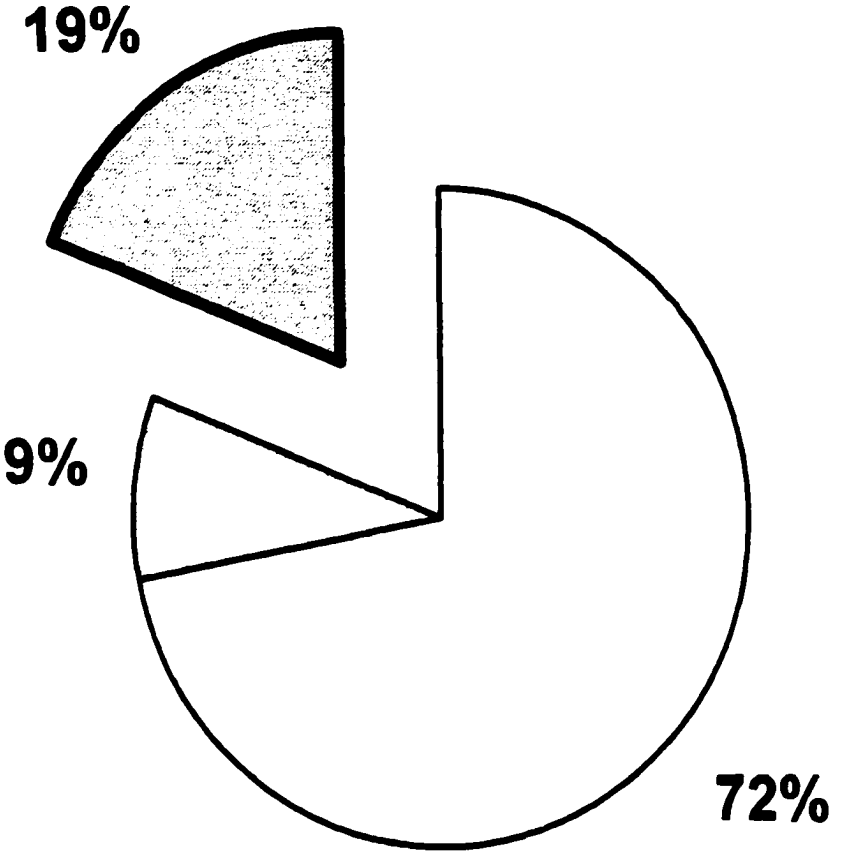

Fig. G.4. Nineteen percent of all boxes that report lightning have only one flash (hatched section-exploded) and nine percent have only 2 flashes (dotted section). Remainder (72%) is for all other categories of flashes (3 to 1175 flashes).